Charles University in Prague

Faculty of Natural Science

Department of Physical and Macromolecular Chemistry

Institute of Macromolecular Chemistry AS CR

Department of Nanostructured Polymers and Composites

Organic-Inorganic Polymer Nanocomposites

Doctoral Thesis

MSc. Sergii Ponyrko

Supervisor: RNDr. Libor Matějka DSc.

Prague 2015

Univerzita Karlova v Praze

Přírodovědecká fakulta

Katedra fyzikální a macromolekulární chemie

Ústav makromolekulární chemie AV ČR, v.v.i.

Oddělení nanostrukturovanych polymeru a kompozitu

Organicko-anorganické polymerni nanokompozity

Disertační Práce

Mgr. Sergii Ponyrko

Školitel: RNDr. Libor Matějka DSc.

Praha 2015

Prohlášení:

Prohlašuji, že jsem závěrečnou práci zpracoval samostatně a že jsem uvedl všechny použité informační zdroje a literaturu. Tato práce ani její podstatná část nebyla předložena k získání jiného nebo stejného akademického titulu.

V Praze, 15.12.2015

Podpis Sergii Ponyrko

.

To my family,

and those who care…

Acknowledgments

First of all, I would like to sincerely thank the persons who supervised this work, to Dr. Libor Matějka, for guiding me all these years, for constant and insightful feedback, availability and constructive guidance and for all the time and efforts. Thank you for always keeping your doors open for me.

Also I would like to thank to the Dr. Adam Strachota for encouragement and helpful discussions, support and his help during my doctoral study. I am very grateful to Eva Miškovská and Iveta Vlasáková for helping me with the arrangements of the labs issues.

I would like to thank to Dr. Jocelyne Galy (INSA de Lyon, France) who hosted me in her laboratory, for her very precious help during my stage in France. I am also grateful to Dr. Marino Lavorgna, Dr. Fabiana Tescione and Dr. Giovanna Buonocore (IPCB-CNR, Italy) who hosted me in their labs in for their help and friendship.

Finally, a special thanks to my parents and my family for their lovely support.

Table of contents

SUMMARY

The research described in this thesis is a part of state founded projects aiming at the design and implementation of new, better materials based on epoxy resins. The epoxy thermosets are organic matrices with excellent heat, moisture and chemical resistance, and good adhesive properties to many substrates; therefore they are mostly applied in the field of coatings, electronic devises, adhesives, laminates and composites. The epoxies, which are very common polymer materials in the industry, have been used as a host to create new, improved materials - nanocomposites. Therefore, this thesis focused on how to improve the thermomechanical properties without deteriorating existing benefits of epoxy materials and on further potential application of this knowledge in "smart" systems.

Organic-inorganic polymer nanocomposites are nanostructured systems containing both organic part and inorganic nanofiller. These systems combine advantages of polymers and inorganic components showing a synergy effect. Synthesis of organic-inorganic nanocomposites can be particularly interesting thanks to their easy applicability to the common processing techniques. In order to improve desired properties, inorganic additives to the epoxy systems are frequently employed. For preparation of epoxy based hybrids/nanocomposites materials, the sol-gel method (hydrolytic polycondensation of alkoxysilanes) is widely used either to modify preformed nanoparticles or to synthesize silica/siloxane domains *in situ* in an epoxy matrix. But classical "aqueous" sol-gel process together with obvious benefits brings a lot of shortcomings such as immiscibility of water with alkoxysilanes and with epoxy resin, necessity of application of a cosolvent which is leading to phase separation and shrinkage of the final product. So the largest part of this work is dedicated to the reinforcement of epoxy thermosets by silica, generated *in situ* under nonaqueous (non-hydrolytic) sol-gel process. For this reason borontrifluoride monoethylamine (BF_3MEA) was chosen as effective catalyst for the formation of nanosilica in epoxy-matrix under thermal heating process.

In order to understand how to reinforce the glassy thermosets by the non-aqueous sol-gel process it was necessary to understand the mechanism of the process and to follow the structure evolution and structure-properties relationships.

Significant attention in this work was given to the use of coupling agents and ionic liquids (IL) to improve compatibilization of the organic matrix and the inorganic part and enhance the interfacial interactions providing chemical bonds between the phases which is reflected in dramatic improvement of thermomechanical and tensile properties.

We proposed the mechanism of the non-aqueous sol-gel process including protolysis of the most typical alkoxysilane (tetraethoxysilane) by using BF_3MEA complex as an initiator. By studying the evolution of the networks growth by dynamic mechanical analysis it was postulated that the generation of silica structures at the nonaqueous process is slower with respect to the classical sol-gel process thus facilitating a better control of the nanocomposite structure and morphology.

As a result of the nonaqueous sol-gel process optimization, we synthesized the high-T_g and heat resistant nanocomposites by combination of the tetramethoxysilane (TMOS) and glycidyloxypropyltrimethoxysilane (GTMS), as coupling agent. At a high GTMS content the silsesquioxane (SSQO) structures, formed by the sol-gel process, percolate and bicontinuous organic-inorganic phase morphology with the strong interphase interaction was formed.

The epoxy-based nanocomposites were applied in the second part of the thesis for the preparation of temperature responsive shape memory polymers (SMP). The investigation was focused on general study of shape memory (SM) behaviour and enhancement of mechanical strength of SMP in order to design and prepare the high performance SMP nanocomposite. The main objective was in improvement of SM key-parameters, such as recovery stress, extent of recoverable deformation, shape fixity, recovery rate. All these parameters were tuned by different structural modifications. The effect of nanosilica, IL, crosslinking density of the epoxy network, physical crosslinking as well as application of the concept of bimodal networks on SM performance was evaluated and discussed. Moreover general recommendation about the SMP testing procedure measurement was presented. The research resulted in the better understanding of the shape memory phenomenon and synthesis of the SMP showing a high recovery stress as well as a high recoverable deformation.

Four articles were published in impacted polymer journals based on this research.

List of abbreviations

ATBN Amine-terminated butadiene copolymer with 18% of acrylonitrile

BF_3MEA Borontrifluoride monoethylamine

DAB 1,4-diaminobutane

DDM diaminodiphenylmethane

DGEBA Diglycidylether of Bisphenol A

DMA Dynamic mechanical analysis

GTMS 3-glycidyloxypropyltrimethoxysilane

IL Ionic liquid

- C_{10}MImBF_4 1-decyl-3-methylimidazolium tetrafluoroborate
- C_4MImCl 1-butyl-3-methylimidazolium chloride
- C_4MImBF_4 1-butyl-3-methylimidazolium tetrafluoroborate
- C_7O_3MImMeS 1-triethyleneglycol monomethylether-3-methylimidazolium methanesulfonate
- CH_2CO_2HMImCl 1-carboxymethyl-3-methylimidazolium chloride
- $C_3H_6CO_2$HMImCl 1-carboxy propyl-3-methylimidazolium chloride

Jeffamine D2000 poly(oxypropylene)diamine M~1970

Jeffamine® D230 poly(oxypropylene)diamine M~230

Jeffamine® D400 poly(oxypropylene)diamine M~400

Laromin 3,3'-dimethyl-4,4'-diaminocyclohexylmethane

NMR Solid-state nuclear magnetic resonance spectroscopy

SAXS Small-angle X-ray scattering

SSQO Silsesquioxanes

SMP Shape memory polymer

TEM Transmission electron microscopy

TGA Thermogravimetric analysis

TEOS Tetraethoxysilane

TMOS Tetramethoxysilane

Symbols

T_g - glass transition temperature

Tc - curing temperature

T_d - deformation temperature (T_d = 100 °C)

T_{trans} – transformation temperature (T_{trans} = T_g or T_m)

Ts – setting temperature (T_s = 25 °C)

$G`$- shear storage modulus

G_r - rubbery modulus

G_s - glassy modulus

tan δ - loss factor (tan δ = $G``/G`$)

D_m - mass fractal dimension

D_S - surface fractal dimension

α_{Si} - condensation conversion

M_C - molecular weight of the elastically active chain between crosslinks

t_{gel} - gelation time

R_f - shape fixity

σ_b – stress at break

σ_r - recovery stress

ε_b - elongation at break

λ_b – strain at break

σ_{rub} - stress under deformation at rubbery state

λ_d – strain at deformation temperature T_d

1. PREFACE

The epoxy thermosets are kind of organic materials with excellent heat, and chemical resistance and with good adhesion properties.[1] Thus, they are mostly applied in the field of coatings, adhesives, printed circuit boards, composites, laminates, the potting of electronic composites, rigid foams and encapsulation of semiconductor devices.[2] However, despite having good thermo-mechanical properties and high heat resistance, the epoxy systems cannot meet all the requirements, especially for the structural and electrical applications.[3] Therefore, mixing of various combinations of epoxy networks and organic or inorganic materials has been very useful for the exploration of new materials combining unique properties and specific performances.[4] These materials, composed of several components, are generally called "composites".[5] The multicomponent polymer composites usually are multiphase heterogeneous materials.[6] The mechanical, electrical, thermal, optical, electrochemical, catalytic properties of the composite will dramatically differ from that of the one-component and homogeneous materials and show a significant improvement after a proper structure and morphology design.[7]

In the 1980`s term polymer/clay based “nanocomposite” came into existence.[8] Nanocomposite is a multiphase material where one of the phases has at least one dimension less than 100 nm, or structures having nano-scale repeated distances between the different phases. Inventing of nanocomposites was reflected in the improving of homogeneity and transparency of multicomponent materials.[9]

Organic-inorganic polymer nanocomposites are nanostructured systems containing both organic and inorganic components.[10] These systems combine advantages of polymers (elasticity, easy processing etc.) and inorganic components (hardness, thermal resistance etc.) showing a synergy effect under proper conditions. The term ‘‘hybrid’’ is used for the composites with components mixed on the molecular level. The term organic-inorganic hybrid materials came out around the late 1980s in the molecular chemistry[11,12] and became prevalent with development of the chemistry of bridged and cubic polysilsesquioxanes.[13,14]

The epoxy matrix filled with silicon based inorganic nanofiller of different structures is an important type of organic-inorganic polymer nanocomposites. The silica nanoparticles[15-17], layered clays[18-20], or the silica and silsesquioxanes domains which are generated *in situ* by the sol-gel process[21-25] are the most common nanofillers.

The thesis deals with organic-inorganic polymer nanocomposites based on epoxy polymer networks. Particularly, the synthesis, structure and properties of epoxy-silica nanocomposites is described in the first part of the thesis and application of this material as high performance shape memory polymers in the second part.

2. INTRODUCTION

2.1 Epoxy networks

In 1909, the Russian chemist Prilezhaev discovered the formation reaction of epoxides.[26] Only ~50 years later, the first industrially-produced epoxy resins were introduced to the market.[27] Generally term “epoxy” is referred to molecule’s functional groups consisting of reactive oxirane rings. The simplest and most common type of an epoxy resin could be prepared by the reaction of bisphenol A with epichlorohydrine.[28] Depending on stoichiometric proportion of those two components, the products of different molecular weight can be obtained. Structure of the common epoxy resin - diglycidylether of bisphenol A (DGEBA) is shown in **Fig.1**.

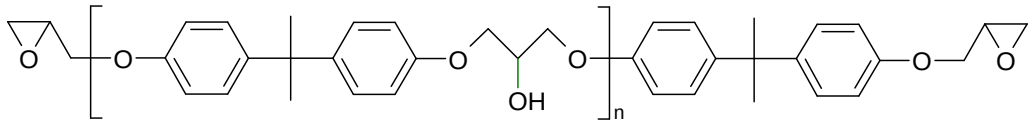

Fig. 1 Diglycidylether of Bisphenol A (DGEBA).

The high reactivity of the epoxy groups, due to the strained ring, makes it possible to use epoxies in a wide variety of polymerization reactions.[29] Epoxy polymers can be produced by step or chain polymerizations or by combination of both mechanisms.[30]

The step-growth polymerization proceeds by alternating addition reactions of the epoxy monomer with a curing agent, such as amines[31-34], amides[35, 36], phenols[37, 38], carboxylic acids[39], anhydrides[40-43] etc. The amines are the most typical curing agents and the corresponding addition reactions of the primary and secondary amine go as shown below:

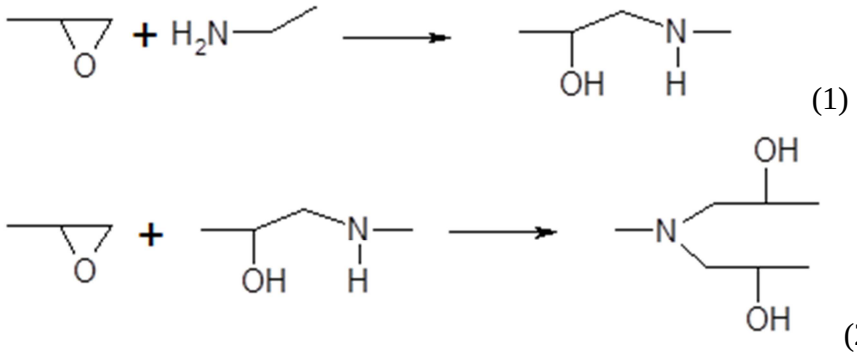

In order to prepare an epoxy network, the multifunctional crosslinking agents with functionality f > 2 are used.[44] In case of amines, the primary amine group -NH_2 is bifunctional with respect to the reaction with an epoxide as shown in Eq.1 and Eq.2.

Consequently, a diamine is the tetrafunctional crosslinking agent, f = 4. Curing of epoxy resin with a diamine occurs in three stages[45, 46]: (i) propagation of the linear chain, (ii) formation of a branched structure, and (iii) gelation and increase in crosslinking density up to fully cured thermoset as shown in **Fig.2.**

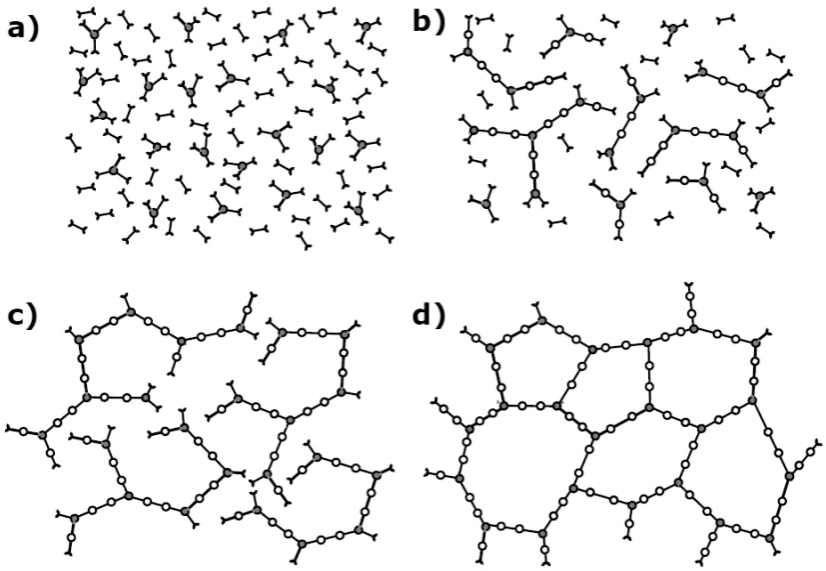

Fig. 2 Curing of the epoxy resin: a) monomers, b) linear growth and branching, c) formation of highly brunched structures, d) fully cured thermoset.

The epoxy-amine reaction is suitable for the synthesis of "model" networks since side reactions do not take place in case of stoichiometric ratios of both reacting functional groups.[47] Among the wide variety of the curing agents available on a market, amine-based hardeners, both aliphatic, cycloaliphatic and aromatic, have been the most common. The amine crosslinkers involve the aliphatic amines such as: ethylenediamine (EDA), diethylene triamine (DETA), triethylenetetramine (TETA), 1,4-diaminobutan (DAB), and Jeffamines D230, D2000 etc., and the aromatic amines e.g.: 4,4′-Diaminodiphenylmethane (DDM), 2,4-Diaminotoluene (DMT), 4,4'-Diaminodiphenylsulfone (DDS), metaxylylene diamine (MXDA). Moreover, the cycloaliphatic amines, such as para-aminecyclohexanemethane, are often used.[48]

The course of polymerization and the properties of the final epoxy network depend on the type of amine curing agent.[49] The reactivity of the amine increases with its nucleophilic character in the series: aliphatic > cycloaliphatic > aromatic. The high reactivity of aliphatic amines makes it possible to accomplish the reaction at room temperature with heat produced by an exothermic reaction, while external heat is required for the curing with aromatic amines.[50] The curing at high temperature results in thermosets of better thermomechanical properties, including higher T_g, strength and

stiffness, compared to those cured at room temperature. By adjusting a proper amine, the final properties of the cured thermosets may be varied from hard and rigid with high crosslinking density to flexible and soft with the low crosslinking density.[51] The most suitable curing agent must be selected according to the use conditions, required properties, application, workability and other factors.

In case of chain-growth polymerizations, the epoxy groups can react with both nucleophilic and electrophilic species which can produce an ion that is an active center of the polymerization.[47] The electron-deficient carbon can undergo nucleophilic reactions, whereas the electron-rich oxygen can react with electrophiles. It is customary in the epoxy chemistry to refer to these reactions in terms of anionic (initiated by e.g. tertiary amines[52]) and cationic[53] (e.g.by Lewis acids[54, 55]) mechanisms of chain-growth polymerizations.

In order to design the epoxy matrix that will show the best properties, the following factors must be considered:

(a) Selection of the proper combination of epoxy resin and curing agent structures;

(b) Epoxy/Curing agent stoichiometric ratio;

(c) Selection of catalyst/accelerator (if needed);

(d) Curing/post-curing processes and conditions;

(e) Selection of modifiers such as fillers, toughening agents, etc.

The precise selection and preparation of epoxy-amine networks leads to the formation of the epoxy-based thermosets with an optimum performance.

2.2. Organic-inorganic nanocomposites

The epoxy-based materials exhibited good thermal stability and mechanical properties.[56, 57] Nevertheless, they do not meet all requirements, so further improvement of the required properties is necessary. As already mentioned above, the use of inorganic nanoparticles can be particularly interesting thanks to their easy applicability to the common processing techniques used for epoxy-based conventional composites. The final properties of the nanocomposite material are affected by several factors, such as intrinsic characteristics of each component, the content, the shape and the dimension of fillers, and the nature of the interface.[58]

Organic-inorganic polymer nanocomposites are multiphase and multifunctional materials. The dispersion of nanoparticles in a polymer is a crucial factor for the final properties of nanocomposites.[59] Nanoparticles tend to form agglomerates and clusters in a

polymer matrix due to their high surface energy.[60] The agglomeration may lead to a deterioration of the aimed properties of the final products.

Generally, there are two different methods how to prepare nanocomposites: top-down and bottom-up approaches[61] (Fig.3). These two methods allow to avoid problems with heterogeneity and to improve properties of the nanocomposites.[62] First method represents disintegration of large microparticles into smaller nanoparticles by a subsequent intercalation and exfoliation. On the contrary, bottom-up approach allows formation of nanostructures starting from molecular level. This is an important and crucial difference because the bottom-up technique enables even better nanofiller dispersion.

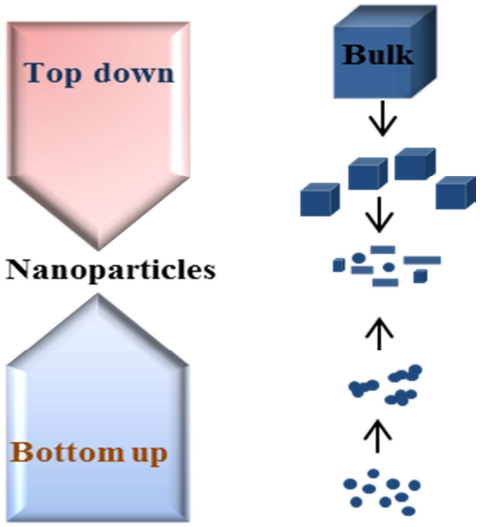

Fig. 3 Top-down and bottom-up approaches of nanocomposite synthesis.

The bottom-up formation of organic–inorganic nanocomposites can be subcategorized in accordance to the manner of formation:

a) Building block approach;

b) *In situ* formation of inorganic nanostructures;

c) Formation of organic polymers in presence of preformed inorganic nanostructured materials;

d) Simultaneous formation of both components, i.e. organic polymer and inorganic nanofiller.

In contrast to traditional polymer composites with high content (~50 wt. %) of micrometre-sized filler particles, polymer nanocomposites are being developed with low content (~10 wt. %) of well-dispersed nanofiller due to high surface to volume ratio (Tab.1).[63]

Table 1. Ratio of particle diameters to the number of contained atoms and to the fraction of surface atoms.[64]

Particle diameter, nm	Number of atoms in a particle	Fraction of surface atoms in a particle, %
20	250.000	10
10	30.000	20
5	4.000	40
2	250	80
1	30	99

The large surface-to-volume ratio of the nanoscale inclusions plays a significant role.[65] Smaller particles display a much larger surface area for interaction with the polymer for the same microscopic volume fraction than larger particles.[66] Majority of the characteristics of nanocomposites are determined by the interactions that occur at nanoparticle-matrix interfaces. Therefore, the mechanical, electrical or thermal properties of nanocomposites are strongly affected by the dispersion state and the quality of the interface between nanoparticles and polymer matrices.[67] The nanofiller as reinforcing material of a polymer can be one-dimensional[68] (nanotubes, fibers, rods), two-dimensional[69] (sheets, plane-like particles, e.g. exfoliated clay stacks) or three-dimensional[70] (particles, e.g. minerals).

The organic-inorganic nanocomposites can be classified into two categories based on the nature of interfacial interaction between the inorganic and organic components:

i) systems with weak interactions between the two phases (Van der Waals, H-bonding or weak electrostatic interactions);

ii) systems with strong chemical interactions between the components (covalent bonds).

The interphase interaction is a crucial factor determining the structure, morphology and properties of the organic-inorganic nanocomposites.[57] Morphology of the organic-inorganic nanocomposites is described by Wilkes model which represent a micro-phase separated polymer and nanoparticle. The model in Fig.4 represents the nanocomposite with silica dispersed in the organic matrix.[12]

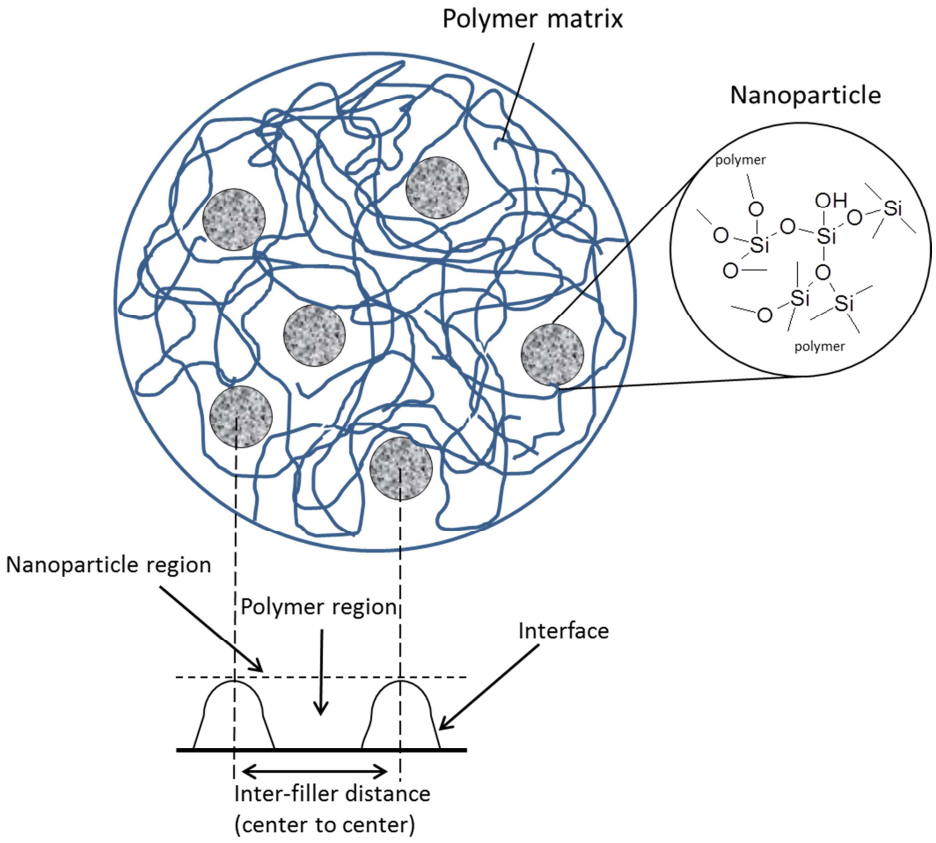

Fig. 4 Wilkes morphological model of the organic-inorganic hybrids.

The silica nanoparticles are the most typical inorganic nanofiller of polymer systems. They are generally introduced in a polymer directly by blending or silica precursors are used in the sol-gel process to generate silica nanostructures *in situ* within the organic matrix. The most widely applied precursors are silicon alkoxides.[71] Usually, the precursors for the sol–gel process are mixed with monomers of the organic polymerization and both processes are accomplished at the same time.[72] Simultaneous formation of the inorganic nanostructures and organic polymers can result in the most homogeneous type of the organic-inorganic nanocomposites.[73]

In particular, the sol-gel process with its unique mild processing characteristics and easiness of control is the most common method for preparing hybrid materials.

2.2.1. Sol-gel process

Since 1930`s the sol–gel process was one of the major driving methods to prepare ceramic precursors and inorganic glasses at relatively low temperatures.[74] The sol-gel reactions proceed by two fundamental hydrolytic polycondensation stages: the hydrolysis of the alkoxide precursors (Eq.3) to introduce a reactive hydroxyl group on the metal and their condensation to form siloxane Si-O-Si bonds (Eq.4) under acidic or basic

conditions.[75-78] Depending on the amount of water and catalyst present, hydrolysis may proceed to completion, so that all of the OR groups are replaced by OH groups, as follows:

$$Si(OR)_4 + 4H_2O \leftrightarrow Si(OH)_4 + 4R\text{-}OH \qquad (3)$$

$$(OR)_3\text{–}Si\text{-}OH + HO\text{–}Si\text{-}(OR)_3 \leftrightarrow [(OR)_3\text{-}Si\text{–}O\text{–}Si(OR)_3] + H\text{-}O\text{-}H \qquad (4)$$

or

$$(OR)_3\text{–}Si\text{-}OR + HO\text{–}Si\text{-}(OR)_3 \leftrightarrow [(OR)_3Si\text{–}O\text{–}Si(OR)_3] + R\text{-}OH$$

In general, the sol-gel process involves the transition of a solution system from a liquid "sol" (mostly colloidal) that acts as the precursor, into a solid "gel" phase. Application of the sol-gel process makes it possible to fabricate advanced materials in a wide variety of forms: ultrafine spherical shaped powders, thin film coatings, fibres, porous or dense materials, and extremely porous aerogel materials.

The goal of sol-gel processing is to control the structure of a material on a nanometer scale from the earliest stages of processing. The most widely used metal alkoxides are the alkoxysilanes, such as tetramethoxysilane (TMOS) - $Si(OCH_3)_4$ and tetraethoxysilane (TEOS) - $Si(OC_2H_5)_4$. However, other alkoxides such as aluminates, titanates, and borates are also commonly used in the sol-gel science, despite a high reactivity with water resulting in the loss of a reaction control.

Furthermore, the nature of the catalyst determines the relative rates of hydrolysis and condensation reactions and therefore it affects the topology of gel in terms of open branched structures or dense network structure (Fig.5).

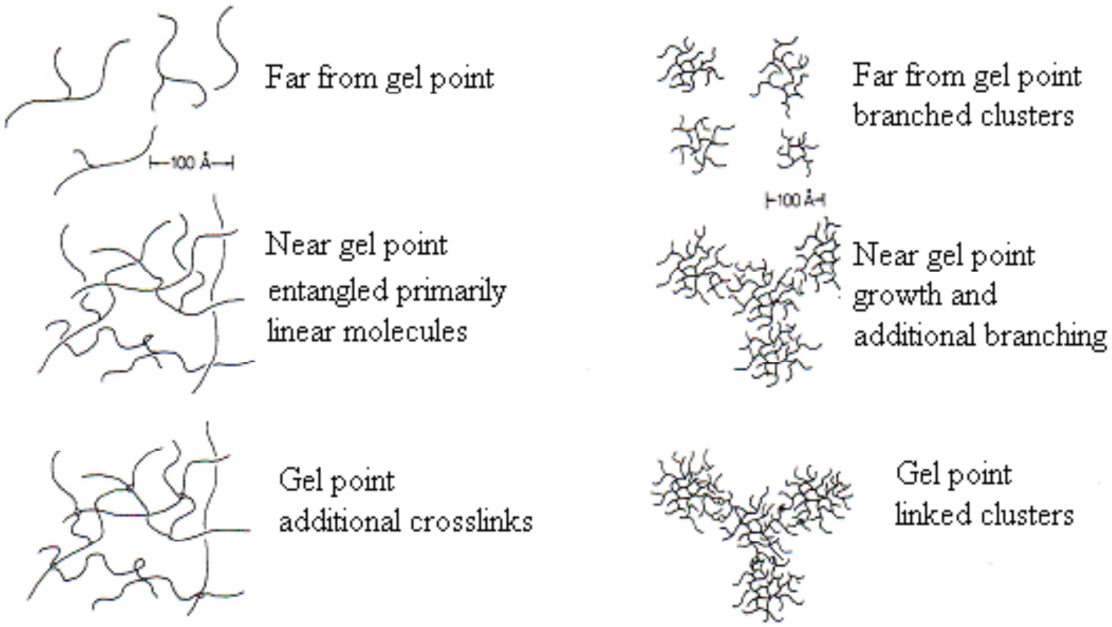

Fig. 5 Gel formation in acid (on the left) and basic catalysed systems (on the right).[74]

Before the gelation point and under acidic conditions, the precursor of the gel consists of linear or randomly branched polymers. Under acidic conditions hydrolysis is complete and fast, resulting in the open branched structures (see Fig.5) formed by the cluster-cluster aggregation mechanism**,** finally having low fractal dimension D_m ~ 2.1. While, under basic conditions hydrolysis is slow and incomplete but polycondensation is fast. In this case the monomer-cluster aggregation mechanism is dominating and dense structures with large compact aggregates and high fractal dimension (D_m ~ 3) are formed.[74] The viscosity at the gelation stage increases asymptotically and a transparent gel is formed.

2.2.2 Epoxy-silica nanocomposites

Epoxy matrix reinforced with *in situ* build silica by the sol-gel process is one of the most typical and widespread type of the organic-inorganic nanocomposite.[79-81] The properties of the final nanocomposites are in general influenced by particle sizes and interaction between the dispersed silica and continuous polymer phases.[57, 82-85]

Catalysis of the sol-gel process affects both, the morphology of the nanocomposites, e.g. homogeneity and size of aggregates, and the interphase interactions between silica structures and epoxy network. As mentioned above in contrast to the base and pH neutral catalysis of the sol–gel process, the acid catalysis promotes fast hydrolysis of the siloxane structures which results in the high contents of Si-OH groups. Strong interphase interaction of epoxy polymer chain with the silica domain through *H*-bond is feasible and preferable. Due to this reason, the application of polyether chains (e.g. Jeffamines) of amines is desirable, since in case of e.g. aliphatic amine less *H*-bond interactions are possible.[76]

Previously one- and two-step acid-base sol-gel procedures were applied for *in situ* generation of silica from TEOS in the DGEBA-polyoxypropylene diamine (D2000) network.[76, 83, 86] The one-step polymerization is a type of epoxy-silica synthesis in which all the organic and inorganic components are mixed altogether and reacted. The sol-gel process, in this case, is base catalysed by the amine crosslinker which acts also as a catalyst of the sol-gel process. The basic catalysis is very efficient for the polycondensation step, however the hydrolysis step is not well promoted. Therefore, only small amount of Si-OH groups is formed resulting in a weak interphase interaction of silica with polyether based polymer chain. The morphology of the network synthesized

by the one-step base-catalysed simultaneous polymerization is the most heterogeneous one and large siloxane aggregates can be detected.

The two step synthesis of a nanocomposite consists of prehydrolysis of TEOS in acid medium in the first stage, followed by polycondensation of siloxanes to form silica structures simultaneously with the build-up of an epoxy network in the second step.[76,78, 83] Therefore, the sol-gel is acid-base catalysed, because the amine is present in the reaction mixture only in the second stage. Hydrolysis is fast under acidic conditions in the first step, thus creating a large number of SiOH and a strong interphase interaction. At the second, basic catalysed step, a fast and complete polycondensation is resulting in formation of well-developed smaller silica nanostructures homogeneously dispersed in the epoxy matrix.

As it was mentioned before, the sol-gel process of alkoxysilanes results in the formation of linear polysiloxanes $(R_2SiO)_n$ or branched and crosslinked silsequioxanes $(RSiO_{3/2})_n$ from trialkoxysilanes as well as silica $(SiO_2)_n$ from tetraalkoxysilanes. For the strengthening the interphase interaction and in order to improve miscibility of the organic-inorganic hybrids coupling agents are frequently used.[87-91] The coupling agent is a type of precursors which contain both organic and inorganic functional group thus can provide a chemical bond between organic and inorganic phases. Organofunctional trialkoxysilanes are the most typical coupling agents.

But along with obvious advantages of the sol-gel process, it has often a problem with loss of morphological and also structural control over the final oxide material, thereby leading to a low reproducibility. Another disadvantage of hydrolytic sol-gel process is immiscibility. Water is immiscible with TEOS or with epoxy resin thus a cosolvent application is required. Furthermore evaporation of water and solvent leads to sample shrinkage and formation of bubbles or cracks in the final product.

2.2.3 Nonaqueous sol-gel process and corresponding nanocomposites

Nonaqueous (or non-hydrolytic) sol-gel processes in organic solvents, generally under exclusion of water, are able to overcome some of the major limitations of aqueous systems and thus represent a powerful and versatile alternative.[92-94]

Nonaqueous processes can be divided into surfactant- and solvent controlled approaches.[95, 96] Surfactant-controlled synthesis routes involve the transformation of the precursor species into the oxidic compound in the presence of stabilizing ligands in a typical temperature range of 250 to 350 °C. An alternative to surfactants is the use of

common organic solvents (ethers, alcohols, ketones or aldehydes) or by the organic constituent of the precursor (alkoxides or acetylacetonates) act as reactant as well as control agent for particle growth, enabling the synthesis of high-purity nanomaterials.[96]

The study, explanation and the conditions for the controlled structure development under the solvent-free nonaqueous sol-gel process[97] is barely described and explored. Application of such a method in the synthesis of epoxy-silica nanocomposite will be the focus of the following chapter.

Nanocomposites by nonaqueous sol-gel process

The non-aqueous solvent-free sol-gel technique provides an improved control over molecular level homogeneity leading to uniform morphologies. The solvent-free sol-gel process to prepare epoxy-silica nanocomposite was recently developed by Phonthamachai.[98] The one-pot synthesis comprises the simultaneous epoxy crosslinking and the sol-gel process of alkoxysilanes in the presence of ammonia solution. The very high postcuring temperature, up to 270 °C, was necessary to prepare the nanocomposites with uniform dispersion of silica and improved thermomechanical properties.

Lee et al.[99] synthesized the nanosilica from TEOS by non-hydrolytic sol-gel process in the epoxy matrix DGEBA-diaminodiphenylsulfone (DDS) catalysed by BF_3MEA. They suggested a catalytic mechanism of BF_3MEA in the reaction with TEOS. The two-step nanocomposite synthesis consisted of (i) preparation of nanosilica in the presence of epoxy resin and the BF_3MEA complex and (ii) formation of DGEBA-DDS-silica network by addition of the diamine. The studied nanocomposite displayed an increase in T_g by 50 °C with respect to the reference epoxy network with addition 40% of TEOS in the initial mixture. The solvent-free non-hydrolytic sol-gel process supported by the BF_3MEA complex was used in order to improve homogeneity of the epoxy nanocomposite and to eliminate problems with a solvent and excessive water removal. And even despite all advantages of the non-hydrolytic procedure, it has been very little studied so far with respect to the synthesis of the epoxy-silica nanocomposites. Such a theme was investigated and discussed in the first three articles

2.2.4. Ionic liquids

Another promising strategy for nanocomposite structure and morphology control is the application of ionic liquids. The ionic liquids (IL) are organic salts with melting temperature usually below 100 °C and are composed of an organic cation and an organic or inorganic anion. ILs possess low flammability, high thermal and chemical stability,

good stability in air and moisture.[100, 101] Due to their low vapour pressure and volatility, they are often used as "green" solvents.[102, 103] The possibility to choose between different counter-ions, allows having a wide range of ILs with different intrinsic properties. Therefore also ILs are widely used as electrolytes in batteries[104], surfactants[102, 103], lubricants in polymers[105], plasticizers[106] or as curing agents in epoxy systems[107].

Moreover, ILs can be applied as "molecular templates" in the sol-gel process due to their special molecular arrangements.[108, 109] Different ILs were used as a catalysts for the sol–gel process[110] and silica structure controllers[111]. In addition, the ILs were found to act like multifunctional agents in synthesis of epoxy-silica nanocomposites. They serve as catalysts of the sol-gel process to form silica structures and modify the epoxy-silica interphase. As a result, they efficiently control the nanocomposite morphology and mechanical properties.[112, 113]

2.3 Shape-memory polymers

Shape-memory polymers (SMP) are an important class of "smart" polymers which, after deformation, can recover their initial shapes under external stimuli (**Fig.6**).[114, 115]. This external stimulus for triggering the shape recovery can be temperature change, electric or magnetic field, light or pH of solution etc.[116] SMP also cover a wide property-range from stable to biodegradable[117], from soft[118] to hard[119], and from elastic[120] to rigid[121], depending on the structural units that constitute the SMP. Thermal-responsive SMPs are one of the most studied smart systems and will be the focus of the following chapter.

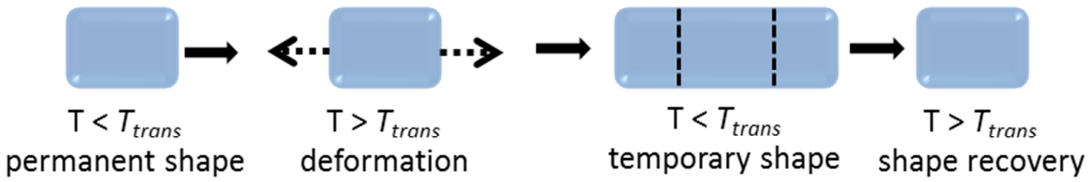

Fig. 6 Schematic representation of the shape-memory effect, where T_{trans} - transformation temperature.

Polymers with a shape-memory effect show both stored (permanent) form and a current (temporary) form.[122] The temporary form can be reached by processing through heating, deformation, and finally, cooling to fix this temporary shape. The polymer keeps new, temporary, shape until the shape change into the permanent form by triggering by a predetermined external stimulus.

In general, suitable shape-memory polymers consist of net-points and molecular switches, which are sensitive to an external stimulus. The net-points of a SMP network, which keep its dimensional stability, could be either covalently or physically crosslinked.[116] The switching phase allows a reversible transfer between hard and soft/liquid states. The glassy and crystalline states serving to fix the temporary shape of a polymer are the most typical.[122] Thermally induced changes of the switching phase, i.e. glass transition or melting, then leads to recovery of the original shape. The most common SMPs are represented by polyolefines[123], polyetheresters[124], polyurethanes[125], acrylates[126], epoxies[127,128] etc.

Generally, SMPs are classified into four main types based on the nature of net-points and switching components[129-131]:

1) chemically crosslinked net-points with amorphous switching components;
2) chemically crosslinked net-points with semicrystalline switching components;
3) physically crosslinked net-points with amorphous switching components;
4) physically crosslinked net-points with semicrystalline switching components.

According to the polymer classification, the first two categories belong to thermosetting polymers and the last two belong to thermoplastics. For the epoxy thermoset, the net-points of network determine the permanent shape of a SMP while fixing of temporary shape is allowed by the glassy state of a sample deformed above T_g.

The temperature-responsive shape memory (SM) properties of polymers are usually evaluated by the thermal SM cycle. Fig. 7 illustrates thermal shape-memory test. It consists of (1) heating the sample above transformation temperature (T_{trans}), corresponding to T_g or T_m, up to deformation temperature T_d, (2) deforming the sample into a new temporary shape, (3) cooling the sample below T_{trans} down to the setting temperature T_s while maintaining the deformation load; the temporary shape is quenched by vitrification or crystallization, (4) the deformation stress is released, (5) re-heating the sample above T_{trans} up to T_d. This step leads to a recovery to the initial permanent shape under nonconstrained conditions (5a) or to a stress recovery at constrained (5b), i.e. the sample is fixed at constant length. During the sample deformation, the elastic energy is generated. At cooling, this energy is stored in the quenched sample. During heating the sample above T_{trans}, the stored energy is recovered and manifested as a recovery stress.

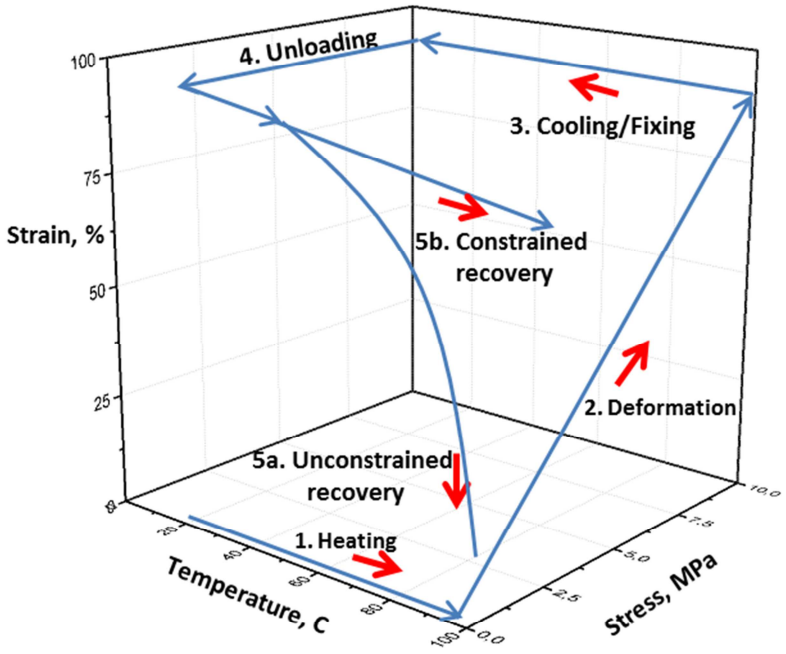

Fig. 7 Representative 3-D plot of thermal shape-memory test.

The SM properties are evaluated by the following parameters, such as shape fixity, shape recovery, rate of recovery and recovery stress σ_r, where shape fixity describes the ability of the net-points and switching segments to fix a mechanical deformation after cooling and unloading. Shape recovery evaluates the ability of the polymer to memorize its initial shape and the recovery stress σ_r is defined as a force that a SMP exhibits during a constrained recovery.[130]

For the possible application, the SMPs are compared with another shape memory material which is shape memory alloy (SMA). The benefits of SMPs with respect to SMA consist in their variability, easier processability, lower costs, light weight and larger deformability.[132] On the contrary, SMAs show higher mechanical strength and faster response to external stimuli. Particularly, a quite low mechanical strength and recovery stress in comparison to shape-memory alloys (SMAs) are the main problem restricting the applications of SMPs with respect to SMA.[132, 133] The mechanical strength is generally enhanced in chemically crosslinked SMPs compared to physical networks. On the other side, however, the physically crosslinked SMPs show a higher deformability which is an important benefit of SMP with respect to SMA.

Incorporating of reinforcing fillers is a common way for improving the mechanical performance and shape recovery stress of SMPs.[134-138] Three different groups of the filler

material can be found, such as nanoparticles (silica, metal, functionalized particles etc.), layered materials (e.g. layered silicate or graphite) and fibres (nanofibers, nanotubes etc.).[116]

In past 10 years a remarkable advances in stimuli-responsive SMPs with the potential applications in medical, aerospace, civil engineering, energy, and bionics areas, were achieved. Numerous possibilities of novel SMPs were described such as multi-SMP, photoactive SMP, and self-healing SMP.[139, 140]

In the fourth paper, the goal was to synthesize and to study the high performance epoxy-based SMP with the high recovery stress and a high deformability, while keeping an excellent shape fixity and recovery. Comprehensive study of the shape-memory nanocomposites properties and determination of relationships between structure and SM properties is discussed in this paper.

AIMS OF THE STUDY

This Thesis has two main objectives of the study:

A) Synthesis of organic-inorganic, epoxy-silica, nanocomposites with silica generated *in situ* by novel nonaqueous solvent-free sol-gel process.

In order to achieve this goal, several points were necessary to be analysed:

- understanding of the epoxy-silica hybrid/nanocomposite formation under non-hydrolytic conditions;
- improvement of silica dispersion in the epoxy matrix and system homogenization;
- improvement of thermo-mechanical and tensile properties.

This part focused on understanding the mechanism of the nonaqueous sol-gel process and a corresponding formation of epoxy-silica nanocomposites. It describes the effect of BF_3MEA complex, amine basicity, presence of the coupling agent, curing temperature, the influence of steric restrictions of the epoxy network affecting the silica structure growth, the evolution of the structure during polymerization, and function of ionic liquids (IL). The nanocomposite hierarchical structure and morphology, as well as the thermomechanical properties were studied in details. The determined relationships between formation, structure and properties of the epoxy-silica nanocomposites made it possible to optimize the synthesis and to control the nanocomposite structure and morphology in order to fit the desired goal.

B) Synthesis of potentially applicable thermo-responsive shape-memory polymers based on epoxy-silica nanocomposites.

In order to achieve this goal, the following points have been studied:

- general understanding of the SM phenomenon;
- relationships between polymer structure - thermomechanical properties - tensile properties - SM properties in order to obtain better SM properties (recovery stress, shape fixity, recoverable deformability etc.);
- design of a polymer structure for the synthesis of high performance SMP.

In order to obtain such a polymer, several parameters were necessary to tailor, such as keeping T_g <100 °C (for easier triggering of the shape recovery), increase storage modulus and tensile properties which is reflected in high recovery stress, high extent of deformation, good shape fixity etc.

The present Thesis consists of four published papers in international journals (Appendices 1 – 4) with an extended introduction and discussion of the content of the papers.

3. METHODS OF CHARACTERIZATION

Transmission electron microscopy (TEM)

TEM image is formed from the interaction of the electron beam which travels through the specimen. The electron microscope operates on the same basic principles as the light microscope; however TEM is capable of imaging at significantly higher resolutions due to the shorter wavelength of electrons (0.02-0.05nm). This measurement was chosen to study morphology assessments because of higher contrast between polymer phase and nanosilica domains. TEM measurements were performed with the microscope JEM 200CX (JEOL, Japan). TEM microphotographs were taken at the acceleration voltage of 100 kV, recorded on a photographic film, and digitized with a PC-controlled digital camera DXM1200 (Nikon, Japan). Ultrathin sections for TEM, approximately 50 nm thick, were cut with ultramicrotome Leica Ultracut UCT, equipped with cryo attachment.

Small-angle X-ray scattering (SAXS)

SAXS is a small-angle scattering technique where the elastic scattering of X-rays, with a wavelength 0.1-0.2 nm, is detected. It is recorded at very low angles (typically 0.1 - 2°). This range contains information about the shape and size of nanoparticles, their distribution, characteristic distances of partially ordered materials, pore sizes etc. The experiments were performed using a pinhole camera (Molecular Metrology SAXS System) attached to a microfocused X-ray beam generator (Osmic MicroMax 002) operating at 45 kV and 0.66 mA (30 W) The camera was equipped with a multiwire, gas-filled area detector with an active area diameter of 20 cm (Gabriel design). Two experimental setups were used to cover the q range of 0.004 - 1.1 A^{-1} where $q = (4\pi/\lambda)\sin\theta$ (λ is the wavelength and 2θ is the scattering angle). The scattering intensities were put on an absolute scale using a glassy carbon standard.

Nuclear magnetic resonance spectroscopy (NMR)

NMR is the type of technique that exploits the magnetic properties of certain atomic nuclei by determination the physical and chemical properties of atoms or molecules in which they are contained. This method relies on the phenomenon of nuclear magnetic resonance and can provide detailed information about the structure, dynamics, reaction state, and chemical environment of molecules. Solid-state ^{29}Si CP/MAS NMR experiments were measured at 11.7 T using a Bruker Avance 500 WB/US NMR spectrometer with double-resonance 4-mm and 7-mm probeheads, respectively. To compensate for frictional heating of the spinning samples, all NMR experiments were

measured under active cooling. The sample temperature was maintained at 308 K. The ^{29}Si CP/MAS NMR spectra were acquired at 99.325 MHz; spinning frequency was $\omega r/2\pi$ = 5 kHz; the number of scans was 2048; spin lock 4 ms and recycle delay was 3s. The spectra were referenced to *M8Q8* (-109.8 ppm). During detection, a high-power dipolar decoupling (TPPI) was used to eliminate strong heteronuclear dipolar coupling.

NMR was used for determination of conversion during the sol-gel process. The condensation conversion α_{Si} was determined as $\alpha_{Si} = \Sigma iQ_i/4$ for TEOS and $\alpha_{Si} = \Sigma iT_i/3$ for GTMS. Q_i and T_i are the mole fractions of the Q_i and T_i structure units with i siloxane bonds Si-O-Si attached to the central silicon. The relative amount of the structural units was obtained from the deconvolution of the ^{29}Si CP/MAS NMR spectra. The assignment of the NMR bands is as follows; Q_0 from -71.7 to -81.9 ppm, Q_1 from -81.5 to -89.3 ppm, Q_2 from -91.2 to -91.5 ppm, Q_3 from -101.2 to -101.6 ppm, Q_4 from -109.3 to -110.1 ppm, T_0 from -42.7 to -43.2 ppm, T_1 from -47.9 to -49.6 ppm, T_2 from -57.3 to -58.3 ppm, T_3 from -66.6 to -66.9 ppm.

^{11}B MAS NMR spectra were measured in 4-mm double resonance probehead at MAS frequency of 5 kHz. The spectra were calibrated using a secondary reference standard $NaBH_4$ (3.2 ppm).

Dynamic Mechanical Thermal Analysis (DMTA)

DMA is most useful for studying the viscoelastic behaviour and general characterization of polymers and composites. The sinusoidal strain is applied and the stress in the material is measured, allowing one to determine the complex modulus. The temperature of the sample or the frequency of the stress are often varied, leading to variations in the complex modulus; this approach can be used to locate the glass transition temperature of the material, as well as to identify transitions corresponding to other molecular motions. Dynamic mechanical properties of the nanocomposites were tested using the ARES G2 apparatus (TA Instruments). An oscillatory shear deformation at the constant frequency of 1 Hz and at the heating rate of 3 °C/min was applied.

ARES G2 rheometer was used also for the chemorheology experiments to follow molecular structure evolution and gelation during polymerization. Oscillatory shear deformation in parallel plates geometry at a frequency of 1 Hz was used. The initial applied maximum strain was 200 % and it was continuously reducing during the reaction in order to keep torque below 20 g*cm to prevent breaking of the formed gel.

Tensile test is one of fundamental test in which sample is subjected to a controlled tension until failure. Properties that are directly measured within a tensile test are tensile

strength, elongation at break and the stress-strain curve provides an information about toughness of the material. The experiments were performed at axial force with the constant linear speed of 0.06 mm/min at T_d = 100 °C. Five rectangular specimens with dimensions 25 x 5 x 1 mm were tested for each sample. The toughness was evaluated as an area under the stress-strain curve.

Shape memory test

Shape fixity R_f was measured in bending mode. The sample was heated and deformed to the angle θ_d = 90° at the T_d. Subsequently, the deformed sample was quickly cooled to the setting temperature and kept at T_S = 25 °C for 8 month. The change of the angle θ in time was recorded. Shape fixity was calculated as, $R_f = 1-[(\theta_f-\theta_d)/\theta_d]$ x100 %, where θ_f - the angle in the frozen state after 8 month.

Shape recovery rate was evaluated in the bending mode by following the angle change of the deformed specimen in time.

Recovery stress σ_r was measured on ARES G2 rheometer. The rectangular sample 25 x 5 x 1 mm was heated up to deformation temperature T_d and extended up to 60% of the previously determined strain at break (λ_b), $\lambda_d = 0.6\lambda_b$, at a rate of 0.06 mm/min. The sample was then cooled down to the setting temperature T_S while keeping the loaded force and kept for 10 minutes to completely freeze and store the stress within the sample. Only then the sample was unloaded. For the constrained recovery the sample was fixed, the length was kept constant and heated up to T_d. The recovery stress induced by heating was recorded.

Stress relaxation was measured using the ARES G2 apparatus (TA Instruments) by transient stress relaxation mode at a strain λ = 1.07 at T_d.

All characterization techniques have been used in cooperation with research teams of the Institute of Macromolecular Chemistry. Some of them are represented as co-authors of the published papers. These people are RNDr. Miroslav Šlouf, PhD. (TEM), Ing. Josef Pleštil CSc. and Mgr. Alexander Zhigunov Ph.D. (SAXS), Ing. Libor Kobera Ph.D. and Ing. Jiří Brus Dr. (NMR), RNDr. Jana Kovářová CSc. (TGA), Ing. Antonín Sikora, CSc. (DSC).

Their help and support is thankfully acknowledged.

4. RESULTS AND DISCUSSION

4.1. Epoxy-silica nanocomposite synthesized by nonaqueous sol-gel process

In the first two papers we were studying epoxy-silica nanocomposites prepared by the nonaqueous solventless sol-gel process. The main focus was dedicated to the analysis of the mechanism of the nonaqueous sol-gel process under action of BF_3MEA. Further evolution of the hybrid structure during polymerization, hybrids gelation, structure, morphology and thermomechanical properties were analysed as well.

In this chapter, the nanocomposites based on a glassy epoxy matrix filled with *in situ* generated nanosilica structures are described [**Appendices 1**]. Four types of the epoxy-amine networks were used as a matrix comprising the diepoxide DGEBA and the following diamine hardeners – aliphatic diaminobutane (DAB), cycloaliphatic Laromin (3,3'-dimethyl-4,4'-diaminocyclohexylmethane), aromatic diaminodiphenylmethane (DDM) and poly(oxypropylene)diamine Jeffamine D230. The networks differ in the rate of gel formation, crosslinking density, glass transition temperature T_g and compatibility with silica nanofiller. This system series thus makes it possible to study the structure-properties relationships. The nonaqueous sol-gel process, promoted by BF_3MEA complex, was applied to generate in the matrix the silica structures from TEOS and TMOS or silsesquioxanes (SSQO) from the coupling agent GTMS. The molecular structure of the coupling agent GTMS enables to function as an intermediary in bonding organic and inorganic materials, since it contains the functional groups reacting both with the organic, epoxy, phase and inorganic, silica phase.

Using the knowledge obtained from the first paper on nonaqueous solventless sol-gel process, the high-performance nanocomposites were synthesized and studied in the second paper. These materials have excellent thermomechanical properties such as indiscrete T_g or high storage modulus (335 MPa) up to 300 °C with only ~10 wt. % loading of *in situ* generated silica.

Third paper is focused on synthesis and characterization of the epoxy-silica nanocomposites by using the imidazolium based ionic liquids (IL) functionalized with carboxylic groups. The ILs enable to control morphology of the nanocomposites and the functional groups allow *in situ* covalent bonding of these ILs to the epoxy based materials and tune the filler-matrix interface interaction in order to improve thermomechanical and tensile properties. In this work we describe an easy and quick procedure to produce

imidazolium functionalized polymers which can open a broad range of possible new materials.

4.1.1. Nanocomposite network formation

The epoxy-amine networks were prepared at a stoichiometric ratio of functional groups (C_{epoxy}:C_{NH} = 1:1) and the epoxy-silica nanocomposites containing in situ build silica were synthesized by the two step synthesis procedure: (i) initiation of the nonaqueous sol-gel process by BF_3MEA complex and (ii) the simultaneous amine catalysed sol-gel polycondensation of TEOS (or TMOS) and the epoxy-amine network formation.

Mechanism of non-aqueous sol-gel process

We determined the mechanism of the non-aqueous sol-gel process initiated by BF_3MEA. By using NMR spectroscopy it was proved that TEOS is protolyzed by amine released from BF_3MEA complex. This step results in production of the Si-OH containing siloxanes [Fig. 8].

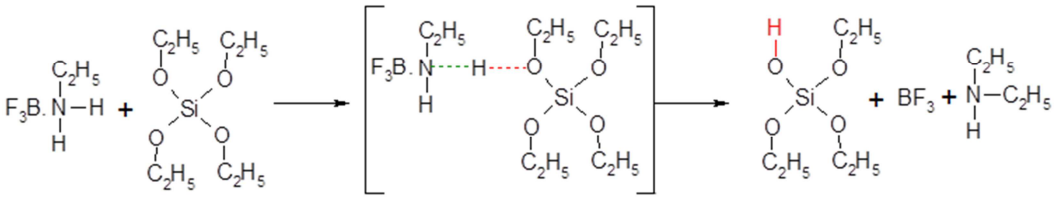

Fig. 8 Protolysis of TEOS under nonaqueous conditions by BF_3MEA complex.

Moreover, it was proved that initiation is more efficient in the presence of epoxy resin as a result of additional protolysis by C-OH of the epoxy resin. Because of small extent of „hydrolysis“ the further structure growth during the second polycondensation step proceeds by the monomer-cluster aggregation mechanism leading to compact structures with fractal dimensions $D_m \sim 3$.[74]

Nanocomposite structure evolution

Structure evolution at formation of the epoxy-silica nanocomposite under nonaqueous conditions was followed by chemorheology. Since the gelation of the two step acid-base aqueous sol-gel procedure is extremely fast, the important benefit of the nonaqueous sol-gel procedure consists in a slower reaction. Lower reaction rates enable a structure control and prevent phase separation.

The nanocomposites based on two epoxy-amine systems displaying the fast (DGEBA-DAB) and slow (DGEBA-D230) network formation were studied. Fig. 9 shows the growth of the shear storage modulus *G'(t)* during build-up of the nanocomposite

networks at constant temperature. The steep increase in modulus in the figure characterizes gelation of the system. The precise gelation time is listed in Tab. 2.

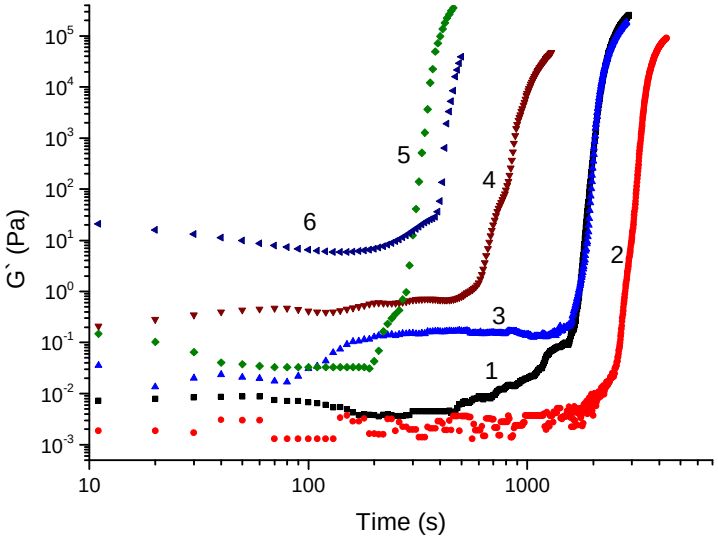

Fig. 9 Shear storage modulus *G'(t)* of the studied systems as a function of time during polymerization at *T* = 80 °C: 1 DGEBA-D230, 2 DGEBA-D230-TEOS, 3 DGEBA-D230-TEOS-BF_3MEA, 4 DGEBA-D230-TMOS-BF_3MEA, 5 DGEBA-DAB, 6 DGEBA-DAB-TEOS-BF_3MEA.

The simultaneous epoxy-amine network build-up and the silica/SSQO structures growth start with addition of a diamine to the mixture. In the epoxy network DGEBA-D230 the gelation is delayed in the presence of silica precursor TEOS due to a corresponding dilution effect (Fig.9 curves 1 and 2). However, addition of the BF_3MEA complex in the DGEBA-D230-TEOS mixture accelerates the gelation of the hybrid and eliminates the dilution effect of TEOS. Furthermore, the figure displays the modulus increase in the pregel stage in the hybrids involving BF_3MEA complex (Fig.9 curve 3). This increase in modulus is due to the fast formation of oligosiloxane/silica nanostructures by the polycondensation catalysed with the added amine. Moreover, according to the proposed mechanism of protolysis by BF_3MEA, initiation of TMOS hydrolysis should proceed faster and easier than protolysis of TEOS due to smaller steric substituent [**Appendices 1, 2**]. This is resulting in the faster sol-gel process and higher pregel stage modulus. The gelation time of TMOS containing hybrids is decreased more than 2 times with respect to hybrids with TEOS (Fig.9 curves 4 and 3).

Table 2. Gelation times of the selected epoxy systems and nanocomposites.

System	Gelation time, min
DGEBA-D230	34
DGEBA-D230-TEOS	52
DGEBA-D230-TEOS-BF_3MEA	33
DGEBA-D230-TMOS-BF_3MEA	15
DGEBA-DAB	5.5
DGEBA-DAB-TEOS-BF_3MEA	6.5

Very strong effect of basicity can be observed in case of substitution D230 by more basic DAB. Both epoxy network formation and silica generation are affected. The DGEBA-DAB gelation is faster than that of DGEBA-D230 (Fig.9 curves 5 and 1). Moreover, the storage modulus rises quickly in less than 2 min in the early pregel stage within DGEBA-DAB mixture (Fig.9 curve 6). The more basic DAB compared to D230 promotes the faster polycondensation and formation of silica aggregates resulting in a higher pregel stage modulus.

4.1.2. Structure and morphology

A homogeneous nanofiller dispersion in a matrix and a strong interphase interaction are well known to be basic factors determining nanocomposite properties. Incorporation of nanosilica in the glassy epoxy matrix DGEBA-Laromin by the classical aqueous sol-gel procedure results in the heterogeneous opaque sample, as shown in Fig.10a, due to the fast polymerization induced phase separation. The nonaqueous sol-gel procedure initiated by BF_3MEA enables preparation of the homogeneous transparent nanocomposites containing up to 40 wt. % TEOS or 80 wt. % of TMOS, corresponding to 12 and 32 wt. % of silica, respectively (Fig.10.b,c). Moreover, no bubbles or cracks in the final product were detected.

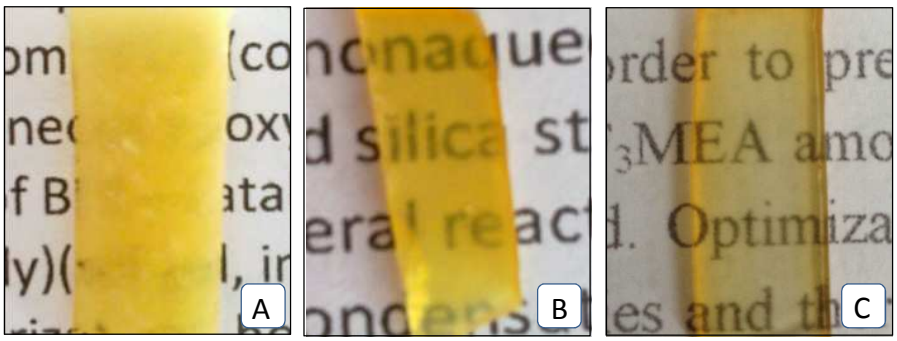

Fig. 10 Epoxy-silica nanocomposite prepared by: (a) aqueous sol-gel process, nonaqueous sol-gel promoted by BF_3MEA from TEOS (b) and from TMOS (c).

An insight into the silica structures on the supramolecular level was obtained from TEM images of nanocomposites without BF_3MEA, with TEOS-BF_3MEA and GTMS-BF_3MEA. TEM micrographs of the epoxy-silica nanocomposites are shown in Fig.11. The aggregates of the size ~300 nm are present in the nanocomposites in case of the synthesis without BF_3MEA (Fig.11). Application of the complex leads to a finer morphology. The results disclose silica aggregates of the size ~70 nm dispersed in the epoxy matrix and composed of primary particles of ~10 nm in diameter (Fig.11b). After the application of the coupling agent GTMS, the corresponding silica/SSQO structures are smaller and better dispersed (Fig.11c).

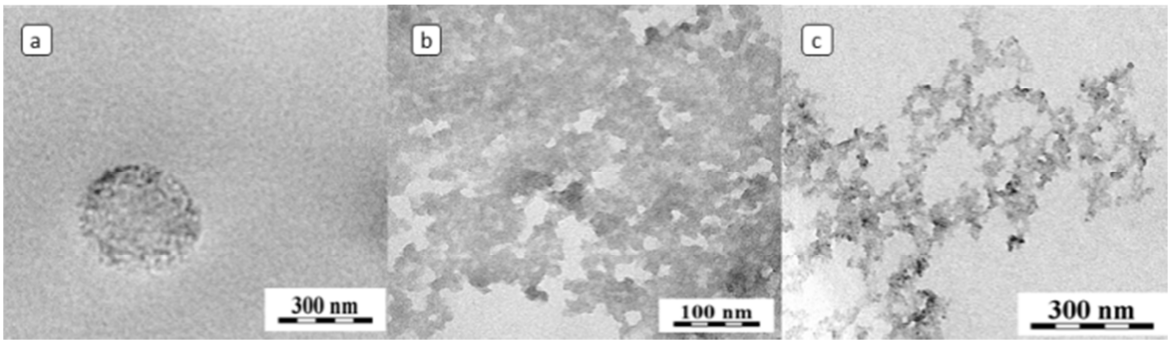

Fig. 11 TEM micrograph of the nanocomposites (a) DGEBA-D230-TEOS (18%), (b) DGEBA-D230-TEOS(18)-BF_3MEA, (c) DGEBA-D230-GTMS-BF_3MEA.

The phase structure was evaluated also by the SAXS analysis since this method gives a geometrical description of the structures from the point of view of fractal dimensions.[57] The mass and surface fractal dimensions, D_m and D_S, determined from the slope β of the log-log profile, measure the compactness of the fractal objects and roughness of their surface, respectively. The high mass fractal dimension, D_m = 2.9, in the case of the nanocomposite DGEBA-D230-TEOS prepared without BF_3MEA and values of surface fractal dimensions *Ds* ~ 2 (*Ds* = 6 - β) in Laromin and DDM containing nanocomposites, disclose compact structures of the aggregates and even smooth surface, respectively [**Appendices** 1]. The synthesis of nanocomposites in presence of the BF_3MEA complex leads to the less compact structure aggregates with the corresponding lower mass fractal dimensions D_m = 2.3 - 2.8. (Fig.12). Moreover, the more open silica aggregates are formed in the case of DGEBA-D230-TEOS compared to Laromin and DDM based networks, due to interaction of the siloxane structures with the polyether chain of D230 in the epoxy network. The knee on the SAXS profile at q = 0.1 A^{-1}

originates from the small particles of a diameter size *D* = 1.9 nm within the silica aggregates (Fig.12 curve 3).

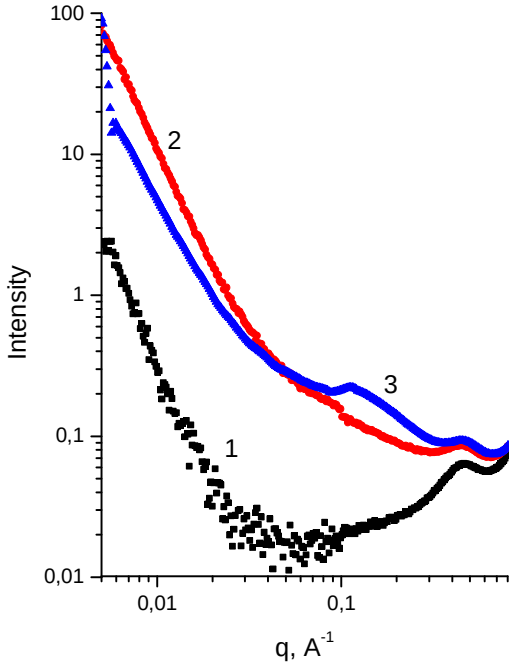

Fig.12 SAXS profile of the epoxy-silica nanocomposites: 1 DGEBA-D230, 2 DGEBA-D230-TEOS, 3 DGEBA-D230-TEOS-BF_3MEA.

The important benefit of the non-aqueous sol-gel procedure consists in a slower reaction. This advantage enables better structure control and prevents phase separation. Acquired knowledge from the studied sol-gel process allows us to propose the course of the hybrid formation. This evolution under both aqueous and non-aqueous conditions is schematically illustrated in Scheme 1 describing also the resulting morphology.

If we apply aqueous two-step, acid-base, sol-gel procedure, the silica gel formation will be extremely fast in the DGEBA-Laromin-TEOS mixture. The heterogeneous milky bulk gel is formed within ~10 sec. The silica network is built much faster than the epoxy-amine (Scheme 1Aa) and the reaction induced separation of organic and inorganic phases takes place (Scheme 1Ab). This results in the opaque final material. Only strong interfacial interactions can prevent a phase separation and the transparent interpenetrating network with the bicontinuous phase structure can be formed (Scheme 1Ac).[83, 141]

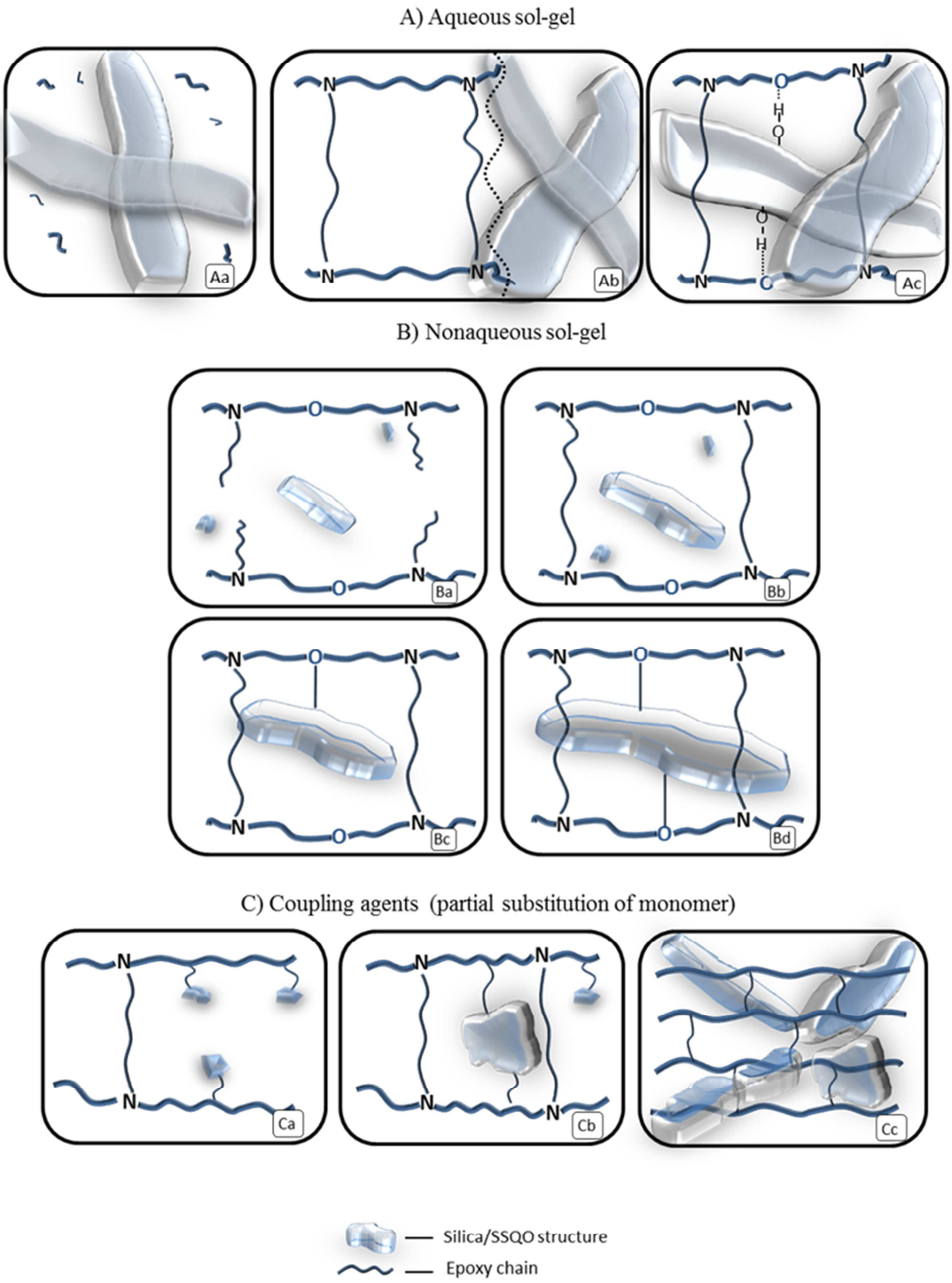

Scheme 1. Schematic description of the formation of the epoxy-silica hybrid/nanocomposite with *in situ* formed silica/SSQO. (The scheme does not correspond to real proportions; the silica structures are bigger compared to the network mesh).

Scheme 1B shows the formation of epoxy-silica nanocomposites under nonaqueous conditions but with the presence of BF_3MEA. In contrast to the aqueous sol-gel process, the silica gel build-up is slower than the epoxy network formation in this case. Under the

non-hydrolytic conditions, no bulk silica gel but only small nanostructures are formed. The difference is given by the small content of Si-OH groups in the siloxanes preformed in the initiating step. This fact leads to a much smaller extent of polycondensation, which is not sufficient for a silica gel formation. Therefore, the hybrid gelation sets in by formation of the epoxy network (Scheme 1Bb). The silica structures further grow and moreover a covalent bonding to the epoxy matrix is produced (Scheme 1Bc). The interface grafting leads to the system compatibilization and precludes the phase separation. Crosslinking of the epoxy chains by silica domains then follows as in Scheme 1Bd. Such a crosslinking can be responsible for the observed acceleration of the hybrid gelation by BF_3MEA.

With coupling agent addition, a fast incorporation in epoxy-amine network can be observed on Scheme 1Ca by the reaction of glycidyl group of GTMS with an amine crosslinker. The sol-gel reactions and formation of the SSQO domains occurs only in the presence of BF_3MEA (Scheme 1Ca,b).[142] The epoxy network is formed in Scheme 1Cb and bridging the epoxy chains by the SSQO junctions contributes to the crosslinking.[143,144] Finally this hybrid displays percolation of the inorganic SSQO network to form co-continuous epoxy-SSQO phase morphology as in Scheme 1Cc.

4.1.3. Thermomechanical properties

Thermomechanical properties are characterized by the glass transition temperature T_g, determined from the maximum of the tan δ curve, and by the shear modulus in rubbery state G_r. The reinforcing of epoxy networks is manifested by reduced mobility of the organic network chains. This is exhibited by a shift of T_g to higher values and drop of the loss factor tan δ amplitudes due to lower fraction of the free relaxing polymer chains.[75, 78, 145]

In order to obtain the best thermomechanical properties applying nonaqueous sol-gel process, several parameters were modified, such as content of BF_3MEA, postcuring temperature, type and amount of silica precursors, and content of coupling agent. Moreover different methylimidazolium based ionic liquid were applied [**Appendices 3, 4**] in order to improve morphological homogeneity of the studied nanocomposites.

All the studied nanocomposites show an increase in rubbery modulus with respect to the corresponding neat epoxy networks, however, both increase and decrease of T_g was found (Fig.13).

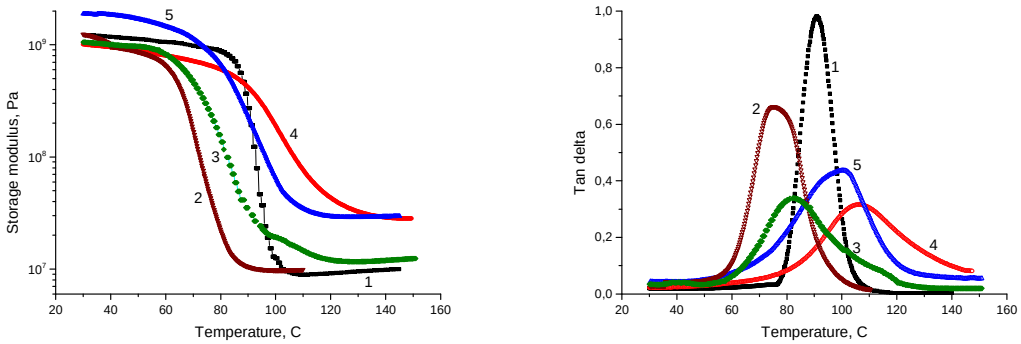

Fig. 13 Storage modulus (a) and loss factor tan δ (b) as functions of temperature of the DGEBA-D230 based nanocomposites prepared from different alkoxysilanes: 1 DGEBA-D230, 2 DGEBA-D230-TEOS-(aqueous), 3 DGEBA-D230-TEOS-BF_3MEA, 4 DGEBA-D230-TMOS-BF_3MEA, 5 DGEBA-D230-TEOS-BF_3MEA-IL.

Although TMOS undergoes much faster sol-gel reactions than TEOS, the structure evolution is under control and well homogeneous nanocomposites are produced. The condensation conversion of TMOS α_{Si} in the nanocomposites prepared under nonaqueous conditions is much higher than those of TEOS under the same conditions [**Appendices 2].** The conversion in the system DGEBA-D230-TEOS even with the BF_3MEA addition is quite low, α_{Si} = 0.46, resulting in the plasticization of the nanocomposites and reduction of T_g with respect to the neat network (Fig.13, curves 3 and 1). In contrast to TEOS, the TMOS containing networks exhibit higher conversion α_{Si} = 0.72 due to smaller steric substituent. Thus significant enhancement of both T_g and rubbery modulus was achieved by application of TMOS (Fig.13, curve 4).

The coupling agent GTMS was used in order to achieve a significant improvement of the thermomechanical properties due to strong interphase interaction and enhanced homogeneity. The content of GTMS was calculated as fraction of epoxy groups of DGEBA replaced by the coupling agent: x = [epoxy (GTMS)] / [epoxy (DGEBA) + epoxy (GTMS)] while keeping the total epoxy groups concentration constant. The SSQO domains formed by the sol-gel reactions of GTMS are covalently grafted to epoxy network chains and it is reflected by T_g enhancement due to the limited chain mobility and topological hindrance. At the certain GTMS fraction the glass transition even becomes indistinct in the case of DGEBA-Laromin based networks (Fig.14 curve 3). These hybrids display percolation of the inorganic SSQO network and formation of co-continuous epoxy-SSQO phase morphology as shown in Scheme 1Cc.

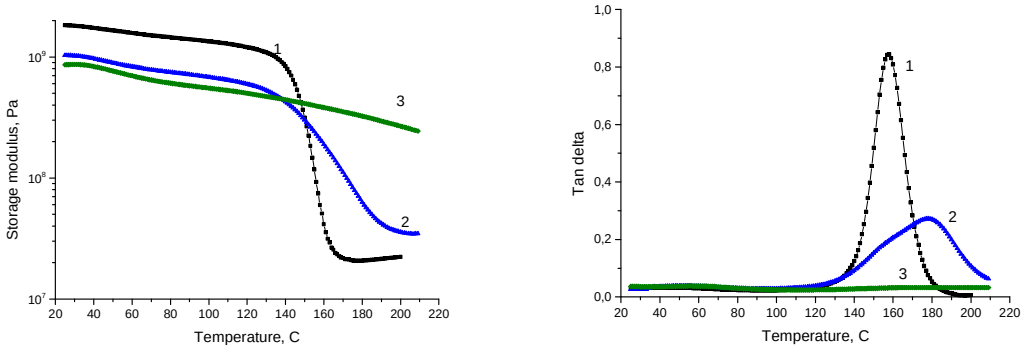

Fig. 14 Storage modulus (a) and loss factor tan δ (b) as functions of temperature of the DGEBA-Laromin with different content of coupling agent: 1 DGEBA-Laromin, 2 DGEBA-Laromin-GTMS(x=0.1)-BF_3MEA, 3 DGEBA-Laromin-GTMS(x=0.3)-BF_3MEA, where GTMS (x =0.1 and 0.3) corresponds to 2.2 and 6.6 wt. % of equivalent silica, respectively.

Finally, based on the obtained results, we have prepared the high-performance hybrids which maintain the mechanical properties up to 300 °C [**Appendices 2**]. We took advantage of the synergy combination of two alkoxysilane TMOS and GTMS. Fig.15 illustrates a dramatic increase of rubbery modulus in the high-temperature region and thermal stability of the nanocomposites with respect to the neat network DGEBA-Laromin. The nanocompsoites containing a low amount of the *in situ* generated silica (~ 10 wt. %) and a small amount of the coupling agent GTMS shows indistinct T_g and the high rubbery modulus (335 MPa) up to 300 °C (curve 4**)**. Probably a percolation of the inorganic structures through the epoxy network takes place and the bicontinous epoxy-silica/SSQO hybrid was formed.

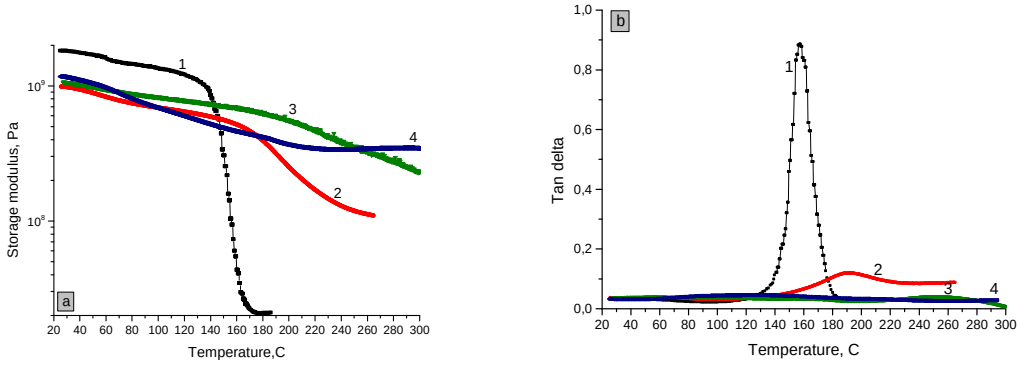

Fig. 15 Storage modulus (a) and loss factor tan δ (b) as functions of temperature of the DGEBA-Laromin based hybrids containing TMOS and GTMS: 1 DGEBA-Laromin, 2 DGEBA-Laromin-TMOS(14)-BF_3MEA, 3 DGEBA-Laromin-GTMS(x = 0.3)-

BF_3MEA, 4 DGEBA-Laromin-TMOS(14)-GTMS(x = 0.3)-BF_3MEA, where 14 % of TMOS corresponds to 5.4 wt. % of equivalent silica.

Another promising strategy for nanocomposite structure and morphology control and enhancement of mechanical properties, is the application of methylimidazolium based ionic liquids **[Appendices 3, 4]**. In the third paper, ILs functionalized with carboxylic groups were studied. These carboxyl groups of the ILs were proved to react with the epoxy groups and create covalent bonds with the epoxy network. The covalently bound ILs are more efficient in control the epoxy-silica interphase in nanocomposites. Homogenization of the nanocomposite system and improved dispersion of the silica nanodomains in the epoxy matrix were achieved. The strengthened epoxy-silica interphase by ILs resulted in significant stiffening and toughening of the system. The DMA shows low T_g in free-IL-nanocomposite (Fig.13 curve 3) with respect to the neat epoxy matrix (Fig.13, curve 1). On the contrary, the increase in both T_g and modulus is achieved in the nanocomposites prepared in the presence of ILs. (Fig.13 curve 5). The IL catalyses the sol-gel process thereby leading to more completely reacted hard silica domains. Moreover, the glassy nanocomposites exhibit a significant enhancement of toughness by more than 100 % [**Appendices 3]**.

Fig. 13 shows also the effect of the sol-gel procedure and enhancement of thermomechanical properties in nanocomposites prepared by the non-aqueous compared to the classical sol-gel process. As it was discussed before, the lack of an interphase interaction, phase separation and increase in free volume by large silica aggregates due to fast gelation are the main reasons of the T_g reduction in case of aqueous sol-gel process (curve 2) with respect to the non-aqueous procedure (curve 3).

The acquired knowledge of epoxy-silica nanocomposites was used for the design and synthesis of epoxy-based shape-memory nanocomposites.

4.2. Thermo-responsive shape-memory nanocomposites

The aim of the fourth paper consists in the synthesis of high performance SMPs showing improved mechanical properties while keeping the perfect shape fixity and recovery. Particularly, the investigation is focused on enhancement of recovery stress and recoverable deformability of SMPs. The potential SM application of these systems is considered in the temperature region T = 25 - 100 °C with the setting temperature T_s = 25°C, transition temperature $T_{trans} = T_g$ and deformation temperature T_d = 100 °C.

From the literature it is known that an increase of rubbery modulus of SMPs is leading to an increase of recovery stress. Furthermore, the theory of rubber elasticity predicts the stress generated in a deformed polymer as

$$\sigma_{rub} = G_r(\lambda_d - \lambda_d^{-2}), \qquad (5)$$

where G_r and σ_{rub} are modulus at rubbery state and stress under deformation at rubbery state, $\lambda = l/l_0$ is the deformation ratio, l and l_0 are the deformed and initial length of the sample, respectively. The recovery stress σ_r presents the elastic energy stored in the sample during the cooling step and one can expect $\sigma_r \sim \sigma_{rub}$, where σ_r is the recovery stress in the fixed-strained material.

Therefore, the study is focused on design of structure of the SMP which makes it possible to control the thermomechanical properties, i.e. rubbery modulus and T_g due to application window (T_g = 25 - 100 °C), as well as tensile properties in order to reach a high deformability λ. Thereby, one can optimize the SM behavior including recovery stress. Moreover, determination of relationships between the nanocomposite structure, thermomechanical and tensile properties and their impact on SM properties can provide better understanding of the SM behaviour.

We have studied the nanocomposite systems based on epoxy networks reinforced with silica nanofiller *in situ* generated by sol-gel process from TMOS. In addition, ILs were used to modify the nanocomposite morphology. Several parameters were taken into account for the designing the epoxy matrix such as, crosslinking density of the network, flexibility of network's chains and possible physical crosslinking. As to the nanofiller, the parameters like content of silica, interphase interaction and quality of the filler dispersion in the polymer matrix, were considered. Moreover, the SM procedure optimization was performed in order to fully investigate a potential of SMP materials.

Synthesis of bimodal networks, involving bimodal distribution of crosslinking density, with silica build *in situ* was selected as another approach of the high performance SMP achievement. Combination of curing agents with different length and flexibility of the chains makes it possible to obtain high network extensibility and thus highly deformable SMP with required T_g.

Fig.16 illustrates the temperature induced SM effect of the epoxy-silica nanocomposite with outstanding recovery.

Fig. 16 SM effect of the epoxy-silica nanocomposite: a) original shape, b) heated, bended and cooled sample, c) reheating up to T_d - 10s, 20s, 30s.

4.2.1 Design of structure

In order to optimize the SM behaviour, the design of the nanocomposites structure and precise tuning of properties is essential. The epoxy-silica nanocomposites were designed as promising high performance SMPs with the applicable T_g in the temperature range of $T_{room} < T_g < 100$ °C. Along with tuning of T_g, the design of a polymer with a high rubbery modulus allowing a high deformation at rubbery state is a way to synthesis of a high performance SMP.

Rubbery modulus of polymer network depends mainly on the crosslinking density ν:

$$G_e = \nu RTA + \text{physical contribution}, \qquad (6)$$

where G_e is equilibrium shear modulus at rubbery state, A is front factor ($A = 1$ for affine networks, $A = (f - 2)/f$ for phantom networks, f is functionality of a crosslinker).

We were investigating the epoxy-amine networks of various crosslinking densities and stiffness of the curing agents. The following networks were prepared by using four types of amine curing agents with different molecular weights M: Jeffamines D230 ($M=230$) and D400 ($M=400$), Laromin ($M=238$) and ATBN ($M=3600$) (Fig. 17). The crosslinking density is inversely proportional to the molecular weight of the chain between net-points which can be regulated by a structure of amines:

$$\nu \sim 1/M_C \qquad (7)$$

where M_C is molecular weight of the elastically active chain between crosslinks.

The increase of crosslinking density or chains stiffness of the crosslinked network, however, leads to growth of both rubbery modulus and Tg. Due to that fact, there are particular limits of network density increase in order to keep T_g in the applicable temperature range. Fig.17 shows that only the epoxy matrices DGEBA-D230 and DGEBA-D400 (showing T_g at 90 °C and 51 °C, respectively) are fitting in the SM application window.

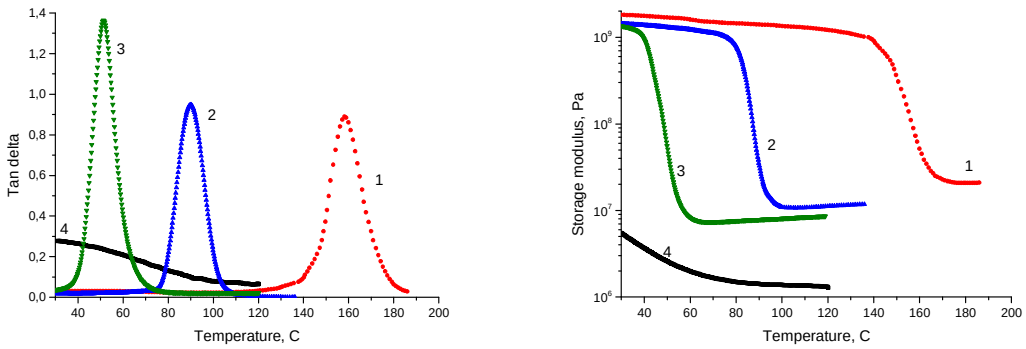

Fig.17 Storage modulus (a) and loss factor tan δ (b) of epoxy networks as functions of temperature: 1 DGEBA-Laromin, 2 DGEBA-D230, 3 DGEBA-D400, 4 DGEBA-ATBN.

The fundamental physical contribution to the modulus in Eq.6 in case of the studied nanocomposites is effected mainly by presence of nanofiller. From the previous study it was found that the most pronounced reinforcement of the epoxy networks was achieved by incorporation of silica nanofiller by nonaqueous sol-gel process and by application of ILs [**Appendices 1 - 3**].

The effect of silica content and presence of ILs on thermomechanical properties of the nanocomposites DGEBA-D400-TMOS is illustrated in Fig. 18. The T_g of the nanocomposites containing 25% of TMOS raised by 15 °C and the rubbery modulus is three times higher compared to matrix. Due to an increase of T_g the application of silica reinforcement is limited to the DGEBA-D400 matrix only. As a result of T_g growth, the DGEBA-D230 based nanocomposite does not fit in the application temperature window. Moreover, broadening of the transition peak with increasing content of silica in the nanocomposite further increases temperature of the recovery triggering.

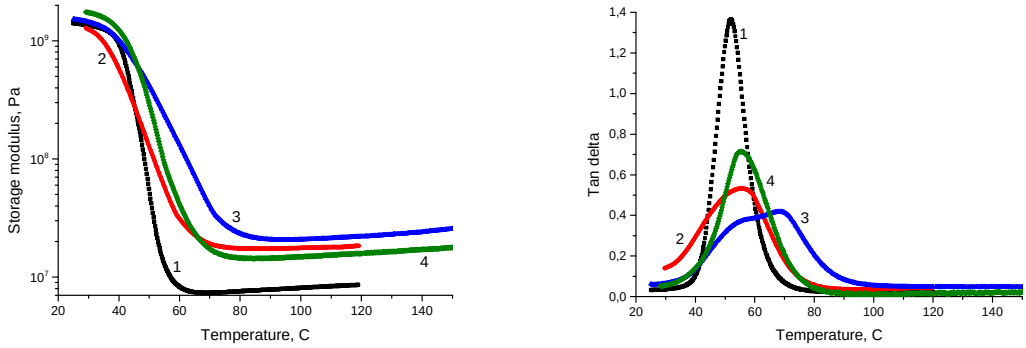

Fig. 18 Storage modulus (a) and loss factor tan δ (b) of the DGEBA-D400 based nanocomposites as functions of temperature: 1 DGEBA-D400, 2 DGEBA-D400-

TMOS(14), 3 DGEBA-D400-TMOS(25), 4 DGEBA-D400-TMOS(14)-IL. Constant content of BF_3MEA.

Application of ILs provides an interphase interaction control and improvement of morphological homogeneity as well as mechanical properties of epoxy-silica nanocomposites [**Appendices 3].** Fig.18 (curve 4) shows a narrowing of glass transition of the nanocomposite supported by the methylimidazolium based ILs which is beneficial for SM properties. The optimized thermomechanical properties were achieved by application of 14 - 25 wt. % of TMOS and with addition of ILs.

In addition to thermomechanical properties also the tensile behaviour of the epoxy-silica nanocomposite at deformation temperature T_d = 100 °C in rubbery state is crucial for SM phenomenon.

The tensile test results of DGEBA-D400 based network and the corresponding nanocomposites with and without ILs are shown in Fig.19. The DGEBA-D400 and DGEBA-D230 based epoxy networks are known to belong among the toughest epoxy thermosets. The reference network DGEBA-D400 shows strain elongation at break and stress at break as 20 % and 2.3 MPa at T_d respectively (Fig.19 curve 1). Dramatic improvement of tensile properties with the addition of *in situ* build silica by nonaqueous sol-gel process was succeeded. Stress at break grows up to σ_b = 4.5 MPa with the addition of 14 wt. % of TMOS showing at the same time only a slight reduction of deformability. Even more pronounced improvement in both extensibility and tensile strength, thus toughness, was achieved with the addition of IL (Fig.19 curve 3). The material toughness is characterized by area under the stress-strain curve and it corresponds to the energy absorbed by a material before break.

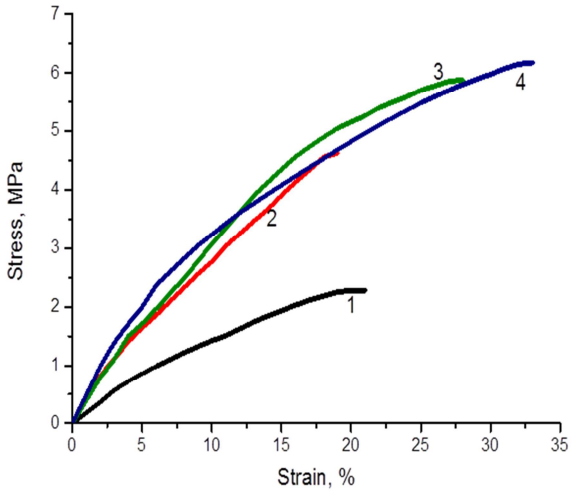

Fig. 19 Stress–strain behaviour of the SM network and nanocomposites at T_d: 1 DGEBA-D400, 2 DGEBA-D400-TMOS(14), 3 DGEBA-D400-TMOS(14)-IL, 4 DGEBA-D400-TMOS(25)-IL.

After evaluation of the obtained results, we found that the polymer toughness is a key materials property controlling SM performance as discussed below. The relationship between toughness and recovery stress was intensely studied in the fourth paper **[Appendices 4]**. Finally, highly extensible tough nanocomposites were synthesized in order to reach excellent SM performance, as follows.

It is known, that strain at break λ_b of a polymer network is related to the crosslinking density, i.e. molecular weight between crosslinks, as $\lambda_b \sim M_c^{1/2}$ and the polymer deformability thus could be increased only at the expense of modulus, as $G \sim 1/M_c$.

The network prepared using high-molecular weight amine-terminated butadiene-acrylonitrile crosslinker (ATBN with M = 3600) shows a high elongation at break ε_b = 280% at deformation temperature T_d (Fig.21 curve 2). However, the DGEBA-ATBN copolymer is rubbery at room temperature, and thus the combination with high-T_g hardener, is necessary (Fig.17). We used Laromin, and the obtained copolymer network of the molar composition, DGEBA-ATBN(n=0.3)-Laromin(n=0.7), exhibits good extensibility ~100% (Fig.21 curve 3), and T_g is shifted into the application window (Fig.20 curve 2). The tan δ curve discloses presence of two phases at the low temperature due to phase separation. Including of ethylene diamine (EDA) as a compatibilizer in the formulation removes a shoulder presented in tan δ peak and leads to a more homogeneous

epoxy network with bimodal distribution of crosslinking density due to application of long and short amines. Additionally, this modification leads to a slight decrease and narrowing of T_g as well as to improvement of rubbery and glassy moduli.

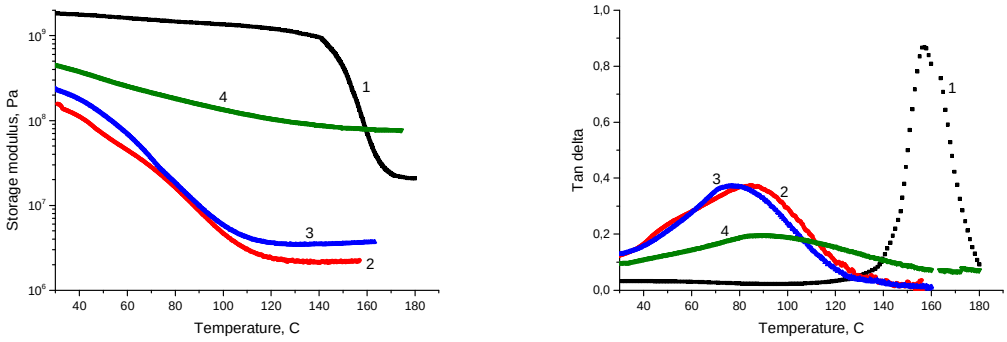

Fig. 20 Storage modulus (a) and loss factor tan δ (b) of the bimodal systems: 1 DGEBA-Laromin, 2 DGEBA-ATBN(0.3)-Laromin(0.7), 3 DGEBA-EDA(0.2)-ATBN(0.3)-Laromin(0.5), 4 DGEBA-ATBN(0.3)-EDA(0.2)-Laromin(0.5)-TMOS(14).

Significant improvement of mechanical properties of the bimodal network was succeeded by the addition of *in situ* build silica. Nanocomposite with 14 wt. % of TMOS shows an increase of rubbery modulus and glassy modulus by more than 10 times and 2 times respectively, while keeping quite high extensibility for the chemically crosslinked thermosets, ε_b = 47% (Fig.21 curve 4).

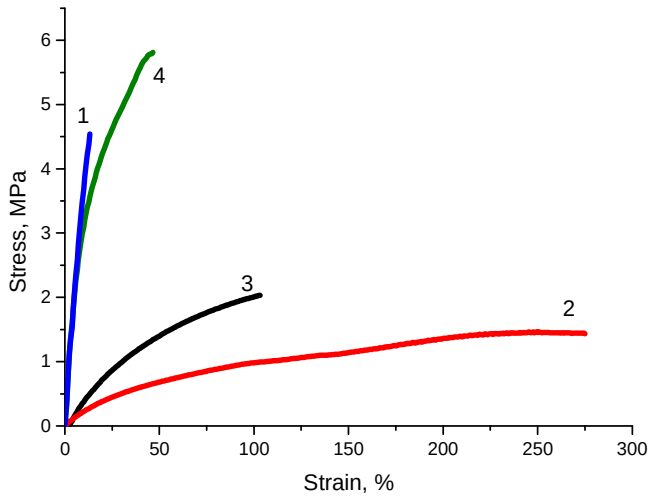

Fig. 21 Stress – strain behaviour of the of the SM nanocomposites at T_d: 1 DGEBA-Laromin, 2 DGEBA-ATBN, 3 DGEBA-ATBN(0.3)-Laromin(0.7), 4 DGEBA-ATBN(0.3)-EDA(0.2)-Laromin(0.5)-TMOS(14).

The following parameters have to be taken into account, in order to obtain a very tough epoxy-based material: (i) increasing of molecular weight of crosslinker, (ii) assimilation of silica nanofiller through *in situ* approach, (iii) application of ILs in synthesis procedure and (iv) formation of nanocomposites based on bimodal networks.

4.2.2 Shape-memory properties of the nanocomposites

To study shape-memory properties, the following SM characteristics were evaluated: shape fixity, shape recovery, rate of recovery and recovery stress. SMPs undergo a shape recovery triggered by heating above the transition temperature up to T_d (unconstrained recovery). In the case of the fixed strain (constrained recovery) the material shows a recovery of the stress.

Fig.22 demonstrates the unambiguous dependence of the experimentally determined recovery stress σ_r of the studied systems on their toughness. The toughest nanocomposites based on bimodal networks and prepared with application of IL shows the highest recovery stress. The obtained experimental results of the thermomechanical, tensile and shape memory properties and the corresponding relationships reveal that the prediction $\sigma_r \sim G_r$ does not match very well. In contrast to the literature data, it was found that the crucial SM parameter, recovery stress, depends on the material toughness rather than on the rubbery modulus [**Appendices 4**].

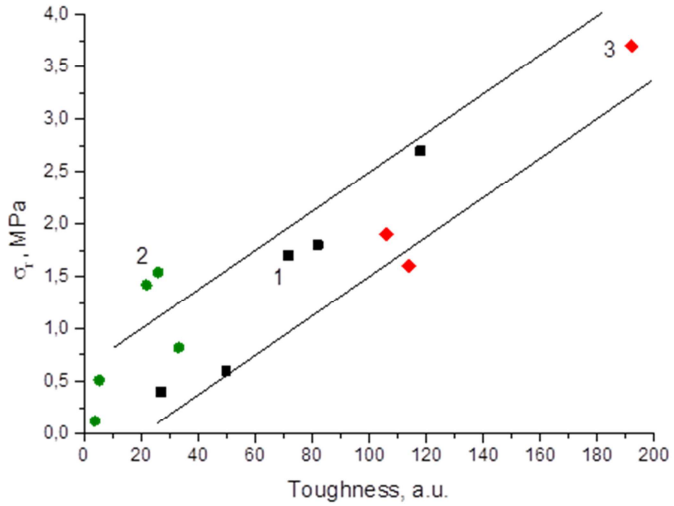

Fig. 22 The recovery stress in SMPs as a function of their toughness for: 1 – DGEBA-D400 and 2 – DGEBA-D230 based systems, 3 – DGEBA-Laromin-ATBN based copolymers.

Moreover, it was proved that SM behavior is governed by viscoelastic properties and materials morphology. Viscoelasticity effect was studied to relate the relaxation phenomenon to the shape memory performance of the material. The polymer relaxation and viscoelasticity effect result in loss of the elastic energy stored in the quenched sample. By controlling the viscoelasticity effect it is possible to increase SM properties of the studied systems. Our results unveil that ILs promoting a fine morphology reduce the viscoelasticity effect and enhance efficiency of the SM performance. So minimizing the stress relaxation is another possibility how to increase the SM efficiency and to reduce the loss of the stored energy.

Majority of the studied systems show the perfect shape fixity R_f = 100 % after 8 months, depending on the glassy modulus at $T_s = T_{room}$. Only, in the case of bimodal network showing a low modulus at setting temperature G_s < 500 MPa (Fig.20) the reduced shape fixity is observed, R_f = 86 - 95 %.

The shape recovery corresponds to typical epoxy systems exhibiting excellent recovery as discussed in details in the **Appendices 4**. Recovery rate was measured in the bending mode as a function of angle change of the deformed specimen in time. All the nanocomposites indicate the complete shape recovery in 15 to 30 s depending on silica content. An increase of recovery time was observed in the silica containing nanocomposites due to lower homogeneity of nanocomposites.

Additionally to the structure design, the SM experimental procedure, including rate and extent of deformation, rate of cooling, was optimized in order to improve SM properties. Rate of cooling the polymer temporary deformed shape is an important parameter for the recovery stress. It was found that fast cooling can decrease stress relaxation and thus to increase SM efficiency and recovery stress.

Finally after procedure optimization, the toughest nanocomposites based on bimodal networks showed the highest value of recovery stress and extensibility σ_r = 3.9 MPa and ε_b = 47 % respectively.

5. CONCLUSIONS

- The mechanism of nonaqueous sol-gel process under application of BF_3MEA complex as initiator was determined.
- Phase and molecular structure evolution during formation of epoxy-silica nanocomposites under nonaqueous conditions was determined and the conditions for the controlled structure development were optimized.
- The relationships formation – structure – thermomechanical properties of epoxy-silica nanocomposites prepared by nonaqueous sol-gel process were clarified.
- The high-T_g, heat resistant and transparent epoxy-silica hybrids have been prepared by the nonaqueous sol-gel technique.
- Application of ionic liquids in synthesis of nanocomposites allowed tuning the interface interactions of nanocomposites by producing a sequence of physical or chemical interactions.
- Enhancement of toughness of glassy epoxy systems by more than 100% was achieved by application of IL.
- Strategy of achieving SMP nanocomposites with both tailored thermomechanical and tensile properties enabling high recovery stress was proposed.
- The high-performance SMPs displaying the high recovery stress and high recoverable deformation were prepared.
- Recovery stress was determined to depend on the material toughness rather than on the rubbery modulus as given in literature.

LIST OF PUBLICATIONS

Impacted publications:

1. S. Ponyrko, L. Kobera, J. Brus, L. Matějka "Epoxy-silica hybrids by nonaqueous sol-gel process" *Polymer* **2013**, 54, 23, 6271.

2. S. Ponyrko, J. Kovářová, L. Kobera, L. Matějka "High-T_g, heat resistant epoxy-silica hybrids with a low content of silica generated by nonaqueous sol-gel process" *J. Appl. Polym. Sci.* **2014**, 131, 40899.

3. S.N. Jaisankar, N. Haridharan, A. Murali, S. Ponyrko, M. Špírková, A.B. Mandal, L. Matějka "Single-electron transfer living radical copolymerization of SWCNT-g-PMMA *via* graft from approach" *Polymer* **2014**, 55,13, 2959.

4. R.K. Donato, M. Perchacz, S. Ponyrko, K.Z. Donato, H.S. Schrekker, H. Benes, L. Matějka "Epoxy-silica nanocomposite interphase control using task-specific ionic liquids via hydrolytic and non-hydrolytic sol-gel processes" *RSC Adv.* **2015**, 5, 91330.

5. S. Ponyrko, R.K. Donato, L. Matějka "High performance shape memory epoxy-silica nanocomposites. Structure design" *Polym. Chem.* **2016**, DOI: 10.1039/c5py01450f

Patents:

1. V. Mentlík, P. Trnka, L. Matějka, S. Ponyrko, K. Vodseďálková, J. Erben "Electro-insulating composite material and methods of its preparation", PV **2015**-899.

Not impacted publications (books of abstracts):

1. S. Ponyrko, L. Matějka „*Temperature responsive shape memory hybrids*", Structure and dynamics of polymer nanocomposites, Montpellier, France, 22-24.06.2015

2. S. Ponyrko, L. Matějka „*Temperature responsive shape-memory nanocomposites*", HINT Training School, Ljubljana, Slovenia, 25-29.05.2015

3. S. Ponyrko, L. Matějka „*Shape-memory nanocomposites based on epoxy networks*", Frontiers in Polymer Science, Riva del Garda, Italy, 19-22.05.2015

4. S. Ponyrko, L. Matějka „*Shape-memory nanocomposites based on epoxy networks*", International Conference on Bioinspired and Biobased Chemistry & Materials, Nice, France, 15-18.10.2014.

5. S. Ponyrko, L. Matějka „*Epoxy-silica nanocomposite by nonaqueous sol-gel process*“, MoDeSt, Portorož, Slovenia, 31.8.-4.9.2014

6. S. Ponyrko, L. Matějka, J. Hodan „*Synthesis of temperature-responsive shape memory hybrids based on epoxy resin*“, workshop "Career in Polymers VI". Prague, CR, 18-19.7.2014.

7. L. Matějka, R. K. Donato, S. Ponyrko „*Reinforcement of epoxy-silica nanocomposites*“, Thermosets 2013 - From Monomers to Components, Berlin, Germany, 18-20.9.2013.

8. S. Ponyrko, L. Matějka „*Preparation and characterization of shape memory hybrids*“, International Conference on Multifunctional, Hybrid and Nanomaterials, Sorrento, Italy, 3-7.3.2013.

9. S. Ponyrko, L. Matějka „*Organic-inorganic nanocomposite based on epoxy resin: nonaqueous sol-gel process*“, Sol-Gel 2013. Madrid, Spain, 25-30.8.2013

10. S. Ponyrko, L. Matějka „*Epoxy-silica hybrids: nonaqueous sol-gel process*“, workshop "Career in Polymers IV". Prague, CR 29-30.6.2012

11. S. Ponyrko, J. Pleštil, M. Pekárek, L. Matějka. „*Nanostructured polymers based on epoxy resin: nonaqueous sol-gel process*“, ECNP Young Scientist Conference and ECNP Short Course on Functional polymers, Prague, CR, 22-24.4.2012.

12. S. Ponyrko, L. Matějka „*Synthesis and characterization of shape memory hybrids based on epoxy resin*“, Annual Conference Yucomat 2012, Herceg Novi, Montenegro, 3-7.9.2012.

13. S. Ponyrko, L. Kobera, L. Matějka „*Preparation and characterization of epox-silica hybrids: nonaqueous sol-gel process*“, NANOCON 2012, Brno, CR, 23-25.10.2012.

14. S. Ponyrko, J. Pleštil, L. Matějka. „*Synthesis and characterization of novel organic-inorganic hybrids*“, ECNP Young Researchers Conference, Lyon, Francie, 7-10.11.2011.

15. S. Ponyrko, L. Matějka „*Synthesis, characterization of modified organic-inorganic nanocomposites: sol-gel technique*“, NANOCON 2011, Brno, CR, 21-23.9.2011

16. S. Ponyrko, L. Matějka, J. Pleštil „*Epoxy-silica hybrid materials: nonaqueous sol-gel process*“, Workshop "Career in Polymers III", Prague, CR, 15-16.7.2011.

17. S. Ponyrko, M. Kubiszyn, L. Matějka „*Preparation and characterization of epoxy-silica hybrid materials: nonaqueous sol-gel process*“, Frontiers in polymer science, Lyon, France, 29-31.5.2011.

18. S. Ponyrko, M. Kubiszyn, L. Matějka „*Epoxy-silica nanostructured polymers: nonaqueous sol-gel process*“, DEMATEN "Processing of Nanostructured Ceramics and Nanocomposites", Brno, CR, 3-05.03.2011.

REFERENCES

1. D. Doran, B. Cather, *Construction Materials Reference Book*, Routledge, 2013
2. M. Dekker, *Epoxy resins-chemistry and technology, 2nd Edition*, New York, 1988
3. A Chatterjee in *Wiley Encyclopedia of Composites*, John Wiley and Sons, 2012
4. G. Kickelbick, *Hybrid Mater.* 2014, 1, 1.
5. T. Saegusa, *Pure & Appl. Chem*., 1995, 67, 1965.
6. B. Pukánszkya, *Europ. Poly. J.* 2005, 41, 4.
7. P.H.C Camargo, K.G. Satyanarayana, F. Wypych, *Mater. Res.*, 2009, 12, 1.
8. A. Okada *Macromol. Mater. Eng*. 2006,291, 1449.
9. G. Kickelbick, *Hybrid Materials: Synthesis, Characterization, and Applications*, Wiley-VCH Verlag GmbH & Co. KGaA, 2007.
10. S. Kalia, Y.Haldorai, *Organic-Inorganic Hybrid Nanomaterials*, Springer, 2014.
11. H. Huang, B. Orler, G.L. Wilkes, *Polym. Bull*., 1985, 14, 557.
12. H. Huang, G.L. Wilkes, *Polym. Bull.*, 1987, 18, 455.
13. F. Ribot and C. Sanchez, *Comments Inorg. Chem*., 1999, 20, 327.
14. R. M. Laine, *J. Mater. Chem.*, 2005, 15, 3725.
15. P. Rosso, L. Ye, K. Friedrich, S. Sprenger, *J. Appl. Polym. Sci.* 2006, 100, 1849
16. B.B. Johnsen, A.J. Kinloch, R.D. Mohammed, A.C. Taylor, S. Sprenger, *Polymer* 2007, 48, 530.
17. M. Preghenella, A. Pegoretti, C. Migliaresi, *Polymer*, 2005, 46, 12065
18. T. Lan, T.J. Pinnavaia, *Chem. Mater.*, 1994, 6, 2216.
19. M.S. Wang, T.J. Pinnavaia, *Chem. Mater.*, 1994, 6, 468.
20. N. Phonthammachai, X. Li, S. Wong, H. Chia, W.W. Tjiu, C. He, *Compos. A: App. Sci. Manuf.*, 2011, 42, 881.
21. F. Mammeri, E.L. Bourhis, L. Rozes, C. Sanchez, *J. Mater. Chem.*, 2005, 15, 3787.
22. L. Matějka, A. Strachota, J. Pleštil, P. Whelan, M. Steinhart, M. Šlouf, *Macromolecules* 2004, 37, 9449.
23. L. Mascia, T. Tang, *J. Mater. Chem.*, 1998, 8, 2417.
24. M. Ochi, R. Takahashi, A. Terauchi, *Polymer*, 2001 42, 5151.
25. W.H. Weng, H. Chen, S.P. Tsai, J.C. Wu, *J. Appl. Polym. Sci.*, 2004, 91, 532.
26. N. Prilezhaev, *Berichte der Deutschen Chemischen Gessellschaft* 1910, 42, 4811.
27. Y.-W. Mai, Z.-Z. Yu, *Polymer Nanocomposites, 1st Edition*, CRC Press, 2006.
28. H. Dodiuk, S. H. Goodman, *Handbook of Thermoset Plastics, 3rd Edition*, 2013.

29. S.R. Sandler, W. Karo, *Polymer syntheses, volumes II*, academic New York, 1977.

30. J.-P. Pascault, R. J. J. Williams, *Epoxy Polymers: New Materials and Innovations*, Wiley-VCH Verlag GmbH & Co. KGaA, Weinheim, Germany 2010.

31. S. Vyazovkin, N. Sbirrazzuoli, *Macromolecules,* 1996, 29, 1867.

32. J. Mijovic, A. Fishbain, J. Wijaya, *Macromolecules*, 1992, 25, 979.

33. J. Mijovic, S. Andjelic, *Macromolecules*, 1995, 28, 2787.

34. P.I. Karkanas, I.K. Partridge, *J. Appl. Polym. Sci.*, 2000, 77, 1419.

35. L.E. Overman, L.A. Flippin, *Tetrahedron Lett.*, 1981, 22, 195.

36. M. Majewski , V. Snieckus. *J. Org. Chem.*, 1984, 49, 2682.

37. D. Gagnebien, P.J. Madec, E. Marechal, *Eur. Polym. J.*, 1985, 21, 273

38. L. Shechter, J. Wynstra, *Indust. & Engin. Chem.*, 1956, 48, 94.

39. E.N. Jacobsen, F. Kakiuchi, R.G. Konsler, J.F. Larrow, M. Tokunaga, *Tetrahedron Lett.*, 1997, 38, 773

40. L. Matějka, J. Lövy, S. Pokorný, K. Bouchal, K. Dušek. *J. Polym. Sci. Part A: Polym. Chem*., 1983, 21, 2873.

41. M. Harsch, J. Karger-Kocsis, M. Holst, *Eur. Polym. J.*, 2007, 43, 1219.

42. E.M. Woo, J.C. Seferis, *J. Appl. Polym. Sci.*, 1990, 40, 1237.

43. K. Dušek, S. Luňák, L. Matějka, *Polym.Bull*., 1982, 7, 145.

44. K. Dušek, *Epoxy resins and composites II*, Springer, 1986.

45. J. K. Fink, *Reactive Polymers Fundamentals and Applications, 2nd Edition*, William Andrew Publishing, Oxford, 2013.

46. M. S. Bhatnagar, *The Polymeric Materials Encyclopedia*, CRC Press, 1996.

47. J.-P. Pascault, R. J. J. Williams, *Epoxy Polymer*, Wiley-VCH Verlag GmbH & Co. KGaA, Weinheim, 2010.

48. I. Hamerton, *Recent Developments in Epoxy Resins,* 1996.

49. C.A. May, *Epoxy resins-chemistry and technology, 2nd Edition*, Marcel Dekker, New York, 1988.

50. H. Lee, K. Neville, *Epoxy resins. Their applications and technology*, McGraw-Hill, 1957.

51. E. Petrie, *Epoxy Adhesive Formulations*, McGraw-Hill Chemical Engineering, 2005.

52. L. Matějka, Š. Podzimek, W. J. Simonsick, Jr., P. Špaček, K. Dušek, *J. Polym. Sci. Part A: Polym. Chem.*, 1992, 30, 2109.

53. H. Morio, H. Murase, Tsuchiya, T. Endo, *J. Appl. Polym. Sci*., 1986, 32, 5727.

54. J.J. Harris, S.C. Temin, *J. Appl. Polym. Sci.*, 1966, 10, 523.

55. S. Mortimer, A. J. Ryan, J.L. Stanford, *Macromolecules*, 2001, 34, 2973.

56. S. Ye, I. Deng, K. Friedrich, *J. Mater. Sci.* 2007, 42, 2766.

57. L. Merhari, *Hybrid nanocomposites for nanotechnology: electronic, optical, magnetic and biomedical applications*, Springer, 2009.

58. R. Gatcher, P.R. Klemchuk, H. Muller, H. Andreas *Plastics additives handbook (4th ed)*, Hanser, Munich, 1993.

59. H. Zou, S. Wu, Shen, *J. Chem. Rev*. 2008, 108, 3893.

60. E. Allen, J. Henshaw, P. Smith, *AEA Technology Engineering Services*, 2001.

61. M. Oliveira, A.V. Machado in *"Nanocomposites: synthesis, characterization and applications"*, Nova Science Pub Inc., 2013.

62. B. Viswanathan, *Introduction to nanomaterials*, Nanomaterials Narosa Publishing House, 2009.

63. L.S. Schadler, L.C. Brinson, W.G. Sawyer, *JOM*, 2007, 3, 53.

64. S. Rätzke, J. Kindersberger, "Erosion behaviour of nano filled silicone elastomers", XIVth International Symposium on High Voltage Engineering, Beijing, China, 2005.

65. R. Kotsilkova, *Thermoset Nanocomposites for Engineering Applications*, Smithers Rapra Technology, 2007.

66. T. Glomann, *Soft Matter*, 2013, 9, 10559.

67. M. Šupová, G.S. Martynkova, K. Barabaszová, *Sci. Adv. Mater.*, 2010, 3, 1.

68. K. Chawla, *Composite Materials*, Springer, 2013.

69. D. Ratna, N.R. Manoj, R. Varley, R.K. Singh, Raman, G.P. Simon, *Polym. Int.*, 2003, 52, 1403.

70. L. Chang, Z. Zhang, C. Breidt, *Appl. Comp. Mater.*, 2004, 11, 1.

71. H. Zou, S. Wu, J. S. *Chem. Rev*. 2008, 108, 3893.

72. G. Kickelbick, *Hybrid Materials: Synthesis, Characterization, and Applications*, Wiley, 2007.

73. F. Mammeri, E. Le Bourhis, L. Rozes, C. Sanchez, *J. Mater. Chem.*, 2005, 15, 3787.

74. J. Brinker, G. W. Scherrer, *Sol-gel Science,* Academic Press, CA. 1990.

75. M. Ochi, R. Takahashi, *J. Polym. Sci. Part B: Polym. Phys.*, 2001, 39, 1071.

76. L. Matějka, O. Dukh, J. Kolarik, *Polymer*, 2000, 41, 1449.

77. L. Matějka in "*Epoxy polymers: new materials and innovation"*, Wiley VCH Verlag GmbH&Co., 2010.

78. H. Beneš, J. Galy, J.F. Gerard, J. Pleštil, L. Valette, *J. Appl. Polym. Sci.*, 2012, 125, 1000.

79. Y. L. Liu, C. Y. Hsu, W. L. Wei, R. J. Jeng, *Polymer*, 2003,44, 5159.

80. M. Preghenella, A. Pegoretti, C. Migliaresi, *Polymer*, 2005, 46, 12065.

81. G. Ragosta, M. Abbate, P. Musto, G. Scarinzi, L. Mascia, *Polymer*, 2005, 46, 10506.

82. W. H. Weng, H. Chen, S. P. Tsai, J. C. Wu, *J. Appl. Polym.Sci*., 2004, 91, 532.

83. L. Matějka, K. Dušek, J. Pleštil, J. Kriz, F. Lednicky, *Polymer*, 1999, 40, 171

84. P. Innocenzi, T. Kidchob, T. Yoko, *J. Sol-Gel Sci. Technol*. 2005, 35, 225.

85. H. Zhang, Z. Zhang, K. Friedrich, C. Eger, *Acta. Mater.*, 2006, 54, 1833

86. L. Matějka, K. Dušek, J. Pleštil, *J. Noncryst. Sol.*, 1998, 226, 114.

87. L. Mascia, L. Prezzi, B. Haworth, *J. Mater. Sci.*, 2006, 41, 1145.

88. F. Piscitelli, M. Lavorgna, G.G. Buonocore, L. Verdolotti, J. Galy, L. Mascia. *Macromol. Mater. Eng.* 2013, 298, 896.

89. J. Macan, H. Ivankovic, M. Ivankovic, H.J. Mencer, *J. Appl. Polym. Sci.*, 2004, 92, 498.

90. M. Spírková, J. Brus, D. Hlavatá, H. Kamisová, L. Matějka, A. Strachota. *J. Appl. Polym. Sci.* 2004, 92, 937.

91. S.R. Davis, A.R. Brough, A. Atkinson. *J. Non-Cryst. Sol.*, 2003, 315, 197.

92. Y.W. Jun, J.S. Choi, J. Cheon, *Angew. Chem. Int*., 2006, 45, 3414.

93. M. Niederberger, M. Antonietti, Nanomaterials chemistry: Recent developments and new directions, chap. Nonaqueous sol-gel routes to nanocrystalline metal oxides, pp. 119–138. Wiley-VCH, 2007.

94. J.N. Hay, H.M. Raval, *Chem. Mater.*, 2001, 13, 3396.

95. M. Niederberger, N. Pinna, *Metal Oxide Nanoparticles in Organic Solvents Synthesis, Formation, Assembly and Application*, Springer, 2009.

96. N. Pinna, M. Niederberger, *Angew. Chem. Int.*, 2008, 47, 5292.

97. K.G. Sharp, *J. Sol-Gel Sci. Technol.*, 1994, 2, 3.

98. N. Phonthamachai, H. Chia, X. Li, F. Wang, W.W. Tjiu, C. He, *Polymer*, 2010, 51, 5377.

99. T.-M. Lee, C.-C. M. Ma, *J. Polym. Sci., Polym. Chem.* 2005, 44, 757.

100. J. Dupont, R.F. de Souza, P.A.Z. Suarez, *Chem. Rev.* 2002, 102, 3667.

101. T. Welton, *Chem. Rev*. 1999, 99, 2071.

102. H. Maka, T. Spychaj, R. Pilawka, *Ind. Eng. Chem. Res.*, 2012, 51, 5197.

103. J. D. Holbrey, K. R. Seddon, *Clean Prod. Process.*, 1999, 1, 223.

104. A. Lewandowski, A. Świderska-Mocek, *J. Power .Sources*, 2009, 194, 601.

105. F. Zhou, Y. Liang, W. Liu, *Chem. Soc. Rev*., 2009, 38, 2590.

106. M.P. Scott, C.S. Brazel, M.G. Benton, J.W. Mays, J.D. Holbrey, R.D. Rogers, *Chem. Commun*., 2002, 13, 1370.

107. H. Mąkaa, T. Spychaja, M. Zenkerb, *J. Ind. Engineer.Chem*, 2015, 31, 192.

108. Y. Zhou, J. H. Schattka, M. Antonietti, *Nano Lett.*, 2004, 4,477.

109. K. Z. Donato, R. K. Donato, M. Lavorgna, L. Ambrosio,L. Matějka, R. S. Mauler, H. S. Schrekker, *J. Sol-Gel Sci. Technol.*, 2015, 76, 414.

110. M. V. Migliorini, R. K. Donato, M. A. Benvegnu, R. S. Gonçalves, H. S. Schrekker, *J. Sol-Gel Sci. Technol*.,2008, 48, 272.

111. R. K. Donato, M. Lavorgna, P. Musto, K. Z. Donato, A. Jager, P. Stepanek, H. S. Schrekker, L. Matějka, *J. Colloid Interface Sci.*, 2015, 77, 447

112. R. K. Donato, L. Matějka, H. S. Schrekker, J. Pleštil, A. Jigounov, J. Brus and M. Šlouf, *J. Mater. Chem*., 2011, 21, 13801.

113. R. K. Donato, K. Z. Donato, H. S. Schrekker, L. Matějka, *J. Mater. Chem*., 2012, 22, 9939.

114. N. Rapoport, *Prog. Polym.Sci.*, 2007, 32, 962.

115. H.Y. Jiang, S. Kelch, A. Lendlein, *Adv. Mater.*, 2006, 18, 1471.

116. A. Lendlein, *Shape-Memory Polymers*, Springer, 2010.

117. A. Lendlein, M. Behl, B. Hiebl, C. Wischke, *Expert Review of Medical Devices* 2010, 7, 357.

118. D. Haiyan, J. Zhang, *Soft Matter.*, 2010, 6, 3370.

119. R. Gouher, H. Luftmann, A. Kraft. *Polymer* 2006, 47, 4251.

120. A. M. Kushner, J. D. Vossler, G. A. Williams, Z. Guan, *J. Amer. Chem. Soc.*, 2009, 131, 8766.

121. S. Ying, M. Yoonessi, R. A. Weiss, *Macromolecules*, 2013, 46, 4160.

122. J. Hu,Y. Zhu, H. Huang, J. Lu, *Prog. Polym. Sci.*, 2012, 37, 1720.

123. C. Liu, S. B. Chun, P. T. Mather, L. Zheng, E. H. Haley, E. B. Coughlin, *Macromolecules*, 2002, 35, 9868

124. K. Sakurai, H. Tanaka, N. Ogawa, T. Takahashi, *J. Macromol. Sci., Phys*., 1997, 36, 703.

125. H. Koerner, G. Price, N. A. Pearce, M. Alexander, R. A. Vaia, *Nat. Mater*., 2004, 3, 115.

126. Y. Kagami, J. P. Gong, Y. Osada, *Macromol. Rapid Commun*., 1996, 17, 539.

127. J. Diani, Y. Liu, K. Gall, *Polym. Eng. Sci*., 2006, 46, 486.

128. N. Zheng, G. Fang, Z. Cao, Q. Zhao, T. Xie, *Polym.Chem*., 2015, 6, 3046.

129. H. Y. Jiang, S. Kelch, A. Lendlein, *Adv. Mater*., 2006, 18,147.

130. C. Liu, H. Qin, P. T. Mather, *J. Mater. Chem*., 2007, 17, 1543.

131. I. A. Rousseau, *Polym. Eng. Sci.*, 2008, 48, 2075.

132. K. Kumar, D. C. Lagoudas, *Shape memory alloys modelling and engineering applications*, Springer, 2008.

133. J. M. Jani, M. Leary, A. Subic, M. A. Gibson, *Materials & Design.* 2014, 56, 1078.

134. K. Gall, M. L. Dunn, Y. Liu, D. Finch, M. Lake, N. A. Munshi, *Acta Materialia*, 2002, 50, 5115.

135. J. Cui, K. Kratz, M- Heuchel, B. Hiebl, A. Lendlein, *Polym. Adv. Technol.*, 2011, 22, 180.

136. Y. Bellouard, *Mater. Sci. Engineer. A*, 2008, 481, 582.

137. E. Hornbogen *Adv. Engineer. Mater.*, 2006, 8, 101.

138. P. Miaudet, A. Derré, M. Maugey, C. Zakri, P. M. Piccione,, R. Inoubli, P. Poulin, *Science*, 2007, 23, 1294.

139. T. Xie, *Nature*, 2010, 464, 267.

140. H. Meng, G. Li, *Polymer,* 2013, 54, 2199.

141. A. Afzal, H.M. Siddiqi, *Polymer*, 2011, 52, 1345.

142. B.J. Bauer, D.W. Liu, C.L. Jackson, J.D. Barnes, *Polym. Adv. Technol.*, 1996, 7, 333.

143. L. Matějka, O. Dukh, H. Kamisová, D. Hlavatá, M. Spirková, J. Brus, *Polymer*, 2004, 45, 3267.

144. K.J.D. MacKenzie, M.E. Smith, Pergamon. In: *Multinuclear solid-state NMR ofinorganic material*, 2002.

145. J. Wen, J.E. Mark. *Rub. Chem. Tech.*, 1994, 67, 807.

APPENDICES 1 - 3

Epoxy-silica nanocomposites by nonaqueous sol-gel process

(1)

S. Ponyrko, L. Kobera, J. Brus, L. Matějka "Epoxy-silica hybrids by nonaqueous sol-gel process" *Polymer* **2013**, 54, 23, 6271.

(2)

S. Ponyrko, J. Kovářová, L. Kobera, L. Matějka "High-Tg, heat resistant epoxy-silica hybrids with a low content of silica generated by nonaqueous sol-gel process" *J. Appl. Polym. Sci.* **2014**, 131, 40899.

(3)

R.K. Donato, M. Perchacz, S. Ponyrko, K.Z. Donato, H.S. Schrekker, H. Benes, L. Matějka "Epoxy-silica nanocomposite interphase control using task-specific ionic liquids via hydrolytic and non-hydrolytic sol-gel processes" *RSC Adv.* **2015**, 5, 91330.

APPENDICES 4

Thermo-responsive shape-memory nanocomposites

(4)

S. Ponyrko, R.K. Donato, L. Matějka "High performance shape memory epoxy-silica nanocomposites. Structure design" *Polym. Chem.* **2016**, DOI: 10.1039/c5py01450f

Polymer 54 (2013) 6271–6282

Contents lists available at ScienceDirect

Polymer

journal homepage: www.elsevier.com/locate/polymer

Epoxy-silica hybrids by nonaqueous sol–gel process

Sergii Ponyrko, Libor Kobera, Jiří Brus, Libor Matějka*

Institute of Macromolecular Chemistry, Academy of Sciences of the Czech Republic, Heyrovský Sq. 2, 162 06 Prague, Czech Republic

ARTICLE INFO

Article history:
Received 31 May 2013
Received in revised form
16 September 2013
Accepted 18 September 2013
Available online 25 September 2013

Keywords:
Epoxy-silica hybrid
Nonaqueous sol–gel process
Gelation

The epoxy-silica hybrids have been prepared by the non-aqueous sol–gel process and the in situ generation of nanosilica from tetraethoxysilane was initiated with borontrifluoride monoethylamine (BF_3MEA). The DGEBA based epoxy networks with aliphatic, cycloaliphatic and aromatic amines were used as matrices. The solventless technique made it possible to avoid drawbacks of the classical aqueous procedure. The "non-aqueous" systems show improved homogeneity and thermomechanical properties in particular at the application of the coupling agent glycidyloxypropyl trimethoxysilane. Mechanism of the non-aqueous sol–gel process under BF_3MEA action and evolution of the hybrid structure during polymerization, followed by chemorheology, are discussed. The nanosilica structure growth is slower under the non-aqueous procedure thus facilitating a better structure control. The hybrids with both particulate and bicontinuous morphologies were prepared and the epoxy-silica interphase bonding and crosslinking through the formed silica domains was proved. The hybrid hierarchical structure and morphology were determined by NMR, SAXS, TEM and DMA.

1. Introduction

The epoxy-silica hybrids are known as efficient materials in the high performance application, for aerospace, automobile and sporting equipment industries, for surface coatings, printed circuit boards, as well as anti-scratch and anti-corrosive materials with better mechanical strength, thermal stability and lower flammability [1,2]. Nanosilica has gained the reputation of the most suitable inorganic filler for epoxy thermosets. The silica nanoparticles, however, are difficult to be well dispersed in a polymer. Therefore, in situ generation of silica in a polymer matrix by the sol–gel process is often used. The sol–gel process involves mostly hydrolysis and polycondensation of alkoxysilane precursors [3], tetraethoxysilane (TEOS) being the most typical one.

The epoxy-silica hybrids show enhanced thermomechanical properties compared to the neat epoxy networks [4–7] and the reinforcement is related mainly to the interphase interaction and to the hybrid morphology. Strengthening the interphase interaction thus is a crucial point in the hybrid synthesis. The common approach consists in grafting, i.e. compatibilization of an organic-inorganic mixture by a covalent bonding between phases. In addition, also physical interphase interactions are used to compatibilize an immiscible system. This is the case of the in situ formed silica by the sol–gel process [8,9]. We have used the two-step acid-base sol–gel procedure to generate silica from TEOS in the epoxy based network from diglycidyl ether of Bisphenol A (DGEBA) and polyether diamine (Jeffamine D2000, amine terminated polyether with M∼2000) [5,10,11]. The acid catalysed step promotes hydrolysis of TEOS to form SiOH groups while the nucleophilic amine D2000 catalyses fast polycondensation in the next step. The hybrid showed a fine morphology with well dispersed silica nanostructures as well as the morphology of co-continuous epoxy and silica phases. This is a result of the strong interphase interaction because of H-bonding between SiOH of silica and polyether based chains of the epoxy network. Due to this interaction and formation of bicontinuous morphology the hybrid modulus increased by two orders of the magnitude at a low silica content.

Generally, however, the separation of the epoxy and silica phases takes place during the polymerization in the systems with a poor interphase interaction. Therefore, coupling agents are used to improve compatibility between phases, the most popular ones being 3-glycidyloxypropyl trimethoxysilane (GTMS) and 3-aminopropyltriethoxysilane. They form covalent interphase links thus preventing a phase separation [7,12–16]. Such hybrids are reported to display both an increase and decrease in glass transition temperature *Tg*. Homogeneous nanofiller dispersion and a strong interphase interaction lead to immobilization of the epoxy chain and a high *Tg* [4,7,17]. In contrast, plasticization by the incompletely cured sol–gel products results in drop in *Tg* [12,13].

The classical sol–gel process, however, suffers by shortcomings such, as immiscibility of water with TEOS and an epoxy system, thus requiring application of a cosolvent. The solvent and excessive water evaporation leads to sample shrinkage and a removal of residual volatile compounds could result in formation of bubbles or

* Corresponding author. +420 296809281.
E-mail address: matejka@imc.cas.cz (L. Matějka).

0032-3861/$ – see front matter © 2013 Elsevier Ltd. All rights reserved.
http://dx.doi.org/10.1016/j.polymer.2013.09.034

cracks in the final product, not even mention the environmental and health issues. The nonaqueous sol–gel process is a method to overcome some of the limitations of the "aqueous procedure". It is a powerful and versatile alternative of the traditional sol–gel process [18,19]. Generally, the fast "aqueous" sol–gel reactions result in a loss of structure control and reproducibility in a hybrid synthesis. In contrast, the non-aqueous sol–gel technique provides an improved control over molecular level homogeneity leading to uniform morphologies. Lee and Ma [20] synthesized the nanosilica from TEOS by nonaqueous sol–gel process in the epoxy matrix DGEBA-diaminodiphenylsulfone (DDS) catalysed by borontrifluoride monoethylamine (BF_3MEA). They proposed the catalytic mechanism of BF_3MEA in the reaction. The two-step nanocomposite synthesis involved (i) preparation of nanosilica in the presence of epoxy resin and the BF_3MEA complex and (ii) formation of DGEBA-DDS-silica network by addition of the diamine. The nanocomposite exhibited an increase in *Tg* by 50 °C with respect to the neat epoxy network by using 40% of TEOS in the initial mixture.

Despite benefits of the non-aqueous procedure, it has been very little studied so far with respect to the synthesis of the epoxy-silica hybrids. Such a theme will be investigated in this paper. The DGEBA based networks cured with diamines were filled with nanosilica in situ formed from TEOS. The solvent-free nonaqueous sol–gel process promoted by the BF_3MEA complex was applied in order to improve homogeneity of the epoxy nanocomposite and to avoid problems with a solvent and excessive water removal. In addition, the coupling agent GTMS was used to strengthen an interphase interaction and improve the hybrid thermomechanical properties, such as *Tg* and rubbery modulus.

The goal of the paper consists in understanding of the epoxy-silica hybrid formation under nonaqueous conditions in comparison to the classical "aqueous" procedure. The paper provides an explanation of the hybrid molecular and phase structure evolution during the simultaneous epoxy network build-up and siloxane/silica structures formation. Attention is paid to an interphase covalent bonding. The main factors governing formation of the hybrids as well as their morphology and final properties are discussed. The paper describes the effect of BF_3MEA complex, amine basicity, content of the coupling agent GTMS, curing temperature or the steric restrictions of the epoxy network affecting the silica structure growth. The evolution of the structure during polymerization was followed by chemorheology. The hybrid hierarchical structure and morphology, as well as the thermomechanical properties were determined by NMR, SAXS, TEM and DMA analysis.

2. Experimental part

We have prepared the hybrids based on a glassy epoxy matrix filled with in situ generated nanosilica structures. Four types of the DGEBA-amine networks were used as a matrix comprising the following diamine crosslinkers – aliphatic 1,4-diaminobutan, cycloaliphatic Laromin, aromatic diaminodiphenylmethane (DDM) and amino-terminated polyether Jeffamine D230. The nonaqueous sol–gel process, promoted by BF_3MEA complex, was applied to generate in the matrix the silica structures from TEOS or silsesquioxanes (SSQO) from the coupling agent GTMS. The two-step synthesis was performed: (i) the nonaqueous "protolysis" of TEOS in the presence of BF_3MEA complex and (ii) the simultaneous amine catalysed sol–gel polycondensation and the epoxy-amine network formation.

2.1. Materials

The epoxides diglycidyl ether of Bisphenol A (DGEBA, $n = 0.17$) based resin, Epilox A 19-03 (Leuna–Harze Gmbh) with the equivalent weight of the epoxy groups $E_E = 187$ g/mol epoxy groups and phenylglycidyl ether (PGE) (Fluka) were used. The following amines were applied as curing agents; poly(oxypropylene) diamine–Jeffamine® D230 (M ~ 230), 4,4′-diaminodiphenylmethane (DDM) (Sigma Aldrich), 1,4-diaminobutan (DAB) (Fluka), butylamine (Fluka) and 3,3′-dimethyl-4,4′-diaminocyclohexylmethane (Laromin® C 260) was received from BASF. Inorganic components: tetraethoxysilane (TEOS) and 3-glycidyloxypropyl trimethoxysilane (GTMS) were purchased from Fluka. Borontrifluoride monoethylamine (BF_3MEA) was obtained from the Aldrich. All chemicals were used as received.

2.2. Synthesis of the hybrid

The epoxy-amine networks were prepared at a stoichiometric ratio of functional groups (C_{epoxy}:C_{NH} = 1:1) and the hybrids were synthesized by the modified two step Lee's synthesis procedure [20]. (i) 2 wt. % of BF_3MEA with respect to TEOS was mixed with the epoxy resin for 30 min at 70 °C. After that, 18 wt. % of TEOS (with respect to DGEBA) was added to the epoxy-BF_3MEA mixture and speedily mixed for 1 h. This composition corresponds to ~5 wt. % of equivalent silica. (ii) Stoichiometric equivalent weight of amine was added to the prereacted mixture of TEOS in the epoxy resin and mixed for 30 min.

The hybrids modified with the coupling agent GTMS were prepared by substituting a fraction of DGEBA by GTMS while keeping the epoxy groups' concentration constant and the total ratio of epoxy and NH functionalities stoichiometric. The content of GTMS (x) in the nanocomposite synthesis was characterized by fraction of epoxy groups of DGEBA replaced by the coupling agent GTMS: x = [epoxy (GTMS)]/[epoxy (DGEBA) + epoxy (GTMS)] and was varying from 0.1 up to 1.0.

The following curing regime was applied: 90 °C for 2 h; 130 °C for 16 h and the posturing under vacuum for 5 h at 190 °C in case of D230 and at 210 °C for Laromin and DDM.

The reference aqueous sol–gel synthesis of the nanocomposite was performed according to the two-step acid–base procedure described in Ref. [10].

2.3. Methods

2.3.1. Transmission electron microscopy (TEM)

Transmission electron microscopy (TEM) was performed with the microscope JEM 200CX (JEOL, Japan). TEM microphotographs were taken at the acceleration voltage of 100 kV, recorded on a photographic film, and digitized with a PC-controlled digital camera DXM1200 (Nikon, Japan). Ultrathin sections for TEM, approximately 50 nm thick, were cut with ultra microtome Leica Ultra cut UCT, equipped with cry attachment.

2.3.2. Small-angle X-ray scattering (SAXS)

The experiments were performed using a pinhole camera (Molecular Metrology SAXS System) attached to a microfocused X-ray beam generator (Osmic MicroMax 002) operating at 45 kV and 0.66 mA (30 W) The camera was equipped with a multiwire, gas-filled area detector with an active area diameter of 20 cm (Gabriel design). Two experimental setups were used to cover the q range of 0.004–1.1 $Å^{-1}$ where $q = (4\pi/\lambda)\sin\theta$ (λ is the wavelength and 2θ is the scattering angle). The scattering intensities were put on an absolute scale using a glassy carbon standard.

2.3.3. Nuclear magnetic resonance spectroscopy (NMR)

Solid-state ^{29}Si CP/MAS NMR experiments were measured at 11.7 T using a Bruker Avance 500 WB/US NMR spectrometer with double-resonance 4-mm and 7-mm probeheads, respectively. To

compensate for frictional heating of the spinning samples, all NMR experiments were measured under active cooling. The sample temperature was maintained at 308 K. The ^{29}Si CP/MAS NMR spectra were acquired at 99.325 MHz; spinning frequency was $\omega r/2\pi = 5$ kHz; the number of scans was 2048; spin lock 4 ms and recycle delay was 3 s. The spectra were referenced to *M8Q8* (−109.8 ppm). During detection, a high-power dipolar decoupling (TPPI) was used to eliminate strong heteronuclear dipolar coupling.

The condensation conversion α_{Si} was determined as $\alpha_{Si} = \Sigma i Q_i/4$ for TEOS and $\alpha_{Si} = \Sigma i T_i/3$ for GTMS. Q_i and T_i are the mole fractions of the Q_i and T_i structure units with i siloxane bonds Si–O–Si attached to the central silicon. The relative amount of the structural units was obtained from the deconvolution of the ^{29}Si CP/MAS NMR spectra. The assignment of the NMR bands is as follows; Q_0 from −71.7 to −81.9 ppm, Q_1 from −81.5 to −89.3 ppm, Q_2 from −91.2 to −91.5 ppm, Q_3 from −101.2 to −101.6 ppm, Q_4 from −109.3 to −110.1 ppm, T_0 from −42.7 to −43.2 ppm, T_1 from −47.9 to −49.6 ppm, T_2 from −57.3 to −58.3 ppm, T_3 from −66.6 to −66.9 ppm.

^{11}B MAS NMR spectra were measured in 4-mm double resonance probehead at MAS frequency of 5 kHz. The spectra were calibrated using a secondary reference standard $NaBH_4$ (3.2 ppm).

^{13}C MAS NMR spectra were recorded at Larmor frequencies $\nu^{13}C = 125.783$ MHz. High power decoupling pulse sequences with a $\pi/2$ (3.4 μs) excitation pulse were applied. The number of scans for the accumulation of ^{13}C MAS NMR spectra was 512 with repetition delay 10 s at 5 kHz magic angle spinning (MAS) frequency of the sample. The isotropic chemical shift of ^{13}C scale was calibrated with glycine as an external standard (176.03 ppm to carbonyl signal).

2.3.4. Dynamic mechanical analysis (DMA)

Dynamic mechanical properties of the nanocomposites were tested using the ARES G2 apparatus (TA Instruments). An oscillatory shear deformation at the constant frequency of 1 Hz and at the heating rate of 3 °C/min was applied.

ARES G2 rheometer was used also for the chemorheology experiments to follow molecular structure evolution and gelation during polymerization. Oscillatory shear deformation in parallel plates geometry at a frequency of 1 Hz was used. The initial applied maximum strain was 200% while keeping torque below 20 g*cm to prevent breaking of the formed gel.

The gel point was determined by using the multifrequency sweep measurement ranging from 1 to 64 rad/s and applying a power-law rheological behaviour at the critical state, $G'(\omega) \sim G''(\omega) \sim \omega^n$ [21]. The loss factor tan δ is independent of measurement frequency at the gel point and therefore, the gelation was evaluated as a crossover of the tan δ for different experimental frequencies during the polymerization.

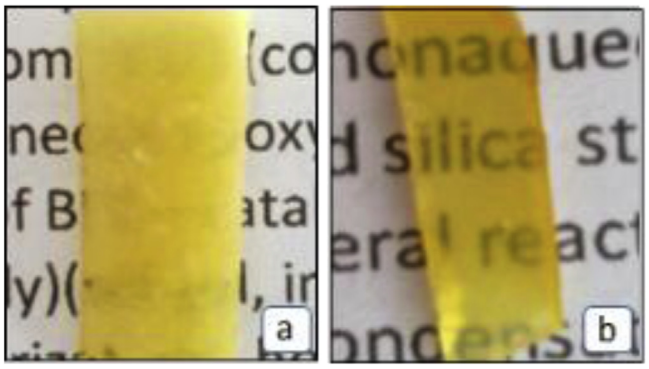

Fig. 1. DGEBA-Laromin-TEOS nanocomposite prepared by (a) aqueous sol–gel process, (b) nonaqueous sol–gel promoted by BF_3MEA.

3. Results

We have studied the epoxy-silica hybrids based on epoxy networks differing in the rate of gel formation, crosslinking density, glass transition temperature *Tg* and compatibility with silica nanofiller. This system series thus makes it possible to study the structure-properties relationships. Silica nanofiller was generated in the matrix by the nonaqueous sol–gel process using BF_3MEA complex.

3.1. Structure and morphology of hybrids

Incorporation of nanosilica in the epoxy matrix DGEBA-Laromin by the classical aqueous sol–gel procedure results in the heterogeneous opaque sample due to the polymerization induced phase separation as shown in Fig. 1a. The nonaqueous sol–gel procedure facilitates preparation of the homogeneous sample illustrated in Fig. 1b. The transparent hybrids containing up to 40 wt. % TEOS are formed at application of BF_3MEA.

The TEM micrographs of fractured surfaces in Fig. 2 indicate the effect of BF_3MEA on dispersion of silica nanostructures in the network DGEBA-D230. The compact aggregates of the size ~300 nm are present in the hybrid in case of the synthesis without BF_3MEA (Fig. 2a). The application of the complex leads to a fine morphology consisting of the branched structure of interconnected silica nanostructures of the size ~20 nm dispersed in the matrix (Fig. 2b). Another improvement of the nanocomposite homogeneity was achieved by using the coupling agent GTMS. The corresponding samples are transparent and the formed SSQO structures are well ramified to create a large interphase in an epoxy medium (see Fig. 2c).

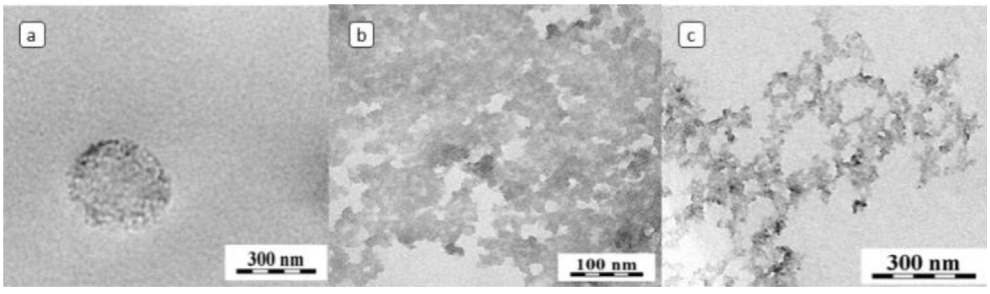

Fig. 2. TEM micrograph of the hybrids: (a) DGEBA-D230-TEOS, (b) DGEBA-D230-TEOS-BF_3MEA, (c) DGEBA-D230-GTMS-BF_3MEA.

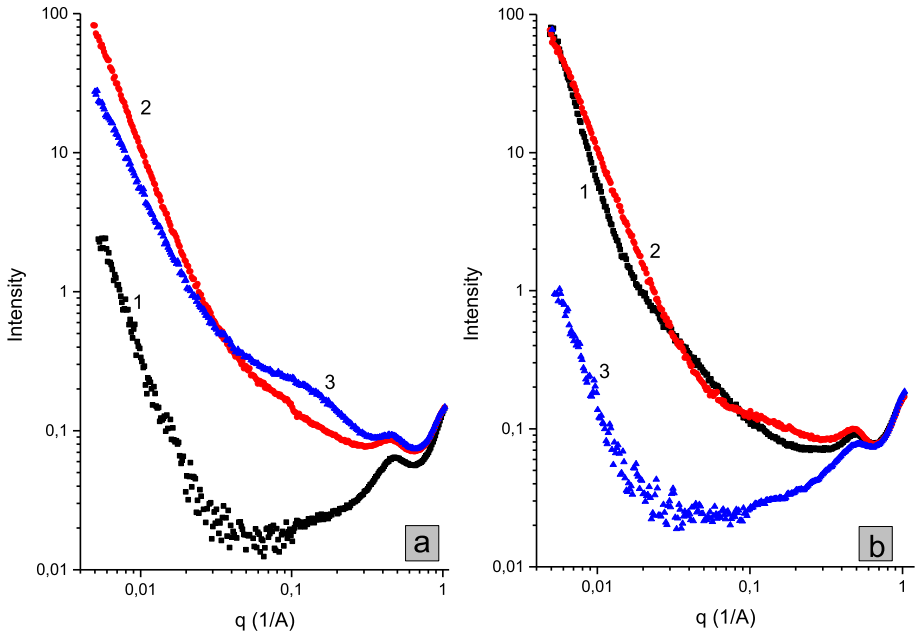

Fig. 3. SAXS profile of the hybrids prepared with or without BF_3MEA: (a) 1 DGEBA-D230, 2 DGEBA-D230-TEOS, 3 DGEBA-D230-TEOS-BF_3MEA; (b) 1 DGEBA-Laromin-TEOS, 2 DGEBA-Laromin-TEOS-BF_3MEA, 3 DGEBA-Laromin-GTMS-BF_3MEA.

An insight into the structure down to the nanoscale was provided by the SAXS analysis. Fig. 3 displays SAXS profiles of the hybrids based on DGEBA-D230 and DGEBA-Laromin networks. The high scattered intensity at low q values in the case of the hybrid DGEBA-D230-TEOS prepared without BF_3MEA in Fig. 3a reveals large silica aggregates of the size out of the SAXS apparatus limit, i.e. >70 nm. The high mass fractal dimension D_m determined from the slope of the log–log profile (see Table 1) implies that the aggregates are quite compact. The smaller slope corresponding to the lower D_m in the case of the synthesis in presence of the BF_3MEA complex characterizes the more open structure aggregates. The knee on the profile at $q = 0.1$ Å^{-1} originates from the small particles of a diameter size $D = 2$ nm within the silica aggregates. The primary particles size was determined from Guinier analysis after subtracting background of the neat epoxy matrix and of the large aggregates curve; $R_g = 0.75$ nm. For the geometrical diameter it holds $D = 2R_g{}^*(5/3)^{1/2}$ assuming spherical particles.

The SAXS profiles of the hybrids prepared from the epoxy network DGEBA-Laromin are illustrated in Fig. 3b. The high value of the slope β of the SAXS profile, $\beta > 3$, reveals a surface fractal structure with the surface fractal dimension $D_S = 6-\beta$. The fractal dimension $D_S = 2$ characterizes the structure with a smooth surface. The results in Table 1 show that the interface in these hybrids is less diffusive and the aggregates with a smooth surface are formed. Consequently, the silica aggregates in these hybrids as well as in the DGEBA-DDM based ones are more compact than those in DGEBA-D230-TEOS. This is a result of a lower compatibility of silica with cycloaliphatic (Laromin) and aromatic (DDM) amines, compared to polyether chain of D230. Again, BF_3MEA makes the silica structure more open with lower fractal dimensions. The primary particles size in the network DGEBA-Laromin is $D = 7.5$ nm and $D = 1.5–2$ nm without and with BF_3MEA, respectively. The hybrids formed using GTMS include smaller SSQO aggregates (see Fig. 2c), however the structure compactness is similar to the TEOS containing hybrids (see Table 1).

The structure of silica aggregates depends mainly on mechanism of its formation during the sol–gel process as discussed below.

Table 1
Fractal dimension of the silica/SSQO nanostructures.

System	D_m, (D_S)[a]
DGEBA-D230-TEOS	2.9
DGEBA-D230-TEOS-BF_3MEA	2.2–2.4
DGEBA-Laromin-TEOS	2.1[a]
DGEBA-Laromin-TEOS-BF_3MEA	2.8
DGEBA-DDM-TEOS	2.0[a]
DGEBA-DDM-TEOS-BF_3MEA	2.6
DGEBA-Laromin-GTMS-BF_3MEA	2.8

D_m–mass fractal dimension.
[a] D_S–surface fractal dimension.

3.2. Nonaqueous preformation of nanostructures

The preformation of nanostructures in the first step of the hybrid synthesis (see Experimental 2.2) was followed by ^{29}Si NMR

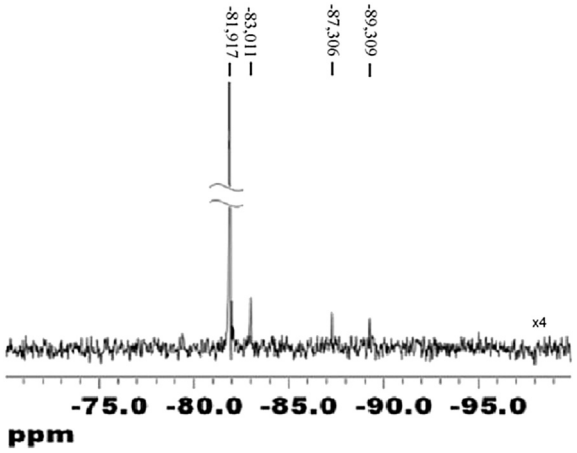

Fig. 4. ^{29}Si NMR spectrum of the reaction mixture TEOS-BF_3MEA complex under nonaqueous conditions.

Table 2
Distribution of Q_i^y units, fraction of SiOH and condensation conversion after TEOS protolysis under non-aqueous conditions.

System	Q_0	Q_0^1	Q_1^1	Q_1^2	Q_1^3	ϕ_{SiOH}	α_{Si}
TEOS-BF_3MEA	0.90	0.018	0.027	0.055	0	0.063	0.025
TEOS-DGEBA-BF_3MEA	0.81	0.06	0.02	0.02	0.09	0.11	0.05

spectroscopy. Fig. 4 shows the spectrum of the reacted mixture TEOS-BF_3MEA. Assignment of the chemical shifts of the structural units Q_i^y in ppm is as follows [3]: $Q_0 = 81.9$, $Q_1^0 = 89.3$, $Q_1^1 = 87.3$, $Q_1^2 = 83.0$, $Q_1^3 = 81.5$. The units Q_i^y correspond to Si atom with y SiOH groups and i siloxane bridges (Si–O–Si).

The distribution of Q_i^y units, sol–gel conversions α_{Si} and the content of silanol groups are given in Table 2. The fraction of silanols ϕ_{SiOH} is defined as $\phi_{SiOH} = \Sigma y Q_i^y/(4-i)$. The results disclose a very small extent of the sol–gel reactions taking place in the presence of 2 wt. % of BF_3MEA complex heated at 70 °C for 1 h corresponding to the applied conditions of the first step. Only 10% of TEOS has reacted as $Q_0 = 0.90$. The conversion, however, is higher in the presence of the epoxy resin in addition to BF_3MEA complex as displayed in Table 2. In that case 19% of TEOS has reacted and the silanol fraction as well as siloxane conversion increased twofold. The results show that the reaction consists in initiation of the nonaqueous sol–gel process by protolysis of TEOS with BF_3MEA (see Discussion 4.1) resulting in formation of the SiOH containing products (Scheme 1). The protolysis of TEOS is more efficient in the presence of the epoxide.

Only low molecular weight products, like disiloxanes, are formed during this reaction step as only Q_0 and Q_1 units were detected. At a high BF_3MEA content (6 wt. %), however, the microgel silica aggregates of the size $D > 100$ nm composed of primary particles are produced in agreement with the results of Lee [20]. Lee applied the more severe reaction conditions ($T = 80$ °C for 4 h) and found the production of small nanoparticles at a low BF_3MEA concentration while large particles of the size >200 nm at a BF_3MEA content higher than 5 wt. %.

3.3. Hybrid network formation

The simultaneous epoxy-amine network build-up and a silica/SSQO structures growth by polycondensation start by addition of a diamine to the mixture of the epoxy and the siloxanes preformed in the first step. The amine serves both as an epoxy crosslinker and a nucleophilic catalyst of the sol–gel polycondensation illustrated in Scheme 2.

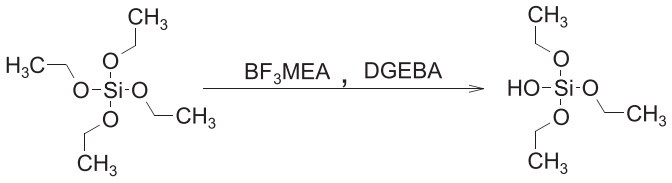

Scheme 1. Protolysis of TEOS under nonaqueous conditions.

Evolution of the hybrid structure and network formation during the cure was followed by chemorheology. Fig. 5 shows the growth of the shear storage modulus $G'(t)$ during build-up of the hybrid networks at $T = 80$ °C. The hybrids based on two epoxy-amine systems displaying the fast and the relatively slow network formations are compared. The "slow network" is represented by DGEBA-D230 system (curve 1) and the "fast" one by DGEBA-DAB (curve 4).

The steep increase in modulus in the figure characterizes gelation of a system. The more precise determination of the gel point was performed by the multifrequency sweep (see Experimental) and the results are given in Table 3. In both epoxy networks the gelation is delayed in the presence of TEOS (curves 2 and 5). This is due to a dilution effect by TEOS slowing down the kinetics of the epoxy-amine reaction. Addition of the BF_3MEA complex in the DGEBA-D230-TEOS mixture, however, accelerates the gelation of the hybrid and compensates the dilution effect (curve 3). Moreover, the figure displays the modulus increase in the pre-gel stage in the hybrids involving BF_3MEA complex (curves 3 and 5).

In addition, we have followed structure evolution of the system with the coupling agent. We have used GTMS partially substituting DGEBA in the hybrid networks. Table 3 shows that GTMS slows down the hybrid gelation and presence of BF_3MEA leads to the acceleration alike in the case of TEOS.

3.4. Structure of silica/SSQO domains in the hybrids

The nonaqueous sol–gel reaction is very slow compared to the aqueous procedure and the rate of the silica/SSQO structures growth depends mainly on basicity of an amine. To find a relation between the formation and structure of the hybrids we have determined the silica/SSQO structure and the sol–gel conversion in four hybrid networks containing the amines with increasing basicity: DDM < D230 < Laromin < DAB. The results are given in Table 4.

Local hybrid structure comprising the structure of silica/SSQO domains was determined by ^{29}Si CP/MAS NMR analysis. The condensation conversion α_{Si} in the hybrids prepared under nonaqueous conditions is lower compared to those in the aqueous sol–gel process. While $\alpha_{Si} = 0.79–0.85$ and 0.85–0.91 in the "aqueous hybrids" DGEBA-D2000-TEOS [5] and GTMS-D2000 [22], respectively, the conversions in the "nonaqueous" network systems reach values in the wide range 0.09–0.65. The results in Table 4 reveal that the conversions α_{Si} increase by (i) catalysis with BF_3MEA complex, (ii) increasing basicity of the curing amine and (iii) decreasing steric hindrance due to an epoxy system.

The latter fact was proved by comparison with the model non-crosslinked epoxy system containing the monoepoxide phenylglycidyl ether (PGE) instead of DGEBA. Only the low molecular weight product is formed by the reaction of PGE with DAB under

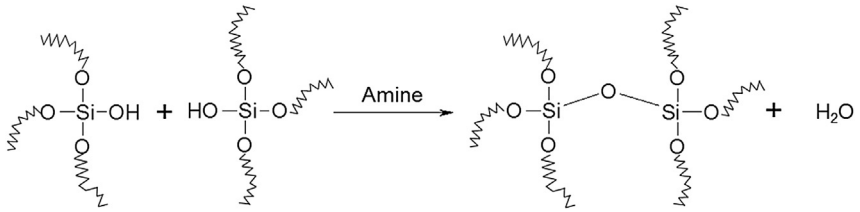

Scheme 2. Sol–gel polycondensation.

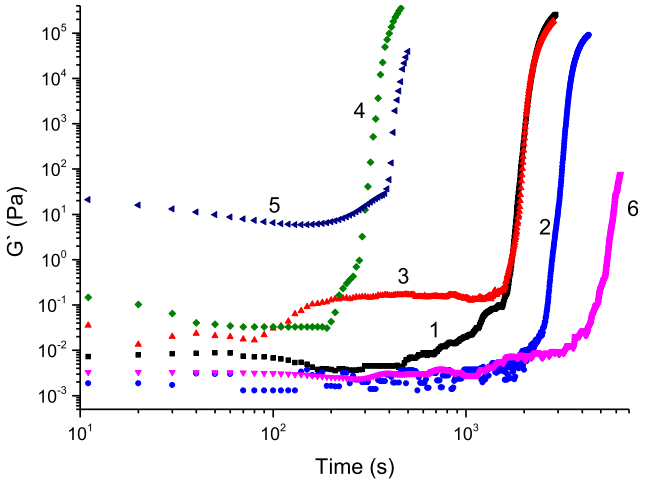

Fig. 5. Shear storage modulus $G'(t)$ of the studied systems as a function of time during polymerization at $T = 80$ °C: 1 DGEBA-D230, 2 DGEBA-D230-TEOS, 3 DGEBA-D230-TEOS-BF_3MEA, 4 DGEBA-DAB, 5 DGEBA-DAB-TEOS-BF_3MEA, 6 GTMS-D230-BF_3MEA.

the stoichiometric composition at a low temperature. The condensation conversion in the model system PGE-DAB-TEOS is high, $\alpha_{Si} = 0.81$, in contrast to $\alpha_{Si} = 0.60$ in the network DGEBA-DAB-TEOS. No fully condensed sterically demanding Q_4 units were found in the network contrary to a relatively high amount, $Q_4 = 0.38$, in the low molecular weight model. This is in agreement with the literature data for "aqueous" hybrids. Lavorgna et al. [13] have found that the fast epoxy network build-up hinders development of silica structures. The restriction of a silica aggregates growth by the formed epoxy network was observed also by other teams [5,16,17].

3.5. Thermomechanical properties

The thermomechanical behaviour of three epoxy networks: DGEBA-Laromin, DGEBA-D230 and DGEBA-DDM as well as the corresponding hybrids are illustrated in Figs. 6 and 7. The figures display dynamic shear storage modulus $G'(T)$ and the loss factor tan δ as functions of temperature. The properties are characterized by the glass transition temperature *Tg*, determined from the maximum of the tan δ curve, and by the modulus in rubbery state G'_r. The results are given in Table 4. All the hybrids show an increase in rubbery modulus with respect to the neat epoxy networks, however, as to the *Tg*, both increase and decrease was found. Mainly application of the coupling agent GTMS leads to a significant enhancement of the thermomechanical properties due to the strengthened interphase interaction and improved homogeneity.

Table 3
Gelation time of the selected epoxy systems and hybrids.

System	Gelation time, min
DGEBA-D230	34
DGEBA-D230-TEOS	52
DGEBA-D230-TEOS-BF_3MEA	33
DGEBA-D230-GTMS ($x = 0.2$)	46
DGEBA-D230-GTMS ($x = 0.2$)-BF_3MEA	34
D230-GTMS-BF_3MEA	97
DGEBA-DAB	5.5
DGEBA-DAB-TEOS-BF_3MEA	6.5
DAB-GTMS-BF_3MEA	13
TEOS-DAB-BF_3MEA	~240

Table 4
Conversion of the sol–gel process in the silica/SSQO domains and the thermomechanical properties of the hybrids.

Sample	α_{Si}	*Tg*, °C	G'_r, MPa[b]
DGEBA-D230		90	9.6
DGEBA-D230-TEOS	0.19	67	11.7
DGEBA-D230-TEOS-BF_3MEA	0.46	82	12.2
DGEBA-D230-TEOS[a]		58	8.1
DGEBA-D230-TEOS-BF_3MEA[a]		76	10.1
DGEBA-D230-GTMS ($x = 0.3$)		65	14.7
DGEBA-D230-GTMS ($x = 0.3$)-BF_3MEA		96	46
DGEBA-Laromin		159	22
DGEBA-Laromin-TEOS	0.63	109	22.2
DGEBA-Laromin-TEOS-BF_3MEA	0.65	160	50
DGEBA-Laromin-TEOS, "aqueous"		145	12.3
DGEBA-Laromin-GTMS ($x = 0.3$)	0.29	150	34
DGEBA-Laromin-GTMS ($x = 0.3$)-BF_3MEA	0.52	>200	
DGEBA-DDM		159	13.4
DGEBA-DDM-TEOS	0.09	109	13.7
DGEBA-DDM-TEOS-BF_3MEA	0.25	139	87.6
DGEBA-DAB-TEOS	0.54		
DGEBA-DAB-TEOS-BF_3MEA	0.60		
PGE-DAB-TEOS-BF_3MEA	0.81		

[a] Final curing temperature $T_C = 120$ °C.
[b] Rubbery modulus G'_r (T_r) determined at temperature $Tr = Tg + 40$ °C.

Fig. 6a demonstrates the effect of GTMS content and presence of BF_3MEA on the properties of DGEBA-Laromin-GTMS hybrid. The rubbery modulus expressively increases with growing content of GTMS. The *Tg* is lower in the absence of BF_3MEA however, the hybrids prepared under BF_3MEA action exhibit the broad loss factor peak tan δ and the remarkable increase in *Tg*. At the GTMS fraction $x = 0.3$ the glass transition even becomes indistinct (curve 5).

The replacement of the diepoxide DGEBA with the monofunctional epoxide GTMS leads to a decrease in the average epoxy functionality and in reduction of the epoxy network crosslinking density. Such an effect of the monofunctional monomer is demonstrated in Fig. 6b by the model epoxy network containing a fraction of the monoepoxide PGE instead of DGEBA. The increasing content of PGE results in diminution of both rubbery modulus and *Tg*. The comparison of the networks with the monoepoxides PGE and GTMS in Fig. 6a and 6b discloses the effect of the sol–gel process producing the SSQO junction domains in the case of GTMS.

An increase in modulus by incorporation of GTMS was observed also in the hybrid of a lower T_g; DGEBA-D230-GTMS in Fig. 6c. In this case, however, only a low amount of GTMS leads to a mild *Tg* growth, while at a higher GTMS content the plasticization dominates and *Tg* drops.

Synthesis of the hybrids with nanosilica generated from TEOS without the coupling agent is less efficient in properties improvement.

The comparison of the nanocomposites DGEBA-Laromin-TEOS prepared by the non-aqueous and aqueous procedures is given in Fig. 7a. The "nonaqueous" hybrid is transparent and shows better thermomechanical properties (curve 2) than the heterogeneous "aqueous" composite displaying decrease both in modulus and *Tg* (curve 3) with respect to the neat network. The "non-aqueous" hybrid exhibits an increase in modulus, however, the improvement of mechanical properties is less significant compared to the hybrid with the GTMS coupling agent. Due to a much lower extent of the covalent interfacial bonding, only a mild immobilization of the epoxy network chains by silica occurs as revealed by a slightly higher loss factor at a high temperature in rubbery region. The glass transition temperature *Tg* is not enhanced, contrary to the GTMS containing hybrid.

The crucial effect of BF_3MEA complex is illustrated in Fig. 7b. The increasing content of the complex up to 2 wt.% in the DGEBA-DDM-

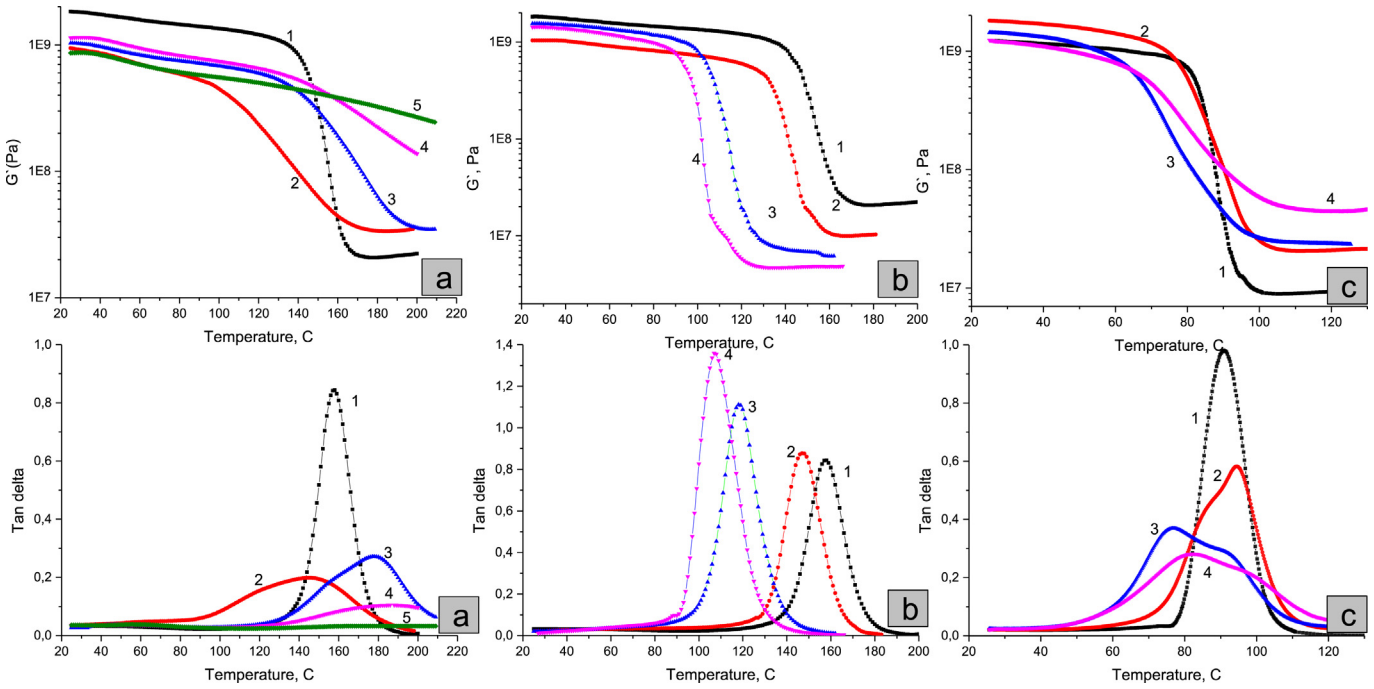

Fig. 6. Storage modulus G' and loss factor tan δ as functions of temperature: a) 1 DGEBA-Laromin, 2 DGEBA-Laromin-GTMS ($x = 0.3$), 3 DGEBA-Laromin-GTMS ($x = 0.1$)-BF_3MEA, 4 DGEBA-Laromin-GTMS ($x = 0.2$)-BF_3MEA, 5 DGEBA-Laromin-GTMS ($x = 0.3$)-BF_3MEA; b) 1 DGEBA-Laromin, 2 DGEBA-Laromin-PGE ($x = 0.1$), 3 DGEBA-Laromin-PGE ($x = 0.2$), 4 DGEBA-Laromin-PGE ($x = 0.3$); c) 1 DGEBA-D230; 2 DGEBA-D230-GTMS ($x = 0.1$)-BF_3MEA, 3 DGEBA-D230-GTMS ($x = 0.2$)-BF_3MEA, 4 DGEBA-D230-GTMS ($x = 0.3$)-BF_3MEA.

TEOS hybrid leads to a gradual enhancement of modulus by up to 560%. The growth of the modulus corresponds to a rise of siloxane conversion at increasing BF_3MEA content. However, the complex concentration ~2 wt. % seems to be optimal (curve 5) because the higher amount, 8 wt. %, results in the drop of modulus (curve 6). Moreover, contrary to the DGEBA-Laromin-TEOS the *Tg* decreases with respect to the epoxy network in the case of DGEBA-DDM based hybrid.

Fig. 7c displays the effect of curing temperature T_c on the hybrid DGEBA-D230-TEOS. The neat epoxy network is completely cured by

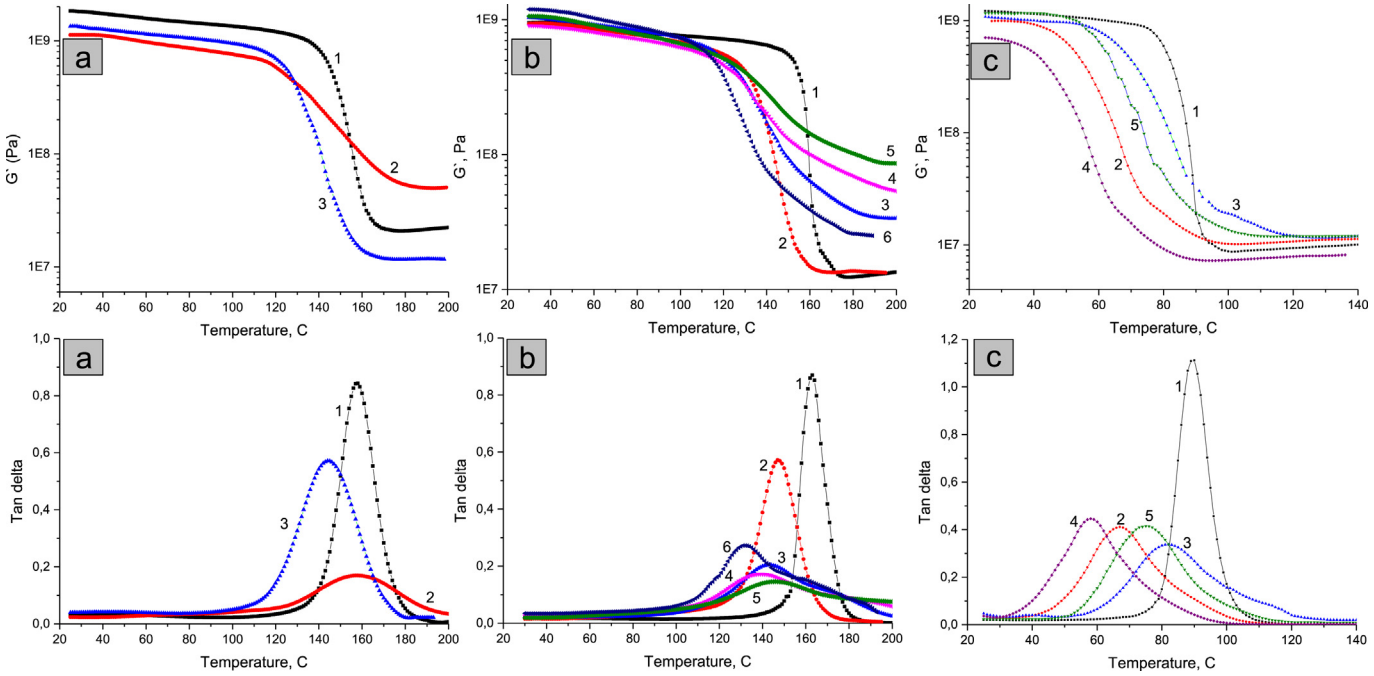

Fig. 7. Storage modulus G' and loss factor tan δ as functions of temperature: a) 1 DGEBA-Laromin, 2 DGEBA-Laromin-TEOS-BF_3MEA, 3 DGEBA-Laromin-TEOS, "aqueous"; b) 1 DGEBA-DDM, 2 DGEBA-DDM-TEOS, 3 DGEBA-DDM-TEOS-BF_3MEA(0.5%)*, 4 DGEBA-DDM-TEOS-BF_3MEA(1%)*, 5 DGEBA-DDM-TEOS-BF_3MEA(2%)*, 6 DGEBA-DDM-TEOS-BF_3MEA(8%)*; c) 1 DGEBA-D230, 2 DGEBA-D230-TEOS, 3 DGEBA-D230-TEOS-BF_3MEA; 4 DGEBA-D230-TEOS, $T_c = 120$ °C; 5 DGEBA-D230-TEOS-BF_3MEA, $T_c = 120$ °C. *Content of BF_3MEA was calculated as wt. % with respect to TEOS.

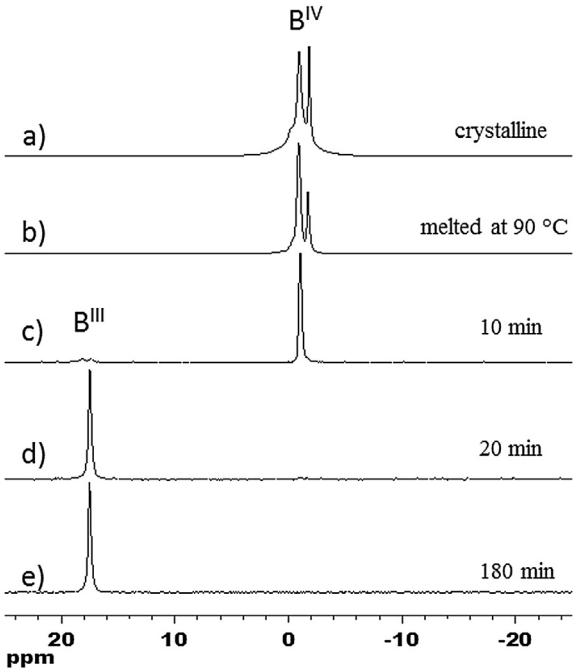

Fig. 8. ^{11}B MAS NMR spectra of $BF_3.NH_2CH_2CH_3$ a) in crystalline state; b) melted at 90 °C; and ^{11}B MAS NMR spectra of $BF_3.NH_2CH_2CH_3$/TEOS mixture recorded during the reaction of TEOS with BF_3MEA after c) 10 min, d) 20 min; e) 180 min.

heating at 120 °C for 3 h. This temperature, however, is not sufficient for the nonaqueous sol–gel condensation within a dense epoxy matrix. The hybrid cured at 120 °C shows a low glass transition temperature, Tg = 76 °C (curve 5), compared to the neat network, Tg = 90 °C (curve 1). The increasing curing temperature T_c to 190 °C and 210 °C leads to an enhancement of Tg to 82 °C (curve 3) and 95 °C, respectively, implying development of a silica phase with growing T_c. For the DGEBA-D230 based hybrid, however, the T_c = 190 °C is optimal because at a higher temperature the thermal degradation of the polyether chain containing epoxy network occurs and modulus decreases. The curing temperature effect of the nonaqueous procedure is even more pronounced in the hybrid synthesis without BF_3MEA as it is obvious from the curves 4 and 2. The application of BF_3MEA significantly decreases the necessary curing temperature.

4. Discussion

4.1. Mechanism of nonaqueous sol–gel process

The non-aqueous sol–gel process is initiated by BF_3MEA. The corresponding mechanism was studied by NMR spectroscopy. The ^{11}B NMR analysis displays that structure of BF_3MEA has been changed during the interaction with TEOS (see Fig. 8). Boron compounds usually occupy tetrahedral (B^{IV}) and trigonal (B^{III}) coordination. The ^{11}B NMR chemical shift ranges of the two boron coordinations are sufficiently well resolved, especially at high magnetic fields. The range of tetrahedral configuration is approximately from ca. 5 to −5 ppm, while trigonal configuration induces chemical shifts ranging from ca. 10 to 20 ppm [23].

The ^{11}B MAS NMR spectrum of crystalline $BF_3.NH_2CH_2CH_3$ is dominated by the asymmetric doublet (Fig. 8a), which indicates presence of nonequivalent molecules in the crystal unit. The spectral pattern is further complicated by the second order quadrupole interaction combined with dipole coupling between ^{11}B and nearest neighbour ^{19}F nuclei. The value of chemical shift of about −1 ppm corresponds with tetragonal coordination. In the melted state the signals are slightly narrowed by released molecular motion (Fig. 8b). The doubling of the signal is, however, still clearly apparent indicating that certain clusters of BF_3MEA molecules persisted. In the reaction mixture with TEOS these clusters disappeared as indicated by the single narrow signal at ca. 0 ppm (Fig. 8c). Furthermore, within 10 min of the reaction a slight signal at ca. 17.5 ppm was detected. This signal can be attributed to the

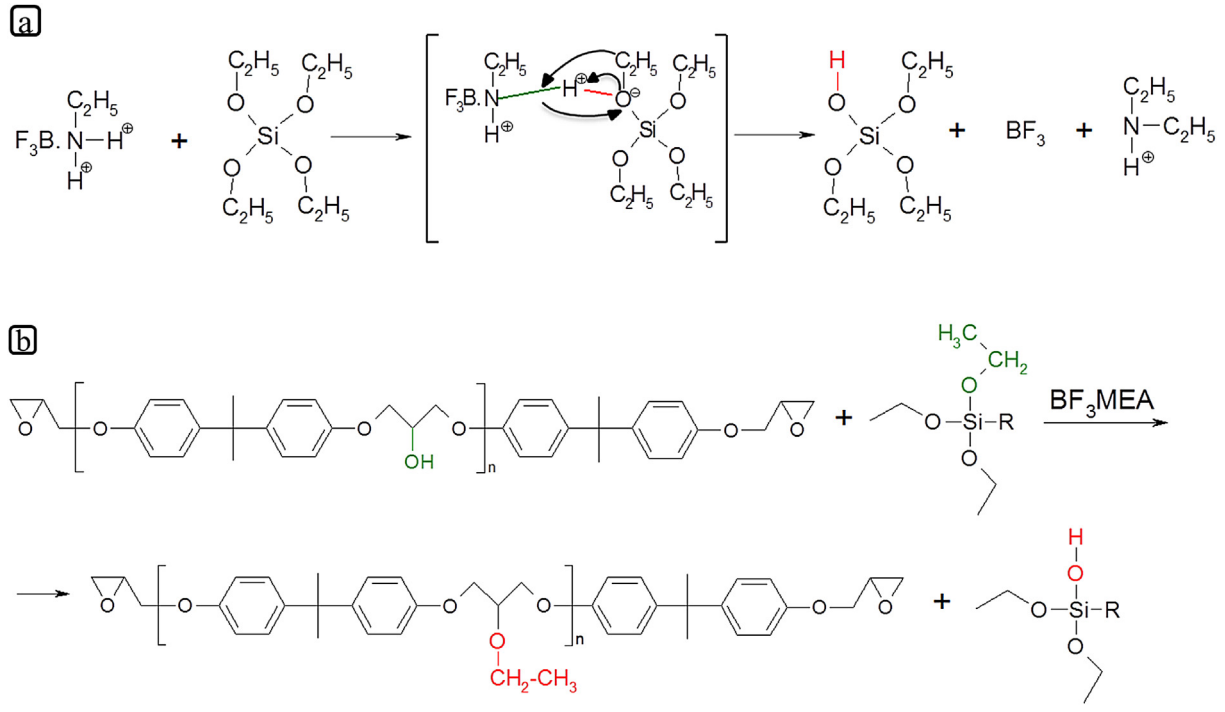

Scheme 3. Protolysis of TEOS under nonaqueous conditions by (a) BF_3MEA complex and by (b) C–OH of the epoxy resin at BF_3MEA activation.

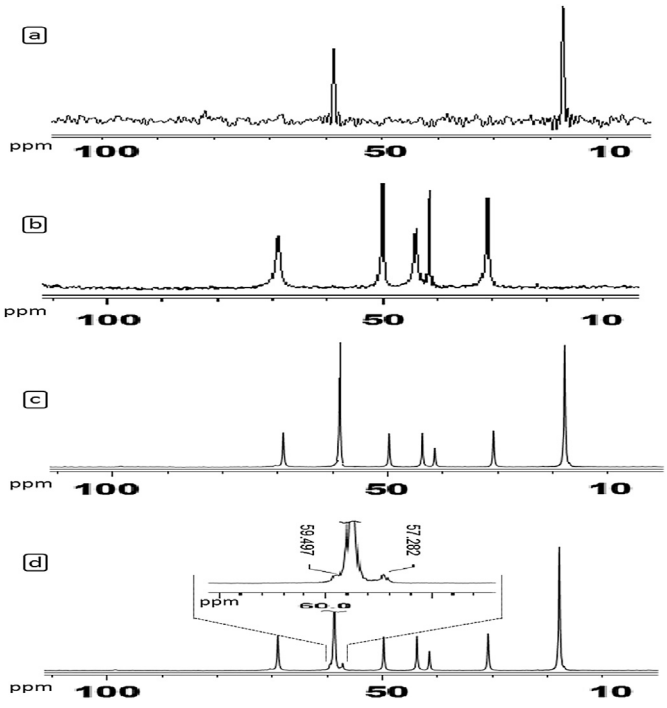

Fig. 9. ^{13}C MAS NMR spectra (a) TEOS, (b) DGEBA, (c) TEOS-DGEBA, $T = 70$ °C, $t = 1$ h, (d) TEOS-DGEBA-BF_3MEA, $T = 70$ °C, $t = 1$ h.

boron species in trigonal (B^{III}) coordination. Subsequently, the signal at 0 ppm completely disappeared while the intensity of the signal at 17.5 ppm significantly increased. This process reflecting conversion of $BF_3.NH_2CH_2CH_3$ from tetrahedral coordination (B^{IV}) to trigonal (B^{III}) coordination is finished within 20 min. No other changes in the ^{11}B MAS NMR spectra were detected during the rest of the reaction.

The results thus reveal that the BF_3MEA complex is splitted and amine released. This structure change implies that BF_3MEA acts like an initiator rather than as a catalyst. Therefore, the amount of the "hydrolysed" TEOS is very small, $\phi_{SiOH} = 0.06$. Based on the ^{11}B and ^{29}Si NMR analysis we suggest the following Scheme 3a displaying protolysis of TEOS by the complex.

Moreover, the higher extent of TEOS conversion in presence of DGEBA (see Table 2) implies that BF_3MEA activates C–OH group of the epoxy resin and promotes protolysis of TEOS by the reaction with C–OH according to the proposed Scheme 3b. This reaction proceeds only in presence of BF_3MEA thus highlighting the activation effect of the complex. The experimental evidence of the reaction was obtained by ^{13}C MAS NMR. Fig. 9 shows the spectra of the initial compounds TEOS (a) and DGEBA (b), as well as their mixtures heated at 70 °C for 1 h in the presence of BF_3MEA (d) or absence of the complex (c). No reaction occurs in the mixture TEOS + DGEBA without BF_3MEA as the spectrum (c) is a sum of the initial ones. An apparent relative increase in intensity of the DGEBA signal at 44 ppm is a result of the peak narrowing after dilution with TEOS and a corresponding higher group mobility. The integrated intensities do not change. On the contrary, in the presence of BF_3MEA, the spectrum in Fig. 9d displays changes in the area of signals $-\underline{CH_2}-O-$ at cca 60 ppm featuring the reaction in Scheme 3b. Presence of new signals at 59.5 and 57.3 ppm, in addition to the $CH_3-\underline{CH_2}-O-Si$ of TEOS, proves formation of new functional groups. In accord with semiempirical predictions of ^{13}C NMR chemical shifts (ACD/Labs program package) and the experimental data obtained for model compounds the signal at 59.5 ppm was assigned to $CH_3-\underline{CH_2}-O-CH<$ group formed by the reaction in Scheme 3b. The peak at 57.3 ppm corresponds to $CH_3-\underline{CH_2}-OH$ from ethanol produced by transesterification reaction of TEOS with COH of DGEBA.

SiOH groups formed by TEOS protolysis initiate polycondensation and development of siloxane/silica structures in the epoxy matrix (see Scheme 2). The ^{29}Si NMR analysis of the preformed siloxanes corroborates the explanation of the hybrid structure determined by SAXS. Because of a small extent of TEOS "hydrolysis" (see Table 2) the further structure growth during polycondensation proceeds by the monomer-cluster aggregation mechanism leading to compact particle-like structures with fractal dimensions $D_m \sim 3$ [3]. The protolysis of TEOS is even smaller in the absence of BF_3MEA. Therefore, the structures are even more compact in this case as determined by SAXS (Table 1). Formation of more open aggregates in the case of DGEBA-D230-TEOS is given by physical interaction of the slowly growing siloxane structures with the polyether chain of D230.

4.2. Evolution of the hybrid structure

Evolution of the hybrid formation during the reaction both in aqueous and nonaqueous conditions is schematically illustrated in Scheme 4 describing also the resulting morphology and mechanical properties.

In the aqueous two-step, acid-base, sol–gel procedure, the silica gel formation is extremely fast in the DGEBA-Laromin-TEOS mixture. The heterogeneous milky bulk gel displayed in Fig. 1a is formed within 10 s. The silica network is built much faster than the epoxy one (Scheme 4Aa) and the reaction induced separation of organic and inorganic phases takes place (Scheme 4Ab). Lack of an interphase interaction and increase in free volume by large silica aggregates could be a reason of the deterioration of mechanical properties with respect to the neat epoxy network as shown in Fig. 7a. Only strong interfacial interactions can prevent a phase separation (Scheme 4Ac) and the transparent interpenetrating network with the bicontinuous phase structure and well improved mechanical properties is formed [5,10,12,17].

The silica gel formation is slowed down by decreasing content of water due to a lower extent of hydrolysis. Small concentration of SiOH (see Table 2) initiating the polycondensation results in the lower final sol–gel conversion of the hybrids prepared under nonaqueous conditions. The slower rate of the sol–gel process, however, facilitates control of a hybrid morphology. The BF_3MEA complex stimulates the sol–gel process, while relatively slow, even at the complete water elimination. The hybrid network evolution under the nonaqueous conditions and presence of BF_3MEA is schematically described in Scheme 4B. The silica gel build-up is slower than the epoxy network formation in this case. The epoxy mixture DGEBA-DAB gels within 5 min while the silica network in the mixture TEOS-BF_3MEA-DAB is formed only in about 4 h (Table 3). However, the storage modulus $G'(t)$ in Fig. 5 rises quickly within 2 min or even less in the early stage in DGEBA-D230-TEOS-BF_3MEA (curve 3) and DGEBA-DAB-TEOS-BF_3MEA (curve 5), respectively. This increase in modulus in the pregel stage originates from the fast formation of siloxane/silica nanostructures by the polycondensation catalysed with the added amine. The modulus at a low frequency scales with the nanofiller content (v_f), $G'_0 \sim v_f^{\mu}$, where $\mu = 3.6$ at a low nanofiller concentration [24]. The rate of condensation depends on basicity of the amine. Hence, the more basic DAB compared to D230 stimulates the faster polycondensation and formation of silica aggregates resulting in a higher pregel stage modulus. The reaction is too fast in the case of DGEBA-DAB-TEOS so that the beginning of the modulus growth cannot be experimentally detected.

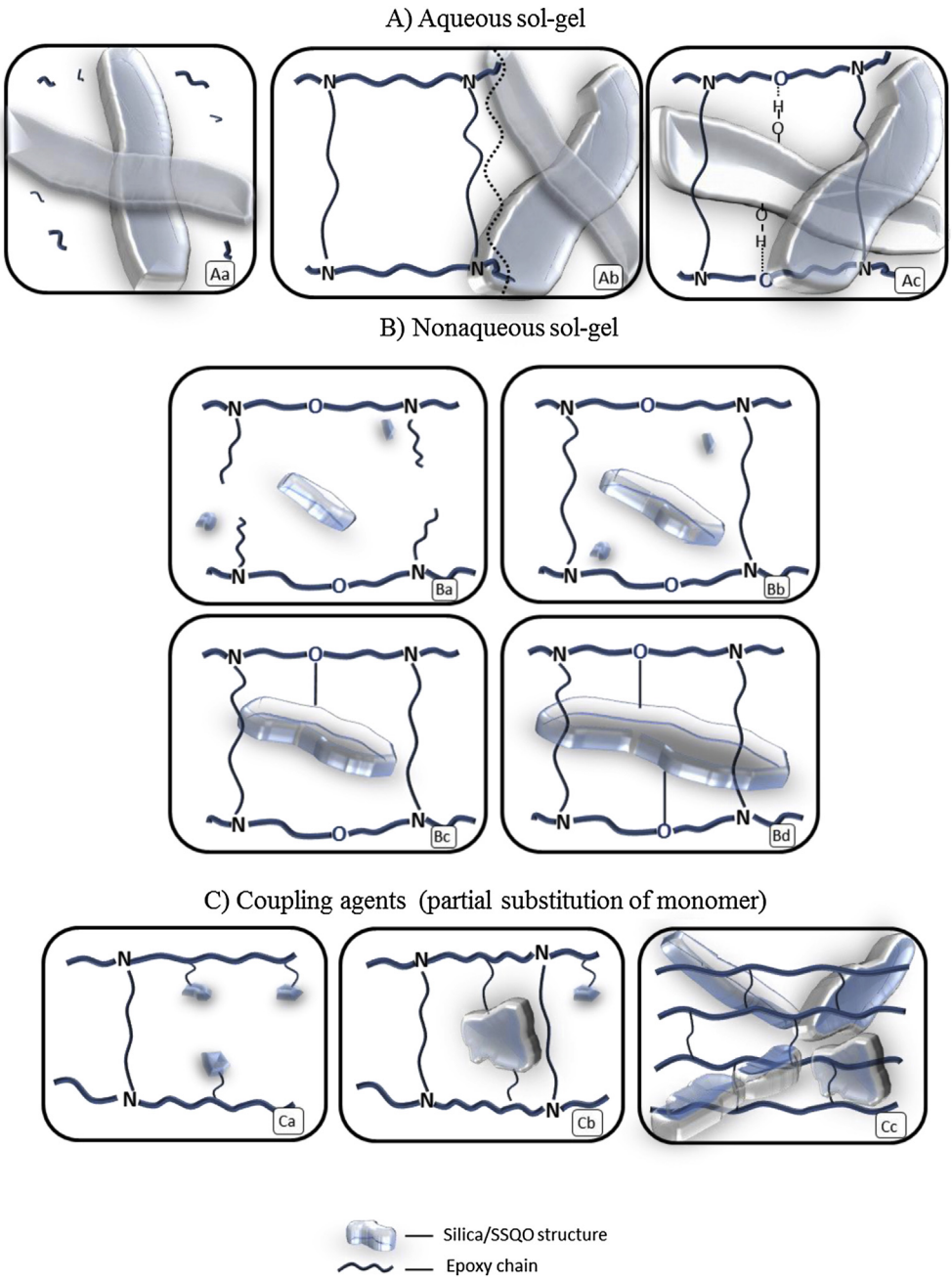

Scheme 4. Schematic description of the evolution of the epoxy-silica hybrid with in situ formed silica/SSQO. (The scheme does not correspond to real proportions; the silica structures are bigger compared to the network mesh.)

Scheme 4Ba illustrates the early pregel stage involving formation of the branched polyepoxy chains and siloxane/silica nanostructures. The fast formation of the silica nanodomains catalysed with the amine in the early stage can be compared to the extremely fast polycondensation in the aqueous two-step, acid-base sol–gel systems [10,11]. In that case, TEOS was completely hydrolysed in the first "acid" step [5,10,13,17] and the polycondensation resulted in the fast silica gelation. Under the nonaqueous conditions, however, no bulk gel but only small nanostructures are formed. The reason consists in the low amount of SiOH. The initial small fraction of silanols, $\phi_{SiOH} = 0.11$, formed in the first step, is quickly consumed during the fast early polycondensation. As a result, the polycondensation and the structure growth as well as modulus evolution slow down in the later pregel stage (see Fig. 5). The new SiOH are only gradually produced by the reaction of TEOS with C–OH of the epoxy-amine reaction products and by hydrolysis of TEOS with water released during condensation. The resulting much smaller extent of polycondensation compared to the "aqueous system", is not sufficient for a silica gel formation. Therefore, the hybrid gelation sets in by formation of the epoxy network (Scheme 4Bb).

However, why does BF_3MEA accelerate the hybrid gelation as shown in Fig. 5? BF_3MEA is known to catalyse cationic homopolymerization of epoxies [25–29]. In our case, the dynamic DSC scan shows an additional small exotherm shoulder in the curing of hybrids in presence of BF_3MEA. This exotherm, possibly related to the homopolymerization, however, appears only at a late reaction stage. The homopolymerization thus is operative only in the post-gel stage under our reaction conditions and does not affect a rate

of gelation. We have excluded also the possible catalytic effect of silanols on the epoxy-amine kinetics, because of their small concentration.

Obviously, it is the formation of silica structures under BF_3MEA action, which plays a role in affecting gelation. However, silica gel is formed from TEOS very slowly under these conditions as mentioned above. Consequently, we suppose that the crucial effect consists in producing a covalent bond between silica structures and the epoxy matrix as illustrated in Scheme 4Bc. The epoxy-silica grafting then leads to crosslinking of the epoxy chains by silica domains (see Scheme 4Bd). Such a crosslinking can be responsible for the observed acceleration of the hybrid gelation by BF_3MEA in case of occurring even to a small extent already in the early pregel stage. The epoxy-silica bonding is produced by the reaction of SiOH in the silica structure and C–OH formed by the reaction of an epoxy with amines or being present in the initial epoxy resin. This reaction shown in Scheme 5 is the topic often discussed and proved in literature [4,5,20,30,31].

In order to prove this interphase bonding and crosslinking by the silica domains we have studied the model diepoxy-monoamine system producing only the linear poly(epoxy-amine) chain with pendant C–OH groups. The mixture DGEBA-butylamine-TEOS serving as the linear model for DGEBA-DAB network, was found to form the transparent gel in 25 min, but only in the presence of BF_3MEA. No epoxy-amine network can be built in this linear system and the silica gel formation is much slower as shown above. One can conclude that the gelation of the model system takes place by the BF_3MEA promoted C–OH + SiOH interphase reaction resulting in crosslinking the linear polyepoxy chains by the formed silica structures.

4.3. Hybrid morphology and thermomechanical properties

Scheme 4Bc shows the growth of the silica structures within the epoxy network and formation of a covalent bonding to the epoxy matrix. The interface grafting leads to the system compatibilization and precludes the phase separation that occurs in the "aqueous" system. Crosslinking of the epoxy chains by silica domains, as in Scheme 4Bd, contributes to increase in rubbery modulus of the hybrid (Fig. 7, Table 4). The nanocomposite exhibits the homogeneous particulate type morphology with silica nanofiller dispersed in and partially grafted to the epoxy matrix. Two effects are responsible for the modulus enhancement; (a) the hydrodynamic reinforcing effect of nanofiller proportional to its volume fraction, which is typical of the particulate composites and usually is expressed by the modified Kerner–Nielsen model [32], and (b) interphase additional crosslinking of the epoxy network by the silica nanodomains.

Both effects depend on sol–gel conversion α_{Si} in silica structures. A low conversion results in formation of undercured soft flexible silica/siloxane domains leading to plasticization of a system and decrease in *Tg* as well as modulus. Content of BF_3MEA catalyst (i), basicity of the curing amine (ii) and the curing temperature (iii) are the most important factors governing α_{Si} and the mechanical properties of the hybrids. (i) Increase in the catalyst content in DGEBA-DDM-TEOS hybrid leads to enhancement of modulus (Fig. 7b). Too high amount of BF_3MEA, however, promotes the noticeable nanocomposite heterogeneity due to formation of large silica aggregates as described above (Section 3.2). The large aggregates show a smaller volume fraction and a smaller interfacial surface area resulting in a lower extent of the interphase crosslinking and diminishing of modulus (Fig. 7b, curve 6). (ii) Due to a low DDM basicity the sol–gel conversion is rather small (see Table 4) and the NMR analysis discloses a high fraction of the unreacted TEOS, $Q_0 = 0.40$, even at a high BF_3MEA concentration. As a result, the corresponding hybrid shows a low *Tg* due to plasticization by low molecular weight species in contrast to the more basic Laromin based system (Fig. 7b and 7a). (iii) The effect of curing temperature on conversion and mechanical properties displayed in Fig. 7c was described above (Section 3.5). The results reveal that the sol–gel process requires a much higher reaction temperature than the epoxy-amine network in order to sufficiently cure silica structures within the hybrid. It was shown that neither 190 °C is sufficient for a silica phase to be well cured. Therefore, the hybrids based on the thermally more stable networks (than the D230 based ones) with Laromin and DDM were cured at 210 °C.

4.4. Hybrid with the coupling agent

Scheme 4C displays an evolution of the hybrids containing the coupling agent. The structure growth proceeds by the simultaneous incorporation of GTMS in the poly(epoxy-amine) chain and the sol–gel reactions to form the SSQO domains [33] taking place only in the presence of BF_3MEA (Scheme 4Ca). The monoepoxide GTMS replacing the diepoxide DGEBA decreases an average functionality of the diepoxy-diamine system. The critical conversion for gelation of the system thus increases [34] leading to delay of the epoxy gel formation as observed for DGEBA-D230-GTMS in the absence of BF_3MEA (Table 3). The complete replacement of DGEBA by GTMS inhibits formation of an epoxy network at all. Despite this fact the mixture GTMS-D230 gels in presence of BF_3MEA by the sol–gel producing SSQO structures and building the network with SSQO junction domains [22,33]. Gelation of GTMS-D230, however, is slow (Fig. 5, Table 3) thus disclosing that formation of the SSQO junctions by the sol–gel process is slower compared to the epoxy-amine reactions to form the epoxy network. Nevertheless, in the DGEBA-D230-GTMS hybrid, such an additional crosslinking through SSQO structures in presence of BF_3MEA accelerates the hybrid gelation.

The epoxy network is formed in Scheme 4Cb and bridging the epoxy chains by the SSQO junctions contributes to the crosslinking and enhancement of rubbery modulus (Fig. 6a, Table 4). *Tg* of the hybrid prepared in the absence of BF_3MEA (Fig. 6a curve 2, Table 4) or cured at a low curing temperature (Fig. 6c), however, decreases due to a low sol–gel conversion (Table 4) and plasticization by flexible undercured siloxane/SSQO structures. The BF_3MEA

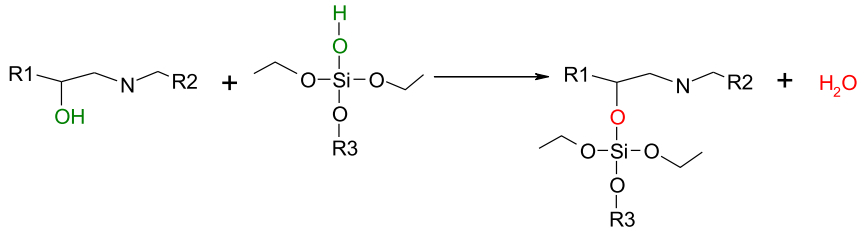

Scheme 5. Bonding between epoxy network and silica phase.

catalysis leads to a higher siloxane conversion and a significant increase in *Tg* of the hybrids (Fig. 6a, Table 4). The strong interphase interaction and immobilization of the epoxy network chains by hard SSQO structures are responsible for this *Tg* enhancement. At a high enough GTMS content the SSQO domains percolate through the system and the bicontinuous morphology with the epoxy and SSQO networks is formed as shown in Scheme 4Cc. The build-up of the SSQO network is in agreement with a high fraction of T_3 units determined by NMR ($T_3 = 0.12$). Transition from the particulate to the bicontinuous organic-inorganic morphology leads to a dramatic increase in modulus and *Tg* (Fig. 6a, curve 5). Similar transition from the particulate nanocomposite to the hybrid containing continuous SSQO phase with increasing GTMS content was found also in the "aqueous" system GTMS-Jeffamine D2000 [22,33].

The effect of curing temperature explains the *Tg* decrease in DGEBA-D230-GTMS at a higher GTMS content (Fig. 6c, curves 3 and 4) unlike the remarkable increase in the Laromin based hybrid in Fig. 6a. The "D230 hybrid" was cured at a lower temperature, 190 °C, compared to 210 °C for the "Laromin hybrid". The curing temperature clarifies also the contradictory results from literature as to the "aqueous" hybrids. Macan et al. [14] and Lavorgna et al. [13] observed plasticization of the DGEBA-D230 network by the sol–gel products while Beneš et al. [7] reported an increase in *Tg* in the corresponding hybrids prepared by the solvent-free technique using water vapour. The former hybrids were cured at 120 °C or 150 °C, respectively, and the curing temperature 180 °C was applied in the latter case.

Structure and morphology are crucial for mechanical properties of the hybrids. In addition to the phase structure, mainly the interphase interaction, grafting and crosslinking result in enhancement of mechanical properties. Moreover, we have proved the effect of BF_3MEA amount, of an amine basicity and the curing temperature on the sol–gel conversions as well as the effect of an epoxy matrix and its thermal stability. Consequently, the hybrid optimization comprises composition and structure of both inorganic and epoxy phases, the reaction conditions as well as presence of the initiator BF_3MEA.

5. Conclusions

The nonaqueous synthesis results in formation of the epoxy-silica hybrids of improved homogeneity and enhanced thermomechanical properties compared to the systems prepared under the classical "aqueous" sol–gel procedure. Mechanism of TEOS protolysis initiating the nonaqueous sol–gel polycondensation is suggested. The generation of silica structures at the nonaqueous process is slower thus facilitating a better control of the hybrid structure and morphology. Evolution of the hybrid structure during the two-step non-aqueous procedure consists of the following stages; (i) initiation of the sol–gel reactions of TEOS by BF_3MEA complex and by C–OH groups of the epoxy resin, (ii) formation of siloxane structures after admixing of an amine, (iii) gelation of the epoxy network, (iv) epoxy-silica grafting and the hybrid crosslinking through the formed silica/SSQO domains, (v) percolation of the SSQO structures in case of a high GTMS content.

The slow silica structure formation and the epoxy-silica interphase bonding, proved by the model system, prevent phase separation and improve the homogeneity as well as mechanical properties. The coupling agent GTMS further enhances the system compatibility. At a higher GTMS content the SSQO structures percolate and bicontinuous phase morphology with the strong interphase interaction is formed. The homogeneous transparent hybrid DGEBA-Laromin-GTMS displays a significant increase in *Tg* with increasing GTMS amount up to the material with the completely indistinct glass transition.

Due to a slow silica structures development the epoxy network formation is faster making thus steric hindrance to a further silica growth within the dense network. As a result, the final sol–gel conversions are low. In order to overcome this limitation the main factors governing the hybrid structure and final properties must be taken into account; (a) presence of an optimum content of the BF_3MEA complex, (b) relatively high amine basicity promoting the polycondensation to reach a high conversion, (c) presence of a proper amount of GTMS, guaranteeing an enhanced interphase interaction, and (d) high curing temperature *Tc* well above the typical one applied for the curing a neat epoxy network.

Acknowledgements

The authors acknowledge the financial support of the Grant Agency of the Czech Republic (P108/12/1459) and the Academy of Sciences for support in the frame of the Program of international cooperation (M200500903).

References

[1] Ye S, Deng I, Friedrich K. J. Mater. Sci. 2007;42:2766–74.
[2] Merhari L. Hybrid nanocomposites for nanotechnology: electronic, optical, magnetic and biomedical applications. New York: Springer; 2009.
[3] Brinker JC, Scherer GW. Sol-gel science: the physics and chemistry of sol-gel processing. New York: Academic Press; 1990.
[4] Ochi M, Takahashi R. J Polym Sci Part B: Polym Phys 2001;39:1071–84.
[5] Matějka L, Dukh O, Kolařík J. Polymer 2000;41:1449–59.
[6] Matějka L. In: Epoxy polymers: new materials and innovation. Weinheim, Germany: Wiley VCH Verlag GmbH&Co.; 2010.
[7] Beneš H, Galy J, Gerard JF, Pleštil J, Valette L. J Appl Polym.Sci 2012;125(2):1000–11.
[8] Landry CJT, Coltrain BK, Brady BK. Polymer 1992;33:1486–95.
[9] Mascia L, Tang T. J Mater Chem 1998;8:2417–21.
[10] Matějka L, Dušek K, Pleštil J, Kříž J, Lednický F. Polymer 1999;40:171–81.
[11] Matějka L, Dušek K, Pleštil J. J Noncryst Sol 1998;226:114–21.
[12] Mascia L, Prezzi L, Haworth B. J Mater Sci 2006;41:1145–55.
[13] Piscitelli F, Lavorgna M, Buonocore GG, Verdolotti L, Galy J, Mascia L. Macromol Mater Eng 2012. http://dx.doi.org/10.1002/mame.201200222.
[14] Macan J, Ivankovic H, Ivankovic H, Mencer HJ. J Appl Polym Sci 2004;92:498–505.
[15] Špírková M, Brus J, Hlavatá D, Kamišová H, Matějka L, Strachota A. J Appl Polym Sci 2004;92(2):937–50.
[16] Davis SR, Brough AR, Atkinson A. J Non-Cryst Sol 2003;315:197–205.
[17] Wen J, Mark JE. Rub Chem Tech 1994;67:807.
[18] Niederberger M, Pinna N. In: Metal oxide nanoparticles in organic solvents synthesis, formation, assembly and application. London: Springer; 2009.
[19] Hay JN, Raval HM. Chem Mater 2001;13:3396–403.
[20] Lee T-M, Ma C-CM. J Polym Sci Polym Chem 2005;44:757–68.
[21] Winter HH, Mours M. Adv Polym Sci 1997;134:165–234.
[22] Matějka L, Dukh O, Kamišová H, Hlavatá D, Špirková M, Brus J. Polymer 2004;45:3267–76.
[23] MacKenzie KJD, Smith ME. Pergamon. In: Multinuclear solid-state NMR of inorganic material 2002.
[24] Kotsilkova R. Thermoset nanocomposites for engineering applications. Shropshire, UK: Smithers Rapra Technology Lim.; 2007.
[25] Morio K, Murase H, Tsuchiya H, Endo T. J Appl Polym Sci 1986;32:5727–32.
[26] Akatsuka M, Takezawa Y, Amagi S. Polymer 2001;42:3003–7.
[27] Li Y-S, Li M-S, Chang F-C. J Polym Sci Polym Chem 1999;37:3614–24.
[28] Chabanne R, Tighzert L, Pascault J-P, Bonneto B. J Appl Polym.Sci 1993;49:685–99.
[29] Matějka L, Chabanne P, Tighzert L, Pascault J-P. J Polym Sci Polym Chem 1994;32:1447–58.
[30] Bauer BJ, Liu DW, Jackson CL, Barnes JD. Polym Adv Technol 1996;7:333–9.
[31] Fasce DP, Williams RJJ, Mechin F, Pascault JP, Lauro MF, Pétiaud R. Macromolecules 1999;32:4757–63.
[32] Nielsen LE, Landel RF. In: Mechanical properties of polymers and composites. New York: Marcel Dekker; 1994.
[33] Matějka L, Dukh O, Meissner B, Hlavata D, Brus J, Strachota A. Macromolecules 2003;36:7977–85.
[34] Stockmayer WHJ. J Polym Sci 1952;9:69–71.

Journal of Applied Polymer Science

High-T_g, Heat Resistant Epoxy–Silica Hybrids with a Low Content of Silica Generated by Nonaqueous Sol–Gel Process

Sergii Ponyrko,[1] Jana Kovářová,[2] Libor Kobera,[3] Libor Matějka[1]

[1]Department of Nanostructured Polymers and Composites, Institute of Macromolecular Chemistry, Academy of Sciences of the Czech Republic, Heyrovský Sq. 2, Prague, Czech Republic

[2]Department of Polymer Processing, Institute of Macromolecular Chemistry, Academy of Sciences of the Czech Republic, Heyrovský Sq. 2, Prague, Czech Republic

[3]Department of NMR Spectroscopy, Institute of Macromolecular Chemistry, Academy of Sciences of the Czech Republic, Heyrovský Sq. 2, Prague, Czech Republic

Correspondence to: L. Matějka (E-mail: matejka@imc.cas.cz)

ABSTRACT: The epoxy-silica hybrids showing high T_g and thermal stability are prepared by the non-aqueous sol–gel process initiated with borontriflouride monoethylamine. Tetramethoxysilane (TMOS) is used as a precursor of silica and 3-glycidyloxypropyl trimethoxysilane as a coupling agent to strengthen the interphase interaction with an epoxy matrix. The basic factors governing the nonaqueous sol–gel process are studied in order to reveal the formation–structure–properties relationships and to optimize the hybrid composition as well as conditions of the nonaqueous synthesis. The formation of the hybrid, its structure, thermomechanical properties and thermal stability are followed by chemorheology experiments, NMR, DMA and TGA. The most efficient reinforcement of the epoxy network is achieved by the combination of both alkoxysilanes, showing synergy effects. The hybrids with a low content (~10 wt %) of the *in situ* generated silica exhibit dramatic increase in T_g and the high modulus, 335 MPa, up to the temperature 300°C.
 J. Appl. Polym. Sci. **2014**, *131*, 40899.

KEYWORDS: glass transition; mechanical properties; nanostructured polymers; structure-property relations; thermal properties

Received 19 November 2013; accepted 17 April 2014
DOI: 10.1002/app.40899

INTRODUCTION

Organic–inorganic nanocomposites have drawn a considerable attention in polymer science in last decades. Among the organic matrices the epoxy thermosets are most widely used due to excellent mechanical and thermal properties. Epoxy resin based organic-inorganic hybrid materials can be employed as tough, transparent and anti-scratch polymer films with good mechanical properties and thermal stability. As to the inorganic filler, silica tends to be the most suitable for epoxy resins. The epoxy-silica nanocomposites are often applied systems and their curing behavior, morphology, mechanical and thermal properties are well investigated.[1–4] Homogeneous dispersion of silica nanoparticles in an epoxy medium, however, brings about crucial synthetic problems. Therefore, silica generated *in situ* by a sol–gel technique has gained a reputation to be a convenient and cost-effective method.[5] The sol–gel process is used for the preparation of epoxy–silica nanocomposites of good homogeneity and improved properties.[6–13] Synthesis and properties of polymer–silica hybrids, prepared both from preformed silica and by the sol–gel process, have been recently reviewed by Zou et al.[14]

Epoxy–silica nanocomposites show high thermal stability and good mechanical properties at high temperatures, which is an important property for a high performance application, electronic packaging industry, coatings etc. Moreover, the coupling agents are often used to strengthen an interfacial interaction and enhance the properties.[15–18] Wang et al.[19,20] prepared heat resistant epoxy-silica hybrids based on diglycidyl ether of Bisphenol A (DGEBA)—diaminodiphenyl sulfone (DDS) epoxy matrix and silica nanoparticles. The great improvement of properties was achieved by using the coupling agent glycidyloxypropyl trimethoxysilane (GTMS). The glass transition temperatures T_g of the hybrids raised with GTMS amount up to 250°C and the modulus above glass transition maintained a very high value up to 300°C. At 30% silica content the hybrid T_g became indistinct. Moreover, the hybrid thermostability determined by TGA was improved. Also Ochi et al.[7,21] reported a significant enhancement of thermomechanical properties of the DGEBA based epoxy network with silica formed by the sol–gel process from GTMS or tetramethoxysilane (TMOS). The epoxy–silica hybrids with GTMS exhibited a strong interphase interaction, increase in the modulus and disappearance of the

Table I. Designation and Compositions of the Hybrids

Designation	Content of TMOS/TEOS (%)	Fraction of GTMS, *x*	Theoretical equivalent of silica (%)
DGEBA-Laromin-TMOS(7), BF_3MEA	7	-	2.6
DGEBA-Laromin-TMOS(14), BF_3MEA	14	-	5.4
DGEBA-Laromin-TMOS(25), BF_3MEA	25	-	9.6
DGEBA-Laromin-TMOS(40), BF_3MEA	40	-	15.2
DGEBA-Laromin-TMOS(60), BF_3MEA	60	-	23.2
DGEBA-Laromin-GTMS(0.1), BF_3MEA	-	0.1	2.2
DGEBA-Laromin-GTMS(0.2), BF_3MEA	-	0.2	4.4
DGEBA-Laromin-GTMS(0.3), BF_3MEA	-	0.3	6.6
DGEBA-Laromin-TMOS(14)-GTMS(0.2), BF_3MEA	14	0.2	9.8
DGEBA-Laromin-TEOS(18), BF_3MEA	18	-	5.4

glass transition at a silica content ~10 wt %. It should be mentioned that the complete vanishing of a glass transition at such low filler content is exceptional.

The sol–gel process consisting of hydrolytic polycondensation of alkoxysilane precursors provides significant benefits in synthesis of hybrids, however, also some shortcomings. The process requires solvents to be used because of incompatibility of alkoxysilanes with water and an epoxy system. The solvent and water evaporation during polymerization results in sample shrinkage and a removal of residual volatiles from the reaction mixture could lead to formation of bubbles or cracks in the final product. These problems can be eliminated by application of the solvent-free non-aqueous sol–gel procedure. Lee and Ma[22] synthesized the nanosilica from tetraethoxysilane (TEOS) by nonaqueous sol–gel process in the epoxy matrix DGEBA-DDS catalyzed with borontrifluoride monoethylamine (BF_3MEA). Recently we have used the Lee's approach to prepare the epoxy–silica hybrids by the nonaqueous sol–gel process and investigated the basic conditions of the nonaqueous procedure.[23] The silica was generated *in situ* from the most common alkoxysilane precursor, TEOS, by using BF_3MEA as an initiator. The initiation mechanism of the non-aqueous process was proposed to involve protolysis of TEOS with BF_3MEA and/or OH groups which are present in the epoxy resin. The sol–gel reactions are relatively slow under nonaqueous conditions thus making possible to control the silica structure evolution and to prevent a phase separation that often occurs during the fast classical "aqueous" sol–gel process. As a result, homogeneous transparent hybrids were prepared. Moreover, GTMS was applied to further improve system homogeneity by interphase grafting. These epoxy–silica hybrids exhibited an enhancement of thermomechanical properties. Nevertheless, a limitation of the nonaqueous sol–gel process exists due to a low TEOS reactivity under nonaqueous conditions leading to an incomplete curing and formation of undercured silica/siloxane domains in the hybrids. This fact resulted in poor mechanical properties in the systems prepared without the coupling agent.

The aim of this article consists in the non-aqueous synthesis of the epoxy-silica hybrids with greatly enhanced thermomechanical properties and thermal stability by overcoming the problems related to an incomplete curing. Instead of TEOS, the more reactive tetramethoxysilane (TMOS) precursor of silica was used, while a structure evolution was still under control so that well homogeneous transparent systems were produced. In addition, an investigation of the factors governing the nonaqueous sol–gel process was performed in order to reveal the formation–structure–properties relationships. These results facilitated optimization of the hybrid synthesis. The coupling agent GTMS was used to strengthen an interphase interaction by covalent bonding with an epoxy matrix. The epoxy network DGEBA—cycloaliphatic diamine (Laromin) was employed as a matrix for synthesis of transparent high-T_g epoxy-silica hybrids showing a high thermal stability.

EXPERIMENTAL

Materials

The diglycidyl ether of Bisphenol A (DGEBA) based resin, Epilox A 19-03 (Aldrich) with the equivalent weight of the epoxy groups $E_E = 187$ g mol^{-1} epoxy groups was used. The following amines were applied as curing agents; 3,3′-dimethyl-4,4′-diaminocyclohexylmethane (Laromin® C 260) was received from BASF and poly(oxypropylene)diamine—Jeffamine® D230 (M~230) (Aldrich). Inorganic components: tetramethoxysilane (TMOS) and 3-glycidyloxypropyl trimethoxysilane (GTMS) were purchased from Fluka. Borontrifluoride monoethylamine (BF_3MEA) was obtained from the Aldrich. All chemicals were used without a further purification.

Synthesis of the Hybrid

The epoxy-amine networks were prepared at a stoichiometric ratio of functional groups (C_{epoxy}:C_{NH} = 1 : 1) and the hybrids were synthesized by the modified two step Lee's synthesis procedure.[22] (i) 2 wt % of BF_3MEA with respect to TMOS was mixed with the epoxy resin for 30 min at 70°C. After that, the specified amount of TMOS, e.g., 14 wt % (with respect to DGEBA) was added to the epoxy-BF_3MEA mixture and speedily mixed for 1 h. All the systems were mixed under weak inert conditions. (ii) Stoichiometric equivalent weight of amine was added to the prereacted mixture of TMOS in the epoxy resin and mixed for 20 min.

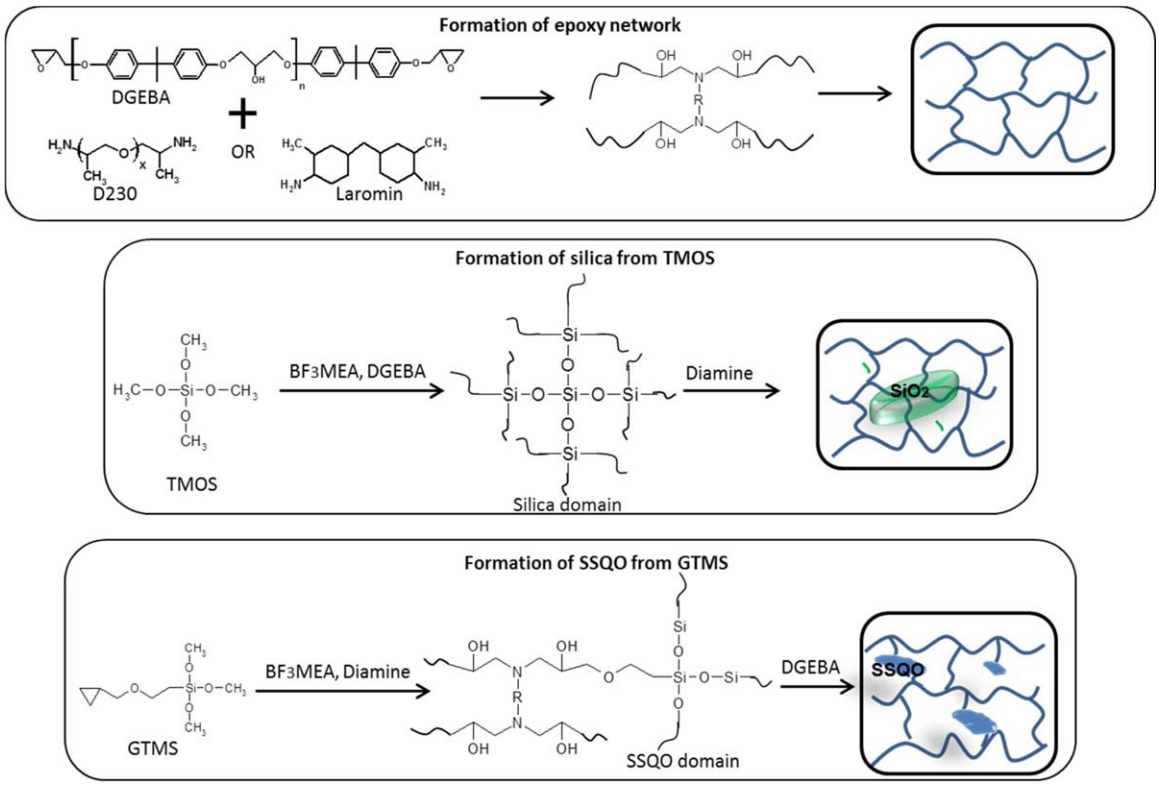

Scheme 1. Formation of the epoxy-silica hybrid with *in situ* formed silica/silsesquioxane (SSQO) domains. [Color figure can be viewed in the online issue, which is available at wileyonlinelibrary.com.]

The hybrids modified with the coupling agent GTMS were prepared by substituting a fraction of DGEBA by GTMS while keeping the epoxy groups concentration constant and the total ratio of epoxy and NH functionalities stoichiometric. The content of GTMS (x) in the nanocomposite synthesis was characterized by fraction of epoxy groups of DGEBA replaced by the coupling agent GTMS: x = [epoxy (GTMS)]/[epoxy (DGEBA) + epoxy (GTMS)] and was varying from 0.1 up to 0.3.

The following curing regime of the sample in inert atmosphere or in the mold was applied: 90°C for 2 h; 130°C for 16 h and the postcuring for 5 h at 190°C in case of D230 and 5 h at 210°C for Laromin. In the special case of the reaction under the air atmosphere the sample was prereacted in the air at 25°C for 2 h.

The hybrids designation indicates the type of epoxy network, content of alkoxysilanes used and alternatively presence of the initiator BF_3MEA during synthesis, e.g. DGEBA-Laromin-TEOS(14)-GTMS(0.1), BF_3MEA shown in Table I.

The schematic structural description of the epoxy network and nanocomposites formation is shown in Scheme 1.

METHODS

Nuclear Magnetic Resonance Spectroscopy (NMR)

Solid-state ^{29}Si CP/MAS NMR experiments were measured at 11.7 T using a Bruker Avance 500 WB/US NMR spectrometer with double-resonance 4-mm and 7-mm probeheads, respectively. To compensate for frictional heating of the spinning samples, all NMR experiments were measured under active cooling. The sample temperature was maintained at 308 K. The ^{29}Si CP/MAS NMR spectra were acquired at 99.325 MHz; spinning frequency was $\omega r/2\pi = 5$ kHz; the number of scans was 2048; spin lock 4 ms and recycle delay was 3s. The spectra were referenced to *M8Q8* (−109.8 ppm). During detection, a high-power dipolar decoupling (TPPI) was used to eliminate strong heteronuclear dipolar coupling.

The condensation conversion α_{Si} was determined as $\alpha_{Si} = \Sigma i Q_i/4$. Q_i is the mole fraction of the Q_i structure units with i siloxane bonds Si—O—Si attached to the central silicon. The relative amount of the structural units was obtained from the deconvolution of the ^{29}Si CP/MAS NMR spectra. The assignment of the NMR bands is as follows: Q_0 from −80.6 to −84.7 ppm, Q_1 from −84.9 to −87.28 ppm, Q_2 from −89.7 to −91.6 ppm, Q_3 from −100.0 to −101.5 ppm, Q_4 from −105.9 to −110.0 ppm.

Dynamic Mechanical Analysis (DMA)

Dynamic mechanical properties of the nanocomposites were tested using the ARES G2 apparatus (TA Instruments). An oscillatory shear deformation at the constant frequency of 1 Hz and at the heating rate of 3°C min^{-1} was applied.

ARES G2 rheometer was used also for the chemorheology experiments to follow molecular structure evolution and gelation during polymerization. Oscillatory shear deformation in parallel plates geometry at a frequency of 1 Hz was used. The initial applied maximum strain was 200% while keeping torque below 20 g cm to prevent breaking of the formed gel.

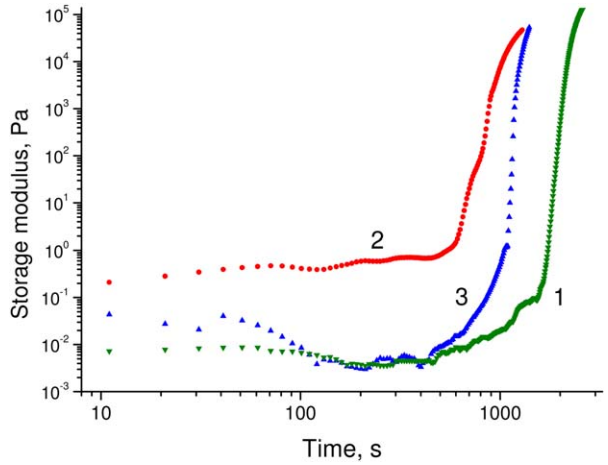

Figure 1. Shear storage modulus $G'(t)$ of the studied systems as a function of time during polymerization at $T = 80°C$: 1 DGEBA-D230, 2 DGEBA-D230-TMOS,BF_3MEA, 3 DGEBA-D230-TMOS. [Color figure can be viewed in the online issue, which is available at wileyonlinelibrary.com.]

The gel point was determined by using the multifrequency sweep measurement ranging from 1 to 64 rad s^{-1} and applying a power-law rheological behavior at the critical state, $G'(\omega) \sim G''(\omega) \sim \omega^n$.[24] The loss factor tan δ is independent of measurement frequency at the gel point and therefore, the gelation was evaluated as a crossover of the tan δ for different experimental frequencies during the polymerization.

Thermogravimetric Analysis (TGA)

TGA measurements were performed on Perkin Elmer Thermogravimetric Analyzer Pyris 1 in air atmosphere. The temperature interval of measurements was 30–880°C, with gradual temperature rise of 10°C min^{-1} and gas flow 50 mL min^{-1} on samples of ~10 mg.

RESULTS AND DISCUSSION

We have studied the epoxy-silica hybrids prepared by the nonaqueous sol–gel procedure initiated by BF_3MEA. The alkoxysilanes TMOS and GTMS were employed for *in situ* generation of nanosilica and grafting of inorganic structures to an epoxy matrix. A comparison with the TEOS based hybrids studied previously[23] is included in order to highlight the TMOS benefits. Two types of epoxy-amine systems were used as hybrid matrices. The DGEBA-Laromin network, involving cycloaliphatic diamine, was used as a high-T_g matrix for the synthesis of high-performance hybrids. In addition, the model low-T_g DGEBA-Jeffamine D230 system, containing amino-terminated polyether D230, was employed to study the hybrid structure evolution and factors governing the non-aqueous sol–gel process in order to disclose relationships between reaction conditions, the hybrid structure and hybrid properties.

Thermomechanical properties of hybrids and their thermal stability were followed by DMA and TGA, respectively.

Formation of Epoxy-Silica Nanocomposites

Structure evolution at formation of the epoxy-silica hybrid under the nonaqueous conditions was monitored by chemorheology. Figure 1 shows the rise of the storage modulus during build-up of the epoxy network DGEBA-D230 (curve 1) and the hybrid DGEBA-D230-TMOS (curves 2 and 3). The steep increase in the modulus indicates gelation of the mixture and the gel times are given in Table II. Figure illustrates that the gelation sets in earlier in the hybrids than in the neat epoxy network. Moreover, the hybrid network formation is faster if the sol–gel process is initiated with BF_3MEA (curve 2). It was proved[23] that the acceleration of the network build-up results from the covalent bonding between the formed silica and epoxy structures. Table II includes for comparison also the gel times of the previously studied "TEOS hybrids."[23] The results reveal a higher reactivity and shorter gel times in case of the TMOS hybrids with respect to the TEOS system.

Table II characterizes the formation–structure–property relationships in the DGEBA-D230-silica hybrids. It shows t_{gel} featuring rate of a hybrid network formation, the sol–gel conversion as characteristics of a silica structure in the hybrid and glass transition temperature T_g of the hybrids describing thermomechanical properties.

The mechanism of the nonaqueous sol–gel process involves protolysis of the alkoxysilane agent, TMOS or TEOS, initiated by BF_3MEA and/or by OH groups in the DGEBA molecule.[23] This initiation occurs in the first synthesis step (see Experimental). The sol–gel conversions and distribution of Q_i structural units after protolysis under different initiation conditions were determined by ^{29}Si NMR. The results are given in Table III showing a comparison between TMOS and TEOS as well as the effect of BF_3MEA on initiation of the sol–gel process. Table proves the higher TMOS reactivity compared to TEOS. While only 13% of TEOS reacted during the protolysis step (Q_0 = 0.87), in the case of TMOS it was more than 50% (Q_0 = 0.48). Moreover, Q_2 units determined in the TMOS mixture after protolysis reveal a presence of short polysiloxane chains. In contrast, only low molecular weight products, like disiloxanes characterized by Q_1 units, were formed in the TEOS mixture. The results disclose that TMOS conversion during protolysis is higher even in the absence of BF_3MEA. The sol–gel reaction is initiated in this case by OH groups of DGEBA.[23]

The initiation of the nonaqueous sol–gel process is a crucial stage. An extent of TMOS protolysis in this initial synthesis step strongly affects the following silica structure evolution within a hybrid. The final sol–gel condensation conversion, $(\alpha_{Si})_{hybrid}$, in both "TEOS and TMOS hybrids" is given in Table II. The comparison of the results in Tables II and III shows that conversions in the hybrids well correlate with the conversions of the pre-reacted mixtures in the first synthesis step, $(\alpha_{Si})_{protolysis}$, revealing an importance of the initiation stage. Also in the hybrids, the conversion of TMOS is higher compared to TEOS even in the case of the reaction without BF_3MEA. The conversion $\alpha_{Si} = 0.72$ in the network DGEBA-D230-TMOS, BF_3MEA is close to that in the classic "aqueous hybrids" DGEBA-D2000-TEOS, which is in the range 0.79–0.85.[25] The curing partially under air atmosphere (see Experimental) is another way of the "non aqueous sol–gel process" initiation. The results disclose that an air humidity promotes the sol–gel reactions and slightly

Table II. Formation-Structure-Property Characteristics of the Hybrids Based on DGEBA-D230 Epoxy Network; Gelation Time, Sol-Gel Conversion and T_g Values

System	t_{gel}[a] (min)	$(\alpha_{Si})_{hybrid}$	T_g,[b] (°C)
DGEBA-D230	34	-	91
DGEBA-D230-TEOS	52	0.19	68
DGEBA-D230-TEOS, air	-	-	62, 75
DGEBA-D230-TEOS, BF_3MEA	33	0.46	82
DGEBA-D230-TMOS	20	0.51	71, 95
DGEBA-D230-TMOS, air	-	0.54	101
DGEBA-D230-TMOS, BF_3MEA	15	0.72	107
DGEBA-D230-TMOS, BF_3MEA, air	-	-	120

[a] For t_{gel} determination see Experimental.
[b] T_g determined from position of the tan δ curve maximum, two T_g values correspond to the two-phase system.

raises the "TMOS hybrid" sol-gel conversion as well as the hybrids T_g values as discussed below (Table II).

The important benefit of the nonaqueous sol–gel procedure consists in a slower reaction enabling a structure control in order to avoid a phase separation.[23] Although TMOS is a much faster silica precursor than TEOS, the structure evolution is under control and well homogeneous hybrids are produced. Figure 2 illustrates the transparent DGEBA-Laromin-TMOS hybrid containing 80% TMOS.

The best properties and homogeneity was achieved by using the coupling agent GTMS. TEM micrographs of the GTMS containing nanocomposites and the reference epoxy network are shown in Figure 3. The results reveal silica aggregates of the size about 70 nm dispersed in the epoxy matrix and composed of primary particles of ~10 nm in diameter [Figure 3(b,c)]. The epoxy matrix [Figure 3(a)] does not display any heterogeneity.

Thermomechanical Properties of the Hybrids

In the previous work dealing with the "TEOS hybrids"[23] it was proved that a covalent bonding between simultaneously formed silica structures and an epoxy network occurs by the reaction of SiOH in silica and C—OH in an epoxy system. This interphase grafting finally leads to crosslinking of epoxy chains through the silica domains. Formation of the hard silica nanofiller structures and the mentioned crosslinking resulted in a rise of the storage modulus above glass transition. Despite this reinforcement, however, the T_g of the hybrids were not improved or even declined with respect to the epoxy network due to a plasticizing effect of soft incompletely cured silica structures. The higher sol–gel conversion in the "TMOS hybrids" is expected to result in the improved properties. The enhancement of the hybrids thermomechanical behavior is the main goal of the work. For this purpose we monitored thermomechanical properties of the hybrids of various compositions prepared under different nonaqueous conditions.

Table III. Distribution of Q_i Units and Condensation Conversion After the TEOS and TMOS Protolysis Under Nonaqueous Conditions

System	Q_0[a]	Q_1	Q_2	$(\alpha_{Si})_{protolysis}$
DGEBA-TEOS, BF_3MEA (ref. 23)	0.87	0.13	0	0.05
DGEBA-TMOS	0.54	0.39	0.07	0.13
DGEBA-TMOS, BF_3MEA	0.48	0.41	0.11	0.175

[a] Q_i is the mole fraction of the Q_i structural units.

A comparison of thermomechanical properties of the hybrids DGEBA-Laromin-silica prepared both from TMOS and TEOS is presented in Figure 4, showing the storage modulus G' and loss factor tan δ $(=G''/G')$ as functions of temperature. The synthesis of hybrids was initiated with BF_3MEA and the composition of both systems corresponds to the theoretical silica content of 5.4 wt %. As discussed above, the TEOS hybrid has a higher modulus with respect to the epoxy network, however, the glass transition temperature T_g is not changed (curve 2). In contrast, by using TMOS a significant enhancement of thermomechanical properties was achieved. The T_g of the hybrid raised by 40°C and the rubbery modulus is by an order of magnitude higher compared to that of the neat network (curve 3). In addition, the figure illustrates the effect of a curing temperature T_C because of a high curing conditions sensitivity of the nonaqueous sol–gel process. The common curing regime used for the epoxy system is not sufficient for hybrids, that had to be cured at a higher temperature, $T_C = 210$°C. Figure 4 presents a substantial drop of T_g by 30–40°C as well as moduli of the hybrids prepared at a lower temperature $T_C = 190$°C (curves 4, 5).

The reinforcement of the DGEBA-Laromin epoxy network by silica formed from TMOS is very efficient and the modulus above glass transition raises as TMOS content increases in

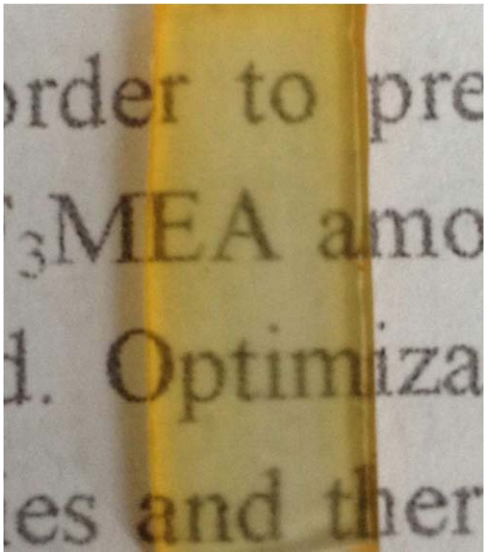

Figure 2. Photo of the hybrid DGEBA-Laromin-TMOS (80%), BF_3MEA. [Color figure can be viewed in the online issue, which is available at wileyonlinelibrary.com.]

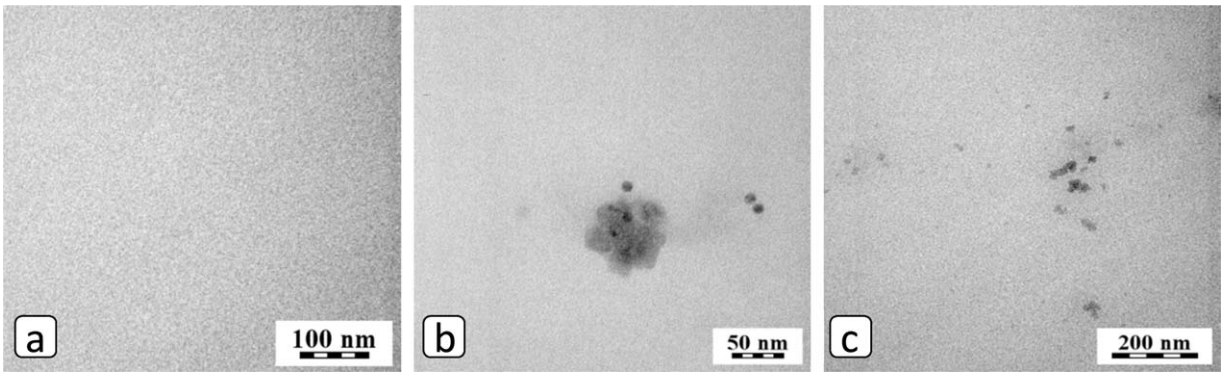

Figure 3. TEM micrographs of (a) epoxy network DGEBA-D230 and (b, c) DGEBA-D230-TMOS (14)-GTMS (0.3), BF_3MEA nanocomposite.

Figure 5(a). T_g values, however, go through a maximum at 14% TMOS (curve 3). At a higher TMOS amount the glass transition becomes less distinct and T_g declines as shown in Figure 5(b). This thermomechanical behavior can be explained as follows:

The silica-epoxy grafting leads to a restriction of the epoxy network chains mobility. This is manifested by a shift of T_g to higher values and drop of the loss factor tan δ amplitudes due to a reducing fraction of the relaxing polymer chains. Moreover, broadening of the loss factor peaks occurs because of a wide distribution of the corresponding relaxation times. The hybrid containing 40% TMOS (i.e., 15 wt % silica) has an almost indistinct T_g and a very high modulus up to 260°C (curve 5) revealing a strong immobilization of the epoxy chains. Moreover, it indicates a good dispersion of silica structures within the matrix because 15 wt % of silica, corresponding to ~ 10 vol %, is sufficient to completely restrict the epoxy matrix and likely to percolate through the hybrid. The high TMOS content in the hybrid implies in addition to a more extensive covalent bonding between phases, also formation of undercured silica structures. An incomplete curing is more likely at a high alkoxysilane content due to severe sterical hindrances for the sol–gel reactions within a densely crosslinked epoxy matrix.[23,26,27] The small relaxation peak at 140°C corresponds to a small fraction of a polymer, which is plasticized by soft less cured inorganic structures. The effect is much more pronounced in the hybrid with 60 % TMOS. In this case the T_g is decreased by 40°C due to a great amount of low-cured plasticizing products. The hypothesis of plasticization with undercured silica domains was proved by postcuring the sample for 1 h at 250°C. Figure reveals the marked properties improvement; T_g raises by 80°C (curve 7).

The initiation of the nonaqueous sol–gel process was shown to be a crucial step in controlling evolution of the silica structure in hybrids featured by the sol–gel conversion. Determination of the effect of initiation conditions on the hybrids final properties is of a high importance in order to optimize the hybrids synthesis. This investigation was performed by using the model hybrid based on the DGEBA-D230 network cured at 190°C.

Figure 6 presents thermomechanical behavior of the DGEBA-D230-silica hybrids prepared under different conditions with respect to initiation of the sol-gel process. The effect of BF_3MEA and an influence of the air humidity on hybrid properties are shown. Both "TEOS and TMOS hybrids" were studied and T_g values of the corresponding systems are given in Table I.

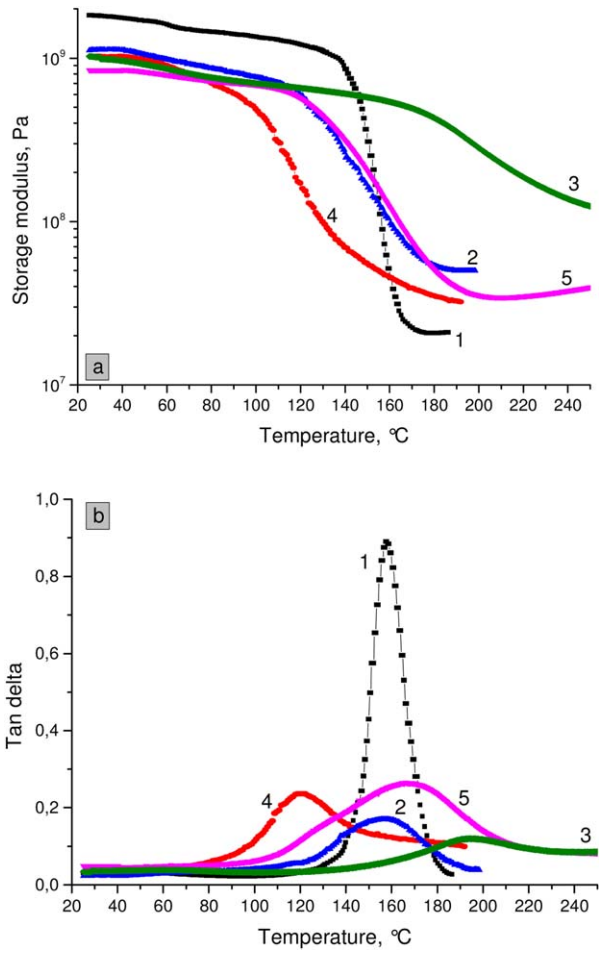

Figure 4. Storage modulus (a) and loss factor tan δ (b) of the DGEBA-Laromin based hybrids as functions of temperature: 1 DGEBA-Laromin, 2 DGEBA-Laromin-TEOS (18) $T_C = 210$°C, 3 DGEBA-Laromin-TMOS (14) $T_C = 210$°C, 4 DGEBA-Laromin-TEOS (18) $T_C = 190$°C, 5 DGEBA-Laromin-TMOS (14) $T_C = 190$°C. Constant BF_3MEA amount. [Color figure can be viewed in the online issue, which is available at wileyonlinelibrary.com.]

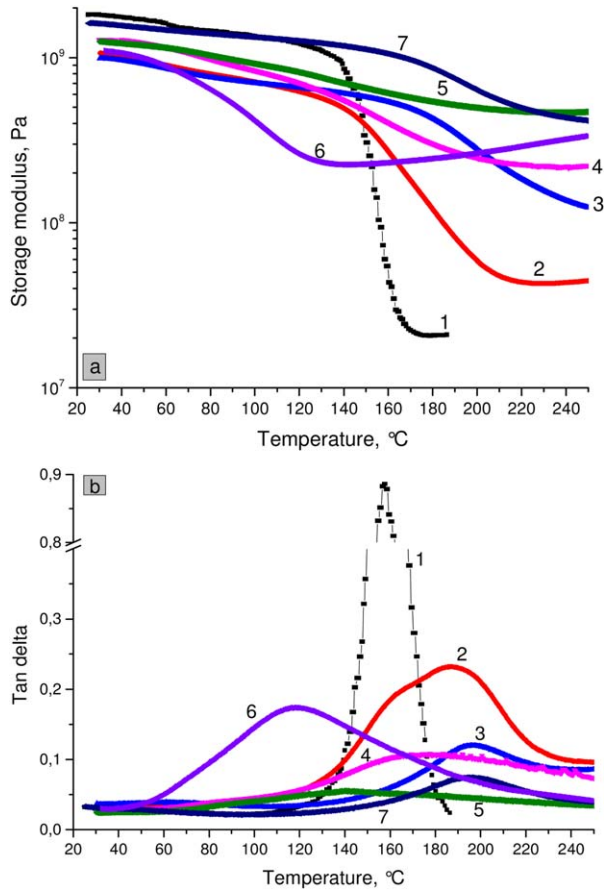

Figure 5. Storage modulus (a) and loss factor tan δ (b) of the DGEBA-Laromin hybrids containing different amount of TMOS, curing temperature $T_C = 210°C$: 1 0%, 2 7%, 3 14%, 4 25%, 5 40%, 6 60%, 7 60%—postcuring at $T_C = 250°C$. Constant BF_3MEA amount. [Color figure can be viewed in the online issue, which is available at wileyonlinelibrary.com.]

While the "TMOS hybrid" prepared in the presence of BF_3MEA (curve 2) exhibits a significant improvement both in T_g and modulus with respect to the epoxy network (curve 1), the TEOS based system shows a drop of T_g (curve 3) due to a low sol-gel conversion (see Table II). The poor properties of the "TMOS hybrid" prepared in the absence of BF_3MEA reveal the importance of the BF_3MEA initiation. In this case a two phase system is formed which is characterized by two loss factor peaks in figure (curve 4). In addition to the polymer phase of a low T_g, which is plasticized by the unreacted TMOS and undercured siloxanes, there is a polymer fraction partly immobilized by better cured silica structures.

The reaction under air atmosphere presents a limiting case of a transition between the aqueous and nonaqueous sol–gel procedures. The figure discloses that the "TMOS hybrid" prepared under air humidity without BF_3MEA (curve 5) exhibits properties which are close to those of the hybrid initiated with BF_3MEA. In contrast, "TEOS hybrid" prepared under air humidity does not show any improvement of properties (see Table II). The best thermomechanical properties were achieved by curing the hybrid under air humidity in the presence of BF_3MEA. The corresponding hybrid shows the T_g rise by 30°C and the high modulus (curve 6). Consequently, in the inert atmosphere the BF_3MEA complex is necessary for the initiation of the non-aqueous sol-gel process. Otherwise the hybrids of poor properties are produced. However, in the case of TMOS, the sol-gel reactions are promoted by air humidity even in the absence of BF_3MEA to form hybrids of improved properties unlike TEOS which is unreactive under the air humidity.

The hybrids thermomechanical properties and T_g values well correlate with the rate of hybrids formation featured by t_{gel} and sol–gel conversions in the hybrids as presented in Table II. The higher rate of the hybrid network formation results in the better cured silica structures and higher T_g of the hybrid.

A homogeneous nanofiller dispersion in a matrix and a strong interphase interaction are known to be principal factors determining nanocomposite properties. As mentioned above, an interphase bonding exits in the TMOS containing epoxy hybrid due to SiOH + COH reactions. In addition, according to the common approach, we employed the coupling agent GTMS to promote an interphase grafting. GTMS is incorporated into an epoxy-amine network by the reaction of glycidyl group with an amine crosslinker. Simultaneously, silsesquioxanes (SSQO) are formed by the sol–gel process producing inorganic domains

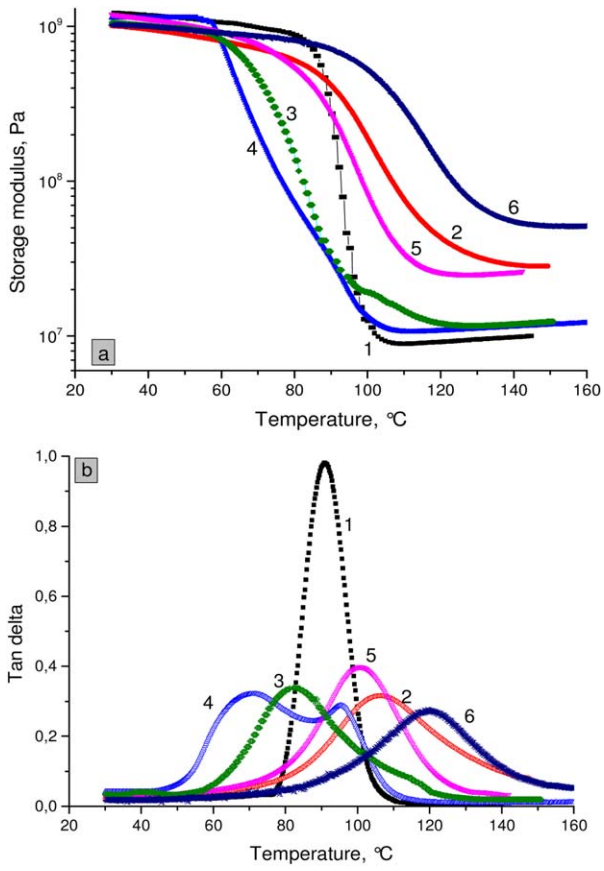

Figure 6. Storage modulus (a) and loss factor tan δ (b) as functions of temperature of the DGEBA-D230 based hybrids prepared under different initiation conditions 1 DGEBA-D230, 2 DGEBA-D230-TMOS,BF_3MEA; 3 DGEBA-D230-TEOS,BF_3MEA; 4 DGEBA-D230-TMOS, inert; 5 DGEBA-D230-TMOS,Air; 6 DGEBA-D230-TMOS,BF_3MEA,Air. [Color figure can be viewed in the online issue, which is available at wileyonlinelibrary.com.]

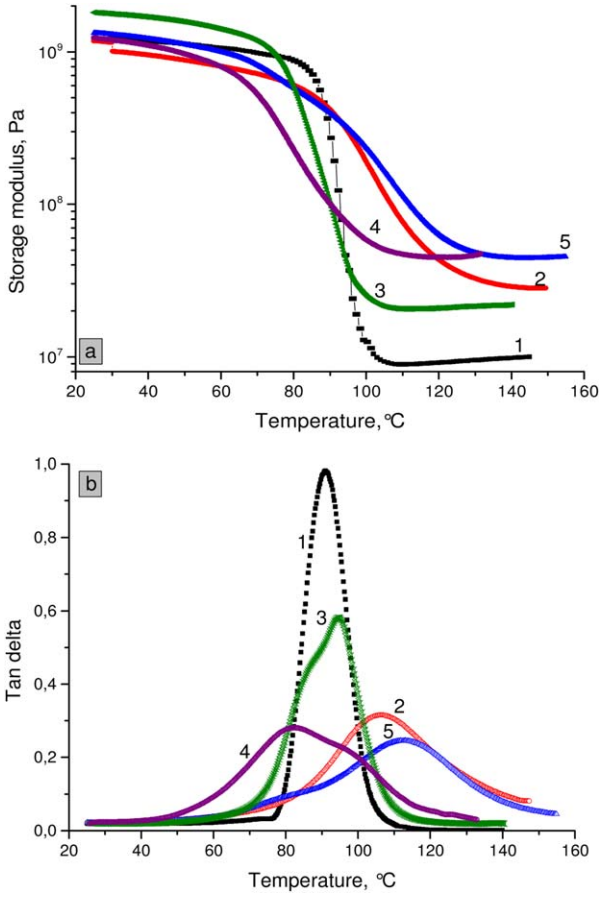

Figure 7. Storage modulus (a) and loss factor tan δ (b) as functions of temperature of the DGEBA-D230 based hybrids containing TMOS or/and GTMS 1 DGEBA-D230, 2 DGEBA-D230-TMOS(14), 3 DGEBA-D230-GTMS(0.1), 4 DGEBA-D230-GTMS(0.3), 5 DGEBA-D230-TMOS(14)-GTMS(0.1). [Color figure can be viewed in the online issue, which is available at wileyonlinelibrary.com.]

which are bound to epoxy network chains. Finally, these domains interconnect the network chains thus functioning as SSQO junctions increasing the hybrid network crosslinking density.[15,28,29]

Figure 7 compares the reinforcing effect of TMOS (curve 2) and GTMS (curves 3, 4) in the hybrid network based on DGEBA-D230. The rise of the hybrids rubbery moduli is slightly more pronounced in the GTMS containing systems, taking into account the theoretical silica content (see Table I). This is a manifestation of the interphase grafting and the hybrid crosslinking via inorganic domains, which is more efficient by using the coupling agent. However, T_g values are lower in the "GTMS hybrids." GTMS undergoes slow sol–gel reactions under nonaqueous conditions and the formed SSQO structures are severely undercured when reacted at 190°C.[23] Mainly at a high GTMS content ($x = 0.3$) T_g drops due to incomplete curing and the network plasticization (curve 4). In contrast, T_g raises with respect to the epoxy network in the "TMOS hybrid" despite low T_C (curve 2). The stronger limitation of the SSQO structure growth from GTMS is likely due to the covalent incorporation in the epoxy network thus being more confined than silica structures formed from TMOS.

The efficient epoxy-inorganic phase grafting by GTMS and the better evolution of inorganic domains within the hybrid in the case of TMOS suggest a hybrid design as a combination of both alkoxysilane reagents. Figure 7 illustrates the best enhancement of properties in the hybrid DGEBA-D230-TMOS(14)-GTMS(0.1), BF_3MEA (curve 5).

On the basis of the results of the model system we have prepared the high-T_g, heat resistant hybrid by using DGEBA-Laromin epoxy network as a matrix. The hybrid was cured at 230°C, which was proved to be sufficient for GTMS to form well developed SSQO domains, while the curing at 250°C already causes some polymer decomposition. The combination of TMOS and GTMS in hybrids leads to outstanding properties at a low inorganic phase content as illustrated in Figure 8. The hybrid DGEBA-Laromin-TMOS(14)-GTMS(0.1) with a silica amount of 7.6 wt % has a very indistinct glass transition and a high modulus up to 300°C; $G' = 335$ MPa at 300°C (curve 5).

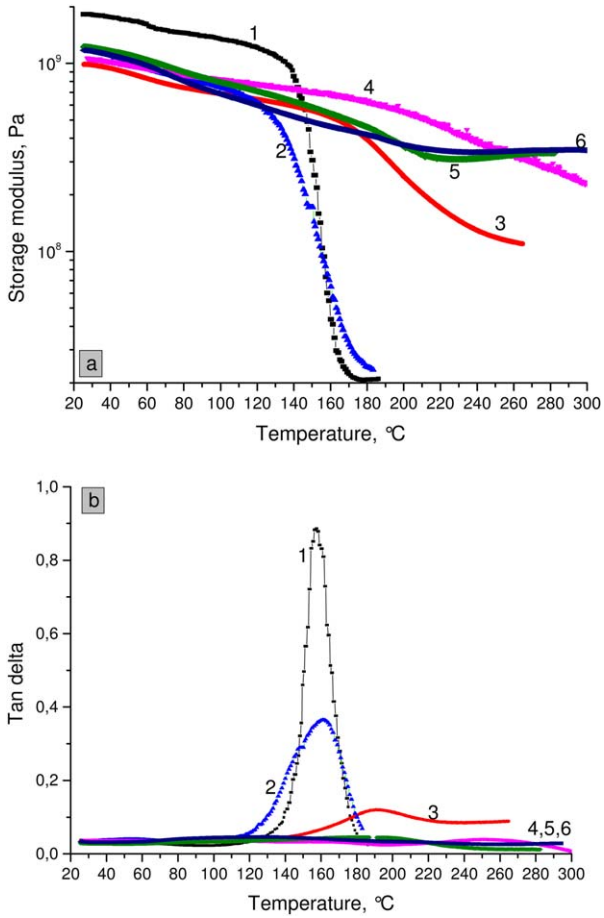

Figure 8. Storage modulus (a) and loss factor tan δ (b) of the DGEBA-Laromin based high-T_g hybrids as functions of temperature 1 DGEBA-Laromin, 2 DGEBA-Laromin-GTMS(0.1); 3 DGEBA-Laromin-TMOS(14); 4 DGEBA-Laromin-GTMS(0.3); 5 DGEBA-Laromin-TMOS(14)-GTMS(0.1); 6 DGEBA-Laromin-TMOS(14)-GTMS (0.3). Constant BF_3MEA content. [Color figure can be viewed in the online issue, which is available at wileyonlinelibrary.com.]

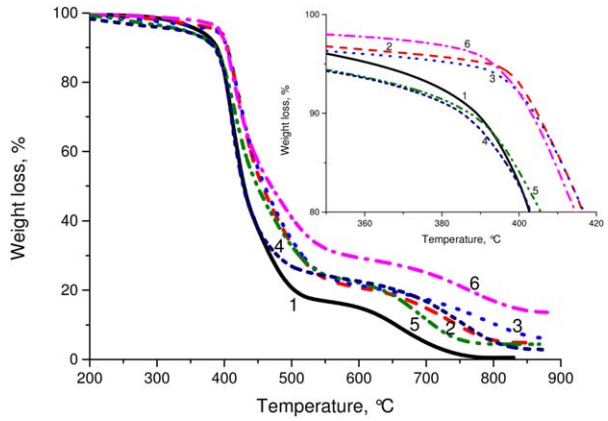

Figure 9. TGA plot of the epoxy network and the hybrids in air 1— DGEBA-Laromin; 2 -- DGEBA-Laromin-TMOS(14),BF_3MEA; 3 ····· DGEBA-Laromin-TMOS(14),Air; 4 ---- DGEBA-Laromin-TMOS(14),inert; 5 ··· DGEBA-Laromin-TEOS(18),BF_3MEA; 6 ·—·— DGEBA-Laromin-TMOS(14)-GTMS(0.2),BF_3MEA. [Color figure can be viewed in the online issue, which is available at wileyonlinelibrary.com.]

The increasing GTMS content in the hybrid DGEBA-Laromin-TMOS(14)-GTMS(0.3) leads to a vanishing of the glass transition before the polymer decomposition (curve 6). Only a very small polymer fraction relaxes in a low-temperature region as revealed by the small amplitudes of the loss factor curves in Figure 8(b). This behavior results from a very strong interfacial interaction and a complete immobilization of epoxy chains by bonding to inorganic structures.

The figure shows also the individual effects of both alkoxysilanes revealing a synergy of their combination in the hybrid. Reinforcement of the epoxy network with TMOS (14), corresponding to 5.4% silica, provides a limited grafting resulting in T_g rise by 35°C (curve 3). However, a severe decline of mechanical properties occurs above 200°C disclosing a lack of the sufficiently strong interfacial interaction. As to the effect of GTMS, the figure displays an appreciable properties dependence on the content of the coupling agent. No properties improvement, only a slight transition broadening, occurs after incorporation of a small amount of GTMS in the hybrid DGEBA-Laromin-GTMS(0.1) (curve 2). Figure illustrates a dramatic increase in the high-temperature modulus as GTMS amount raises; the curve 4 corresponds to the hybrid with GTMS content, $x = 0.3$, i.e. 6.6 wt % equivalent silica. The interphase interaction and crosslinking are more efficient and the modulus is higher compared to the TMOS containing hybrid. However, also in this case a drop of the modulus sets in above 200°C. Only the combination of both alkoxysilanes even at small contents, TMOS (14) and GTMS (0.1), results in the hybrid which maintains the mechanical properties up to 300°C without worsening. Obviously, there is a synergy effect. GTMS is very efficient in an interphase grafting and homogenization of the system, while it is low reactive. The TMOS high sol–gel reactivity ensures formation of well developed silica structures even under conditions of the nonaqueous procedure; however an extent of interphase grafting is low. The combination thus leads to the strong grafting with well cured structures because of cocondensation of silica and SSQO domains. Very likely a percolation of the inorganic structures through the hybrid occurs and the bicontinous epoxy-silica/SSQO hybrid is formed.

Thermal Stability

The incorporation of the silica *in situ* formed from TMOS into the epoxy network results in a significant enhancement of thermal stability. Figure 9 and Table IV present the results of thermal gravimetric analysis (TGA) of the DGEBA-Laromin based hybrids. The thermal stability was characterized by the temperature T_5, at which 5% loss of mass occurs in the air atmosphere.

The TGA results show a dramatic difference between "TEOS" and "TMOS" hybrids. While the TEOS based hybrid exhibits a reduction of thermal stability with respect to the epoxy network, the thermal stability of DGEBA-Laromine-TMOS hybrids considerably enhances. The best results were achieved in the hybrids containing both TMOS and GTMS. The hybrid DGEBA-Laromin-TMOS(14)-GTMS(0.2) displays a rise of the thermal stability by 31°C (curve 6). Also the second decomposition step corresponding to the high temperature thermal oxidative degradation is shifted in the hybrid by ~100°C to higher temperatures. The residue which remained after analysis (in the air) is by 50% higher than the theoretical content of the inorganic phase (see Table IV) indicating a considerable char formation. This high residue reveals that a part of a polymer phase is well protected from thermal and thermal oxidative degradation due to strong interphase interaction in the hybrid and formation of a silica layer on a polymer surface.

The hybrid prepared without BF_3MEA shows a pronounced drop of decomposition temperature T_5 by 50–60°C compared

Table IV. Thermal Stability of the Epoxy Network and the Hybrids

System	T_5[a]	Experimental residue (%)	Calculated residue (%)
DGEBA-Laromin	362	0.52	0
DGEBA-Laromin-TEOS(18), BF_3MEA	341	4.4	5.4
DGEBA-Laromin-TMOS(14)	335	2.8	5.4
DGEBA-Laromin-TMOS(14), air	384	6.1	5.4
DGEBA-Laromin-TMOS(14), BF_3MEA	392	4.9	5.4
DGEBA-Laromin-TMOS(14),BF_3MEA, $T_C = 190$°C	379	4.8	5.4
DGEBA-Laromin-TMOS(14),GTMS(0.2), BF_3MEA	393	13.6	9.8

[a] T_5 – 5 % loss of mass occurs.

to the "initiated hybrids." This sample exhibits a lower residue than the theoretical one due to incompletely cured silica. Only small improvement of thermal stability was observed in the systems cured at a low temperature, $T_C = 190°C$. In contrast, a relatively high thermal stability was achieved in the hybrids reacting partially under air atmosphere (see Experimental) even without BF_3MEA. The corresponding hybrid, moreover, has a slightly higher residue. We assume that a protective skin silica layer of a higher sol–gel conversion is formed on the surface in the air humidity atmosphere.

CONCLUSIONS

The high-T_g, heat resistant and transparent epoxy-silica hybrids have been prepared by the nonaqueous sol–gel process initiated with borontriflouride monoethylamine. The hybrids containing a low amount of the *in situ* generated silica (~10 wt %) show indistinct T_g and the high modulus (335 MPa) up to 300°C. The thermal stability of the hybrids characterized by T_5 value (temperature of 5% mass loss) increased by ~30°C with respect to the epoxy network and the high temperature thermal-oxidative degradation was delayed by ~100°C. The outstanding thermo-mechanical properties result from a very strong interphase interaction by covalent bonding leading to a complete immobilization of epoxy network chains and formation of the silica skin protective layer during a thermo oxidative hybrid degradation.

The epoxy network DGEBA-cycloaliphatic diamine (Laromin) was used as an organic matrix, TMOS as a precursor of silica formed by the sol-gel process and the coupling agent GTMS was employed to strengthen the interphase interaction. We took advantage of the synergy combination of both alkoxysilanes. The best properties were achieved in the hybrid of the following composition: DGEBA-Laromin-TMOS(14)-GTMS(0.1).

The model hybrid based on the network DGEBA-D230 was used to study the basic factors governing the nonaqueous sol–gel process. The results enabled to reveal the formation–structure–properties relationships in order to optimize the hybrid composition and conditions of the nonaqueous synthesis. The nonaqueous technique was employed due to better control of the structure evolution compared to the classical sol–gel process facilitating the synthesis of homogeneous transparent hybrids.

ACKNOWLEDGMENTS

The authors acknowledge the financial support of the Grant Agency of the Czech Republic (P108/12/1459) and the Academy of Sciences of the Czech Republic for support in the frame of the Program of international cooperation (M200501203).

REFERENCES

1. Liu, Y. L.; Hsu, C. Y.; Wei, W. L.; Jeng, R. J. *Polymer* **2003**, *44*, 5159.
2. Preghenella, M.; Pegoretti, A.; Migliaresi, C. *Polymer* **2005**, *46*, 12065.
3. Ragosta, G.; Abbate, M.; Musto, P.; Scarinzi, G.; Mascia, L. *Polymer* **2005**, *46*, 10506.
4. Rosso, P.; Ye, L. *Macromol. Rapid Commun.* **2007**, *28*, 121.
5. Brinker, J. C.; Scherer, G. W. Sol–Gel Science: The Physics and Chemistry of Sol–Gel Proces; Academic Press: New York, **1990**.
6. Mascia, L.; Tang, T. J. *Mater. Chem.* **1998**, *8*, 2417.
7. Ochi, M.; Takahashi, R.; Terauchi, A. *Polymer* **2001**, *42*, 5151.
8. Weng, W. H.; Chen, H.; Tsai, S. P.; Wu, J. C. *J. Appl. Polym. Sci.* **2004**, *91*, 532.
9. Matějka, L.; Dušek, K.; Pleštil, J.; Kříž, J.; Lednický, F. *Polymer* **1999**, *40*, 171.
10. Innocenzi, P.; Kidchob, T.; Yoko, T. *J. Sol-Gel Sci. Technol.* **2005**, *35*, 225.
11. Matějka, L. In Hybrid Nanocomposites for Nanotechnology; Merhari, L., Eds.; Springer Verlag: New York, **2009**, p 3.
12. Zhang, H.; Zhang, Z.; Friedrich, K.; Eger, C. *Acta Mater* **2006**, *54*, 1833.
13. Matějka, L. In Epoxy Polymers—New Materials and Innovation; Pascault, J. P.; Williams, R. J. J., Eds.; Wiley-VCH Verlag: Weinheim, **2010**, p 137.
14. Zou, H.; Wu, S.; Shen, J. *Chem. Rev.* **2008**, *108*, 3893.
15. Mascia, L.; Prezzi, L.; Haworth, B. *J. Mater. Sci.* **2006**, *41*, 1145.
16. Battistella, M.; Cascione, M.; Fiedler, B.; Wichmann, M. H. H.; Quaresimin, M.; Schulte, K. *Compos. A*, **2008**, *39*, 1851.
17. Liu, Y.-L.; Wu C.-C.; Chiu Y.-S.; Ho W.-H. *J. Polym. Sci. A Polym. Chem.* **2003**, *41*, 2354.
18. Nazir, T.; Afzal, A.; Siddiqi, H. M.; Ahmad, Z.; Dumon, M. *Prog. Org. Coat.* **2010**, *69*, 100.
19. Yang, P.; Wang, G.; Xia, X.; Takezawa, Y.; Wang, H.; Yamada, S.; Du, Q.; Zhong, W. *Polym. Eng. Sci.* **2008**, *48*, 1214.
20. Xia, X.; Wang, G.; Yang, P.; Kagawa, H.; Wang, H.; Suzuki, M.; Zhong, W.; Du, Q. *Polym. Polym. Compos.* **2010**, *18*, 443.
21. Ochi, M.; Takahashi, R. *J. Polym. Sci. B Polym. Phys.* **2001**, *39*, 1071.
22. Lee, T.-M.; Ma, C.-C. M. *J. Polym. Sci. Polym. Chem.* **2005**, *44*, 757.
23. Ponyrko, S.; Kobera, L.; Brus, J.; Matějka, L. *Polymer* **2013**, *54*, 6271.
24. Winter, H. H.; Mours, M. *Adv. Polym. Sci.*, **1997**, *134*, 165.
25. Matějka, L.; Dukh, O.; Kolařík, J. *Polymer*, **2000**, *41*, 1449.
26. Davis, S. R.; Brough, A. R.; Atkinson, A. *J. Non-Cryst. Sol.*, **2003**, *315*, 197.
27. Piscitelli, F.; Lavorgna, M.; Buonocore, G. G.; Verdolotti, L.; Galy, J.; Mascia, L. *Macromol. Mater. Eng.* **2012**, *298*, 896.
28. Matějka, L.; Dukh, O.; Meissner, B.; Hlavatá, D.; Brus, J.; Strachota, A. *Macromolecules* **2003**, *36*, 7977.
29. Matějka, L.; Dukh, O.; Kamišová, H.; Hlavatá, D.; Špirková, M.; Brus, J. *Polymer*, **2004**, *45*, 3267.

RSC Advances

PAPER

View Article Online
View Journal | View Issue

Cite this: *RSC Adv.*, 2015, **5**, 91330

Epoxy–silica nanocomposite interphase control using task-specific ionic liquids *via* hydrolytic and non-hydrolytic sol–gel processes

R. K. Donato,*[ab] M. Perchacz,[b] S. Ponyrko,[b] K. Z. Donato,[ab] H. S. Schrekker,[a] H. Beneš[b] and L. Matějka*[b]

Received 8th September 2015
Accepted 12th October 2015

DOI: 10.1039/c5ra18387a

www.rsc.org/advances

Carboxylic-functionalized task-specific imidazolium ionic liquids (carboxylic-ILs) presented selective high reactivities with epoxy-functionalized compounds, even in highly complex epoxy–silica nanocomposite systems. The carboxylic-ILs induced the *in situ* covalent bonding with epoxy based materials and tuning of the nanocomposites' filler–matrix interphase when applied either *via* hydrolytic or non-hydrolytic sol–gel processes. Structural modifications in the carboxylic-ILs allowed fine morphology control and promoted the formation of well dispersed silica nanodomains. This approach resulted in nanocomposites with improved mechanical properties, without a negative effect on the glass transition temperature, for both rubbery and glassy epoxy–silica nanocomposite systems with a very small IL content (~0.2 wt%). The best properties were achieved with the application of IL 1-carboxypropyl-3-methylimidazolium chloride, which produced a toughness increase of more than 7 times for the rubbery and almost twice for the glassy epoxy systems, when compared to their IL-free equivalents. These easy and quick procedures to produce imidazolium functionalized materials have the potential to open up a broad range of new conductive, responsive, smart and tunable reinforced materials.

1. Introduction

Tailoring materials' properties is a desirable but difficult task, especially due to the need for specific and selective reactions. The application of silica nanofillers formed *in situ* by the sol–gel process is a feasible option, where the silica containing polymer nanocomposites properties are mainly governed by the silica structure, the nanocomposite morphology and the matrix–filler interphase interactions and bonding.[1]

The network reinforcement by *in situ* formed silica is generally defined as a simultaneous increase in stiffness (modulus), tensile strength and toughness.[2,3] The rubbery modulus enhancement is given by the hydrodynamic effect of hard filler particles in a soft matrix.[4] This refers to strain amplification due to the presence of inextensible particles and by interphase filler–matrix interactions. As a consequence, the interfacial polymer layer is immobilized, thus increasing the effective filler volume.[5,6] The modulus increase by hard fillers is often accompanied by a decrease in the material extensibility and toughness. Hence, the challenge of this approach consists in the optimization of the balance among stiffness, strength and toughness. Reinforcing glassy-epoxy networks is an even more complex task, as they are much more sensitive to the filler aspect ratio effect due to their much smaller internal volume compared to rubbery networks.[7] Thus, the need for an effective method for producing highly dispersed filler, forming strong interphase bonding, is critical. Recently, significant advances were reported by our group concerning the epoxy matrices reinforcement with silica fillers, within which the application of ionic liquids (ILs) has been shown as a promising strategy for nanocomposite structure and morphology control.[8,9]

The ILs are organic salts, with ionic–covalent crystalline structures, that are liquid at temperatures of 100 °C or below. They present favorable properties, such as: insignificant flammability and volatility, high thermal and chemical stability, high ionic mobility and stability in the presence of air and moisture.[10,11] Initially, ILs were applied for replacing conventional volatile solvents and transforming hazardous processes into recyclable environmentally friendly ones.[12] Later on, the application scope was broadly expanded with, *e.g.*, their use as electrolytes in batteries and in the preparation of nanomaterials. In particular, the imidazolium cation based class of ILs have been applied in a variety of processes and materials, which is mainly due to their easily tunable properties *via* both cation and anion structural changes.[13,14]

Various imidazolium-based ILs have been used as catalysts for the sol–gel process,[15–17] silica morphology controllers[16,18–20] and epoxy–silica compatibilizers.[8,9] Furthermore, ILs can act as

[a]*Laboratory of Technological Processes and Catalysis, Institute of Chemistry, Universidade Federal do Rio Grande do Sul, Av. Bento Gonçalves 9500, Porto Alegre, RS, Brazil. E-mail: donatork@gmail.com*

[b]*Institute of Macromolecular Chemistry, Academy of Sciences of the Czech Republic, Heyrovsky Sq. 2, 162 06 Prague 6, Czech Republic. E-mail: matejka@imc.cas.cz*

"molecular templates" in the sol–gel silica process due to their special self-organization and selective interaction features.[18–23] Thus, the use of different ILs leads to not only different filler sizes, morphologies and dispersions but also to a completely different matrix–filler interphase behavior.[8,9,16]

For instance, ILs with long aliphatic chains attached to their cations produce nanocomposites with very well dispersed silica nanodomains and significantly increased stiffness, due to physical crosslinking by the ordered domains of decyl-substituents. However, the associated high brittleness makes them lack toughness.[8]

On the other hand, ether-functionalized ILs (ether-ILs) promoted a fine nanocomposite morphology with well dispersed silica nanodomains, presenting good matrix–filler interface interaction. This allowed a good balance between stiffness and toughness in the nanocomposites, especially when these ILs were applied synergistically with a covalent coupling agent, *e.g.* 3-glycidyloxypropyltrimethoxysilane (GTMS). The covalent bonds created by GTMS together with the capacity of ether-ILs to make multiple H-bonds[16,22,23] allowed tuning of the interphase bonding and the production of tough nanocomposites without considerable stiffness loss, which is a frequent drawback associated with the application of covalent coupling agents.[9]

In previous papers we reported about the effect of ILs and GTMS on the tensile properties of epoxy–silica nanocomposites. The epoxy network was composed of diglycidyl ether of bisphenol A (DGEBA) and poly(oxypropylene)diamine and was reinforced with *in situ* formed silica from TEOS, GTMS (coupling agent for interphase bonding) and ILs (with aliphatic or ether functionalities in the cation side chain for enhancing and balancing the nanocomposites' tensile properties).[8,9] At that point, the drawback was that such systems were easily applicable for rubbery networks but hard to adapt for glassy ones.

Following this idea, in this work we applied ILs functionalized with carboxylic groups (carboxylic-ILs) presenting different chain lengths between the imidazolium ring and the carboxyl functionality (Fig. 1). The IL carboxyl groups were expected to react with the DGEBA epoxy groups, covalently bonding the IL to the matrix and creating nanocomposites with optimized matrix–filler interphase. Thus, a model reaction, *i.e.* phenylglycidylether (PGE) reaction with the carboxylic-ILs, was used to detect the spontaneity of the epoxy–carboxyl reaction at room temperature, as the PGE carboxyl groups present the same reactivity as the DGEBA ones. Furthermore, the different cation chain lengths also provided information about the interphase hindrance influence in the final nanocomposite properties, which allowed evaluation of the ideal interphase flexibility for achieving the best properties. The obtained nanocomposites' performances were compared to the ones with an ether-IL (Fig. 1), which was able to produce only physical interactions within the interphase. Furthermore, two amine hardeners were applied to produce rubbery and glassy DGEBA–diamine nanocomposites *via* both hydrolytic and non-hydrolytic processes, exploring the applicability of a broad range of systems. Within this context, carboxylic-ILs could work as a substitute for both ILs and GTMS in the previous systems presented by our group.[8,9] This type of IL holds the functionalities to form covalent-physical interphase coupling, different from the GTMS covalent–covalent interphase coupling. This could contribute to higher nanocomposite toughness, making these ILs potential multifunctional agents for tuning nanocomposite morphology, filler dispersion and interphase bonding.

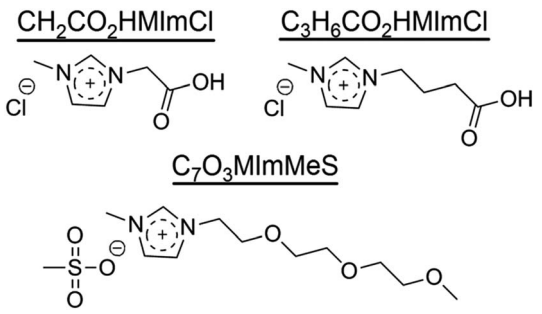

Fig. 1 Carboxylic and ether-ILs used in this study.

2. Experimental

2.1 Materials

2.1.1 Organic system components. Diglycidyl ether of bisphenol A (DGEBA) based resin, Epilox A 19-03 was purchased from Leuna–Harze GmbH. Poly(oxypropylene)diamines, Jeffamine® D2000 ($M = 1970$) and Jeffamine® D230 ($M = 230$) were purchased from Huntsman Inc. Borontrifluoride monoethylamine ($BF_3 \cdot MEA$) and phenylglycidylether (PGE) were obtained from Sigma Aldrich. All reactants were used as received.

2.1.2 Inorganic system components. Tetraethoxysilane (TEOS) was purchased from Fluka and used as received.

2.2 IL synthesis

The carboxylic[24] and ether-ILs[25] were synthesized as described in the literature: 1-carboxymethyl-3-methylimidazolium chloride ($CH_2CO_2HMImCl$), 1-carboxy propyl-3-methylimidazolium chloride ($C_3H_6CO_2HMImCl$) and 1-triethyleneglycol monomethyl ether-3-methylimidazolium methanesulfonate (C_7O_3-MImMeS) (Fig. 1). The purities of the synthesized ILs were checked by ^{1}H- and ^{13}C-NMR and were in accordance with published data. To avoid water and solvent contamination, the ILs were dried under vacuum at 80 °C for at least 5 h and further stored under an argon atmosphere.

2.3 Epoxy network formation

The epoxy networks were prepared by curing DGEBA with diamines as cross-linking agents. The equivalent weight of the epoxy groups in DGEBA was $E_E = 187$ g mol^{-1}, and the equivalent weights of the NH group in the diamines were; $E_{NH} = 492$ g mol^{-1} NH groups for D2000 and $E_{NH} = 60$ g mol^{-1} NH groups for D230.

2.4 Synthesis of the epoxy–silica nanocomposites

The nanocomposites were prepared from a stoichiometric mixture of the organic components, DGEBA and diamine (the ratio of functionalities $C_{NH} : C_{epoxy} = 1 : 1$) and the inorganic phase components, TEOS and H_2O. IL was used as the catalyst/additive where indicated. The hybrids were synthesized at the ratios of functionalities DGEBA : diamine : TEOS = 1 : 1 : 4 (TEOS is a tetrafunctional reagent with respect to the sol–gel process). This composition corresponds to ~7.5 wt% of silica (*i.e.* ~3.0 vol%) according to TGA analysis of the composition residues.

2.4.1 Synthesis of the epoxy–silica nanocomposites *via* hydrolytic sol–gel process. A two-step synthetic procedure was employed.[6,8,9] In the first step, TEOS was pre-hydrolyzed in the presence of HCl, iPrOH and IL at room temperature for 1 h. In the second step, the pre-hydrolyzed TEOS with IL was mixed with the organic phase components, DGEBA and diamine. The mixtures were mechanically stirred during the whole synthesis process, up to the curing stage when they were transferred to a Teflon wafer mold and cured to form 2 mm thick samples. The samples were cured for 20 h at 130 °C, followed by a post-curing and drying process under vacuum at 150 °C for 2 h. The neat matrix and nanocomposites formed without the addition of IL were used as the references. The IL content present in the final systems was ~0.2 wt%.

2.4.2 Synthesis of the epoxy–silica nanocomposites *via* non-hydrolytic sol–gel process. The nanocomposites were synthesized according to a sequential synthesis procedure.[26] First, BF_3·MEA was mixed with DGEBA for 30 min at 70 °C followed by TEOS addition to the epoxy–BF_3·MEA mixture and strong stirring for 30 min. Finally, IL was added and mixed for another 30 min, followed by the addition of a stoichiometric content of amine and 30 min stirring. The final mixtures were transferred to a Teflon wafer mold and cured to form 2 mm thick samples. The specimens were cured for 20 h at 130 °C, followed by a post-curing at 190 °C for 5 h. The neat matrix and nanocomposites formed without the addition of IL were used as the references. The IL content present in the final systems was ~0.2 wt%.

2.5 Epoxy-IL model reaction

For evaluating the IL bonding in the epoxy matrix, a model reaction of the carboxylic functionality of the IL with the epoxy functionality of phenylglycidylether (PGE) in acetone (50% w/v solutions) was analyzed by FTIR, considering the identical reactivity of PGE and DGEBA. In this manner, the reduced number of functionalities enabled more defined spectra, without peak overlaps at the epoxy range. Aliquots were collected to follow the reaction evolution after 30 min, 1 h, 5 h, 24 h and 48 h.

2.6 Methods

2.6.1 Transmission electron microscopy (TEM). TEM was carried out with two standard microscopes (Tecnai G2 Spirit Twin 12, FEI; and JEM 200CX, JEOL). The nanocomposite specimens were ultramicrotomed (Leica Ultracut UCT ultramicrotome; Leica) in order to obtain 50 nm, ultrathin sections; the sections were transferred to the TEM carbon-coated copper grids and covered with a ~5 nm carbon layer (Vacuum evaporation device JEE-4C; JEOL) in order to eliminate sample damage under the electron beam. The specimens were observed in the TEM microscope in bright field at an accelerating voltage of 120 keV.

2.6.2 Small-angle X-ray scattering (SAXS). The experiments were performed using a pinhole camera (Molecular Metrology SAXS System) attached to a microfocused X-ray beam generator (Osmic MicroMax 002) operating at 45 kV and 0.66 mA (30 W). The camera was equipped with a multiwire, gasfilled area detector with an active area diameter of 20 cm (Gabriel design). Two experimental setups were used to cover the q range of 0.004–1.1 $Å^{-1}$, where $q = (4\pi/\lambda)\sin\theta$ (λ is the wavelength and 2θ is the scattering angle). The scattering intensities were adjusted to an absolute scale using a glassy carbon standard. The nanocomposites were measured as thin films.

2.6.3 Dynamic mechanical analysis (DMA). A rheometer ARES (Rheometric Scientific) was used to follow the dynamic mechanical behavior of the networks. The temperature dependence of the complex shear modulus of rectangular samples was measured by oscillatory shear deformation at a frequency of 1 Hz and a heating rate of 2 °C min^{-1}. Also tensile mode experiments were carried out at 22 °C at a crosshead speed of 1 mm min^{-1}, as a manner of checking the tensile tests reproducibility. At least five specimens were tested for each sample. The tensile stress and elongation were evaluated. In addition, the energy to break obtained from the area under the stress–strain curve was determined as a standard measure of the specimen's toughness.

2.6.4 Tensile tests. Tensile tests were carried out at 22 °C using an Instron 5800 apparatus at a crosshead speed of 1 mm min^{-1}. At least five dumb-bell shaped specimens from at least two different syntheses (~10 specimens) were tested for each sample. The Young's modulus, E, the stress to break, σ_b, and elongation to break, ε_b, were evaluated. In addition, the energy to break obtained from the area under the stress–strain curve was determined as a standard measure of the elastomer toughness.

2.6.5 Fourier transformed infra-red spectroscopy (FTIR). FTIR spectra of the PGE-IL mixtures in acetone (50% solutions) were obtained using a PerkinElmer Spectrum 100 equipped with a universal ATR (attenuated total reflectance) accessory with a diamond crystal. In all cases, the resolution was 4 cm^{-1} and the spectra were averaged over 16 scans. The reaction between the PGE epoxy group and the IL carboxylic group was evaluated by the consumption of the epoxy band at 914 cm^{-1}, relative to the stretching C–O of the oxirane group. Acetone was chosen as a solvent that does not present signals overlapping the peak of interest.

3. Results and discussion

The polycondensation of TEOS to form silica *via* both hydrolytic and non-hydrolytic sol–gel processes was strongly affected by

the IL used. As the sol–gel process is highly sensitive to acids and bases, we previously demonstrated that ILs can be used to affect the final silica morphology due to their different acidity profiles.[8,17] We also observed that the reaction kinetics are dependent on the IL anion, and in the presence of methanesulfonate (MeS) a slow gelation is promoted with a homogeneous transparent gel build-up. The IL C_7O_3MImMeS generates acidic species in the presence of water,[17,27] thus acting as an acid catalyst.

For this reason, together with its multiple H-bond capacities,[16,19] C_7O_3MImMeS was selected as a reference IL to form a nanocomposite with fine morphology but presenting only physical interactions at the filler–matrix interphase.[9] The carboxyl-ILs also present acidic character,[24] but with an available functional group that can easily react with the substrates. The similar character of the two types of IL allowed the evaluation of their action over silica formation excluding pronounced catalytic differences during the first hydrolysis–protolysis step.

The ILs presented in Fig. 1 were tested for their effects on rubbery and glassy epoxy systems by using different diamines (Jeffamines D2000 and D230), under both hydrolytic and non-hydrolytic sol–gel processes. As a manner of systematically discussing the IL effects over the different systems, the results are presented segregated into hydrolytic and non-hydrolytic sol–gel approaches, as these classes presented the most dramatic differences. The *in situ* produced silica led to the epoxy network reinforcement, which varied with the resulting nanocomposite morphology and could be tuned by the sol–gel reaction conditions.

Several of these conditions have been extensively discussed in the literature,[1,6,28] thus we will direct our evaluations to the best pre-established of those and limit our discussions to the IL effect.

3.1 Nanocomposites *via* hydrolytic sol–gel approach

Via the hydrolytic sol–gel approach, homogeneous nanocomposites were only obtained when Jeffamine D2000 was used as a cross-linker. Contrarily, applying IL to the epoxy resin cured with Jeffamine D230 led to the formation of highly heterogeneous films with very brittle character. It is known[1,8,9] that the two-step acid–base polymerization promotes an extremely fast epoxy–silica gelation in the second step, after the acidic pre-hydrolysis of TEOS. Therefore, the extremely quick condensation was a consequence of the IL's presence in the first step (acid catalysis), followed by the presence of D230 (basic catalyst) in the second step, inducing the system to condense before its homogenization. Thus, as D2000 is a weaker base, only the rubbery DGEBA-D2000 based systems were homogeneous enough to be characterized. Furthermore, the IL content set (~0.2 wt%) was detected as ideal to form all the hydrolytic systems. When higher carboxylic-IL amounts were applied the gelation was too quick to pour the suspensions onto the molds and the formation of homogeneous films was not possible. This also confirmed the strong IL catalytic effect on the sol–gel process.

3.1.1 Structure and morphology. The dynamic-mechanical and tensile properties of these epoxy–silica elastomer nanocomposites are directly dependent on the system's morphology and interfacial interactions. Previously, we demonstrated that different applied ILs can have drastically different effects on the structure and morphology of such type of materials.[8] Carboxylic-ILs also follow this rule, as they have a strong influence on the size of silica aggregates formed during the synthesis.

A nanocomposites' SAXS investigation showed that carboxylic-ILs exert a strong homogenizing effect on the formed silica domains. The comparison between acid-catalyzed IL-free and IL-modified nanocomposites is displayed in Fig. 2. Both carboxylic-ILs produce nanocomposites with open structures of aggregates (fractal dimension $D = 1.7$). This value coincides exactly with the one for the two-step acid-catalyzed epoxy–silica synthesis,[29] or for the nanocomposite applying the ether-IL C_7O_3MImMeS.[8] This implies a cluster–cluster diffusion-limited aggregation mechanism, which is opposite to the monomer–cluster aggregation characteristic for basic catalysis or application of IL C_{10}MImBF$_4$ (presenting $D \sim 3$).[8]

Compared to the IL-free and C_7O_3MImMeS systems (Fig. 2a and b), both nanocomposites with carboxylic-ILs presented a plateau in the low q region, suggesting the formation of very small silica structures with $d \sim 50$–90 nm, where $d = 2\pi/q$ and q corresponds to the beginning of the plateau (Fig. 2c and d).

For confirming the SAXS predictions, TEM images were taken from the nanocomposites without and with carboxylic-ILs (CH_2CO_2HMImCl and $C_3H_6CO_2$HMImCl, Fig. 3). In complete agreement with the SAXS results, the IL-free epoxy–silica system presented non-uniform aggregates of dense particles with a broad size distribution (Fig. 3a). Both systems with carboxylic-ILs presented very small (5–20 nm), more uniform and well dispersed particles, which formed only small aggregates (<50 nm) loosely packed all over the matrix (Fig. 3b and c). The nanocomposite with CH_2CO_2HMImCl displayed small

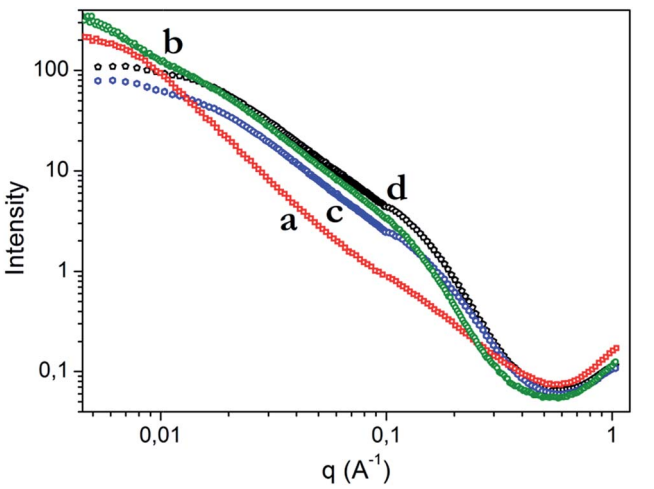

Fig. 2 SAXS profiles of the nanocomposites; (a) IL-free reference, and with ILs (b) C_7O_3MImMeS, (c) CH_2CO_2HMImCl and (d) $C_3H_6CO_2$HMImCl.

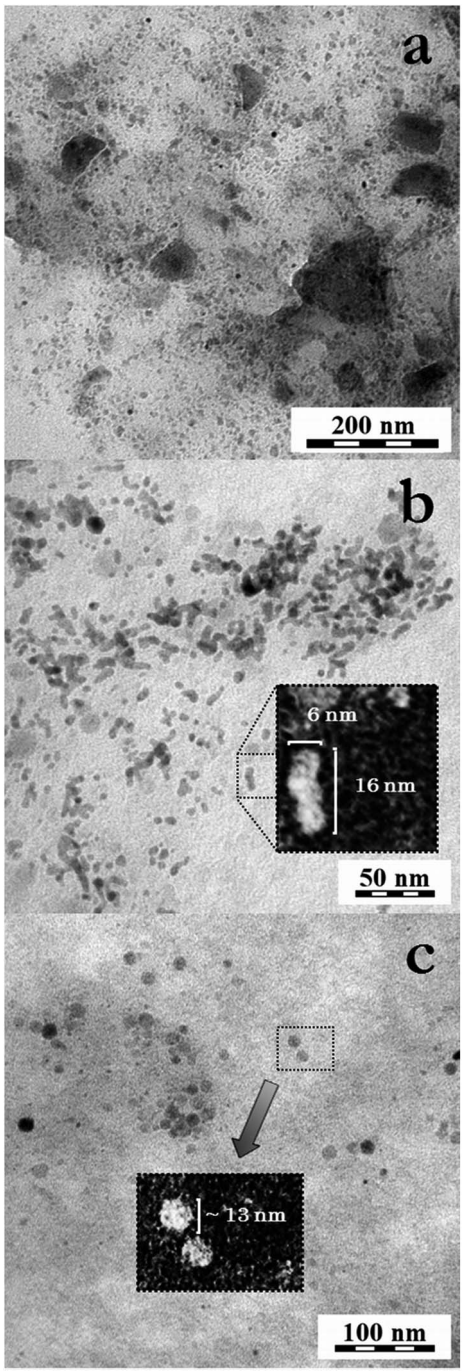

Fig. 3 TEM images of nanocomposites; (a) reference IL-free, and with ILs (b) $C_3H_6CO_2HMImCl$ and (c) $CH_2CO_2HMImCl$. In the insets are shown magnified negative images of the highlighted particles.

spherical particles ($D \sim 13$ nm), presenting few loose aggregates, well distributed through the network (Fig. 3c). Interestingly, the nanocomposite with $C_3H_6CO_2HMImCl$ presented even smaller particles ($D \sim 6$ nm), which frequently were found aggregated linearly in groups of a few particles (Fig. 3b).

3.1.2 Dynamic-mechanical and tensile properties. Fig. 4 displays the dynamic shear storage modulus G' and the loss factor tan δ as functions of the temperature.

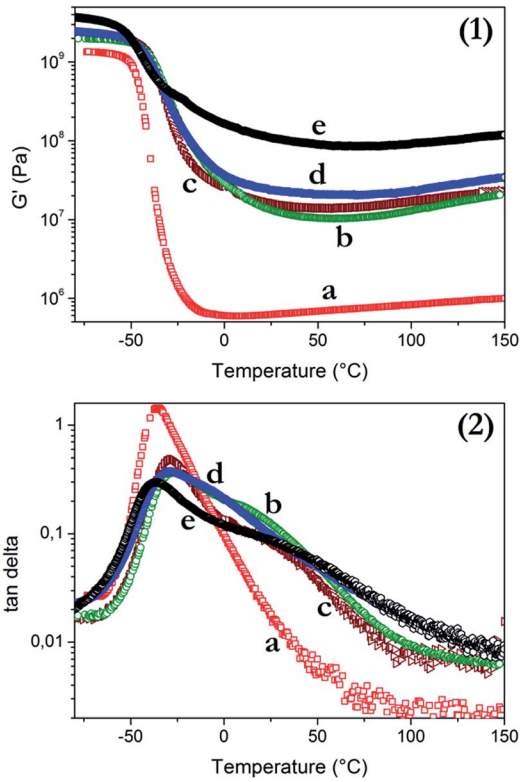

Fig. 4 Shear storage modulus (1) and loss factor tan δ (2) as functions of temperature of the; (a) reference neat epoxy network, epoxy–silica nanocomposites (b) without IL, and with (c) $C_7O_3MImMeS$, (d) $CH_2CO_2HMImCl$ and (e) $C_3H_6CO_2HMImCl$.

The glass transition temperature (T_α) was determined from the tan δ curve maximum, while the G' by the modulus at the beginning of the rubbery plateau (50 °C). The systems' dynamic-mechanical properties were compared with both the neat epoxy-D2000 matrix (Fig. 4(1a)) and IL-free epoxy-D2000–silica nanocomposite (Fig. 4(1b)). The systems with $C_7O_3MImMeS$ (Fig. 4(1c)) and $CH_2CO_2HMImCl$ (Fig. 4(1d)) showed good moduli improvements, but the nanocomposite with $C_3H_6CO_2HMImCl$ (Fig. 4(1e)) presented the best performance, with a modulus two orders of magnitude higher than the neat epoxy matrix and one order of magnitude higher than the IL-free system.

None of the nanocomposites showed a T_α decrease (Fig. 4(2), Table 1), suggesting no plasticization or considerable cross-linking density decrease in the final network. Despite presenting worse modulus reinforcement performance, only the systems with $CH_2CO_2HMImCl$ and without IL showed some increase in T_α (Fig. 4(2b) and (c)).

Nevertheless, the system with $C_3H_6CO_2HMImCl$ kept the same value as the neat epoxy network (Fig. 4(2d)). Most importantly, phase separation, represented as bimodal peaks on the loss factor curves, can be clearly observed, especially for the $C_3H_6CO_2HMImCl$ system. This, most probably, is a consequence of the IL-matrix covalent bonding, which physically attracts silica structures, resulting in the formation of strongly immobilized interphase layers.

Table 1 Mechanical properties of the rubbery DGEBA-D2000 epoxy–silica nanocomposites obtained *via* the hydrolytic sol–gel approach

Entry	IL	T_α (°C)	E (MPa)	Tensile strength (MPa)	Elongation at break (%)	Toughness (MJ m^{-3})
1[a]	—	−36	4.3 ± 0.2	0.8 ± 0.1	22 ± 2	0.10 ± 0.02
2[b]	—	−28	21.9 ± 1.8	4.3 ± 0.4	24 ± 2	0.6 ± 0.1
3[c]	C_7O_3MImMes	−28	44.4 ± 0.8	8.0 ± 0.5	20 ± 1	0.9 ± 0.1
4[d]	CH_2CO_2HMImCl	−30	37.5 ± 4.7	7.6 ± 2.2	50 ± 18	3.1 ± 1.6
5[e]	$C_3H_6CO_2$HMImCl	−37	71.5 ± 4.4	8.5 ± 1.8	58 ± 9	4.5 ± 0.9

[a] Neat epoxy. [b] IL free epoxy–silica. [c] Epoxy–silica with C_7O_3MImMeS. [d] Epoxy–silica with CH_2CO_2HMImCl. [e] Epoxy–silica with $C_3H_6CO_2$HMImCl.

The nanocomposites' tensile properties confirmed the morphological contributions in reinforcement, where all the nanocomposites with ILs presented significant improvements (Fig. 5). All these hybrids showed similar tensile strength improvement (one order of magnitude higher than the neat matrix and 100% higher than the IL-free nanocomposite) (Table 1). This suggests a stronger contribution of the silica morphology and dispersion for this property, while the interphase bonding has only a secondary role.[30] Differently, the tensile modulus and toughness suffered significant effects depending on the IL applied.

Both C_7O_3MImMeS and CH_2CO_2HMImCl caused significant increases in tensile modulus (both one order of magnitude in relation to the neat matrix and 100% in relation to the IL-free nanocomposite). The IL CH_2CO_2HMImCl also induced a pronounced increase in extensibility (100% in relation to both the neat matrix and the IL-free nanocomposite), which resulted also in high toughness (more than 5 times higher than the IL-free nanocomposite).

The best mechanical performances were achieved with $C_3H_6CO_2$HMImCl, which induced an outstanding 200% higher tensile modulus, and toughness almost one order of magnitude higher than the IL-free nanocomposite. These high toughness values are a result of the high tensile modulus together with the higher extensibility presented (almost 200% higher than the neat matrix and IL-free nanocomposite) (Table 1 and Fig. 5).

In summary, both CH_2CO_2HMImCl and $C_3H_6CO_2$HMImCl produced very strong polymer–filler interphase bonding, most probably caused by covalent-physical crosslinking rather than only physical interactions. Also, as the total IL amount applied was very small (~0.2 wt%), the crosslinking reinforced the nanocomposites without causing brittleness. Also, the length of the chain between the imidazolium ring and the functional group seemed to have a significant influence on the nanocomposite's final properties. The IL with longer propyl chain reinforced, but still allowed some interphase flexibility and release of part of the stress, conferring higher toughness.

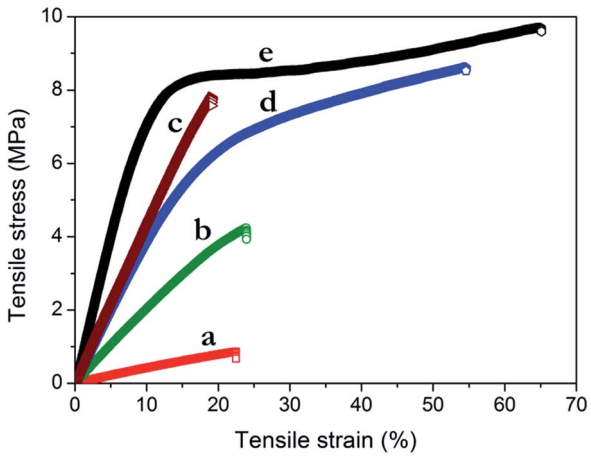

Fig. 5 Stress–strain curves of (a) reference neat epoxy network, hybrids (b) without IL, (c) with C_7O_3MImMeS, (d) with CH_2CO_2HMImCl and (e) with $C_3H_6CO_2$HMImCl.

3.2 Nanocomposites *via* non-hydrolytic sol–gel approach

The solvent-free nonaqueous sol–gel process, promoted by the BF_3·MEA complex, was applied in order to improve the epoxy nanocomposite homogeneity, avoiding problems with excessive solvent and water removal. An important benefit of this approach consists in a slower reaction, enabling structure control, avoiding phase separation and resulting in transparent hybrids, even without the application of a co-solvent. In fact, this system suffered a behavior inversion when compared to the hydrolytic one. The most suitable systems were the glassy DGEBA-D230 networks, exactly the ones unsuitable for the hydrolytic sol–gel.

3.2.1 Structure and morphology. For evaluating the IL effect also in this type of system, TEM images were taken from nanocomposites without and with the IL that produced the best performance in the hydrolytic systems, $C_3H_6CO_2$HMImCl (Fig. 6). The TEM micrographs indicated that, as for the hydrolytic process, the use of IL also considerably improved silica dispersion in the non-hydrolytic sol–gel process. The IL-free epoxy–silica system presented non-uniform partially condensed particles, forming large aggregates (~500 nm, Fig. 6a). The system with $C_3H_6CO_2$HMImCl displayed much smaller aggregates (10–100 nm), loosely packed all over the matrix (Fig. 6b).

3.2.2 Dynamic-mechanical and tensile properties. As both hydrolytic and non-hydrolytic systems followed the same morphological trends, DMA was used for studying the main parameters governing the hybrids' thermomechanical properties. Only a weak enhancement of G' and a decrease by ~10 °C in the T_α was observed when TEOS was applied to the

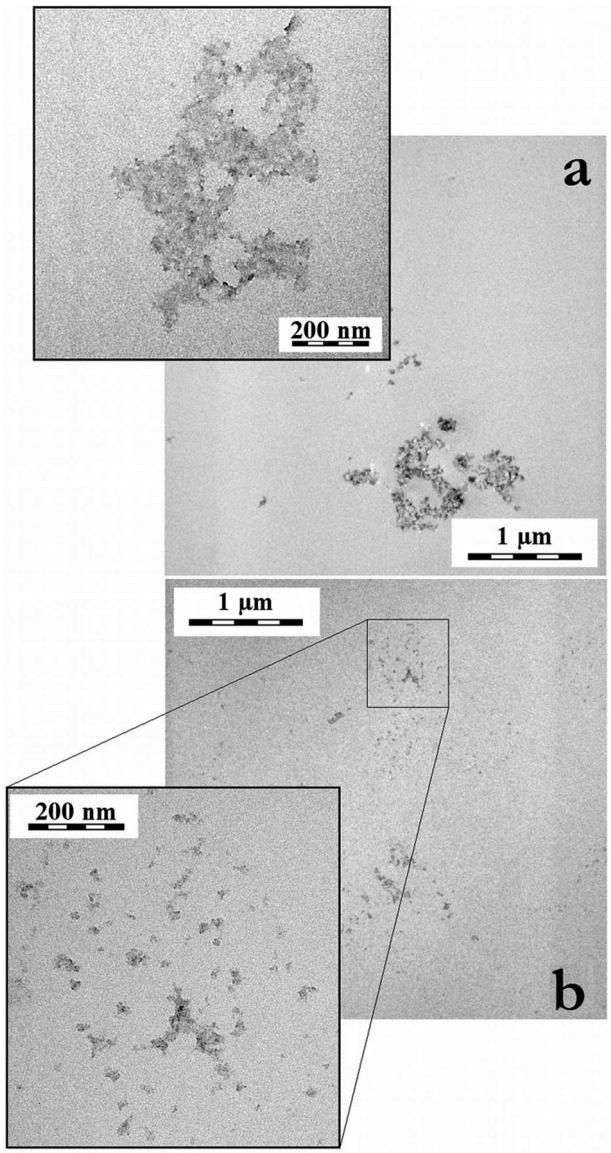

Fig. 6 TEM images of (a) reference IL-free nanocomposite and (b) nanocomposite with $C_3H_6CO_2HMImCl$ obtained by the non-hydrolytic sol–gel approach.

IL-free system, when compared to the neat DGEBA-D230 network. This indicates an incomplete condensation, resulting in plasticization of the system (Fig. 7, Table 2). Differently, all systems with ILs presented a G' increased by at least 150%, followed by the T_α increase. The highest T_α was observed for the $CH_2CO_2HMImCl$ system (~10 °C higher than the neat network, Fig. 7, Table 2). The tensile properties of the systems with applied ILs also showed considerable reinforcement (Fig. 8, Table 2).

When considering only the silica contribution, the IL-free system showed a slight elastic modulus (E') decrease, keeping the tensile strength practically the same. As a probable reflex of the previously observed plasticization, the increase in elongation at break (~50%) caused a consequent increase in toughness by about 30%.

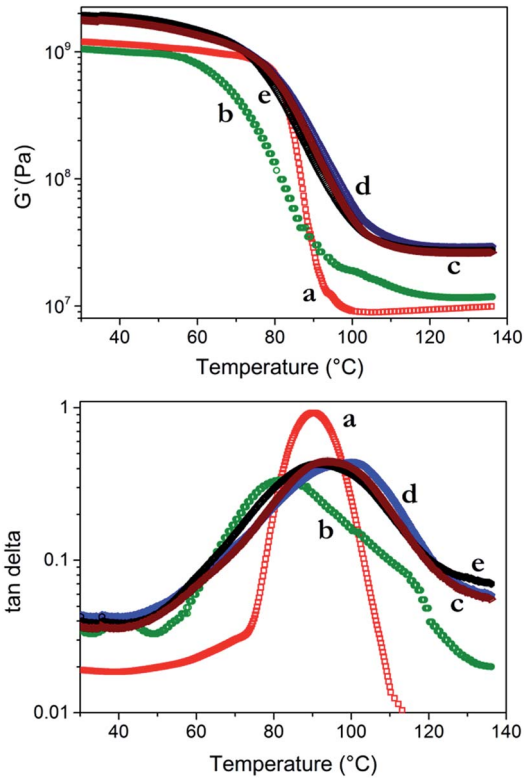

Fig. 7 Shear storage modulus (1) and loss factor tan δ (2) as functions of the temperature of the; (a) reference neat epoxy network, hybrids (b) without IL, and with IL (c) $C_7O_3MImMeS$, (d) $CH_2CO_2HMImCl$ and (e) $C_3H_6CO_2HMImCl$.

A much more significant reinforcement was observed for the $C_7O_3MImMeS$ system, where both tensile strength (~10%) and elongation (~120%) increased, consequently producing a significant increase in toughness (more than twice in comparison with the neat DGEBA-D230 network). On the other hand, the IL $CH_2CO_2HMImCl$ produced a good tensile strength improvement (~25%) but the elongation was lower than for the IL-free system, which nevertheless caused a toughness increase (~50%). The best properties balance was produced by $C_3H_6CO_2HMImCl$, causing both the tensile strength (~45%) and the elongation to increase considerably (~100%), producing a much tougher hybrid (~130% higher than the neat network) (Fig. 8, Table 2).

Very defined yielding could be observed for the C_7O_3-MImMeS and $C_3H_6CO_2HMImCl$ systems, possibly due to interphase gradual breakage. This showed that both ILs strongly reinforce the nanocomposite's interphase, although the $C_3H_6CO_2HMImCl$ application allows it under a much higher stress.

The absence of yielding for the $CH_3CO_2HMImCl$ system clearly demonstrates the IL side chain's importance for interphase reinforcement, where the short side chain restricts the IL bonding function.

3.3 Diamine and IL catalytic effect

As previously mentioned, the sequential acid (IL) and basic (diamine) catalytic effects govern the system's homogeneity.

Table 2 Mechanical properties of the glassy DGEBA-D230 epoxy–silica nanocomposites obtained *via* the non-hydrolytic sol–gel approach

Entry	IL	T_α (°C)	E (GPa)	Tensile strength (MPa)	Elongation at break (%)	Toughness (MJ m^{-3})
1[a]	—	90	2.1 ± 0.2	52 ± 3	5.5 ± 0.6	2.1 ± 0.5
2[b]	—	82	1.9 ± 0.1	53 ± 7	8.1 ± 2.0	2.7 ± 0.5
3[c]	C_7O_3MImMeS	94	2.1 ± 0.2	58 ± 6	12.0 ± 3.2	4.4 ± 0.6
4[d]	CH_2CO_2HMImCl	101	2.0 ± 0.2	64 ± 3	7.3 ± 0.8	3.1 ± 0.6
5[e]	$C_3H_6CO_2$HMImCl	93	2.4 ± 0.3	75 ± 6	11.1 ± 1.7	4.9 ± 0.7

[a] Neat epoxy. [b] IL free epoxy–silica. [c] Epoxy–silica with C_7O_3MImMeS. [d] Epoxy–silica with CH_2CO_2HMImCl. [e] Epoxy–silica with $C_3H_6CO_2$HMImCl.

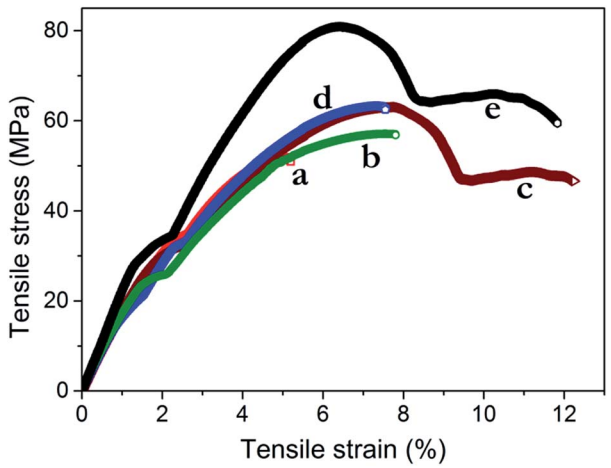

Fig. 8 Stress–strain curves of (a) reference neat DGEBA-D230 network, hybrids (b) without IL, (c) with C_7O_3MImMeS, (d) with CH_2CO_2HMImCl and (e) with $C_3H_6CO_2$HMImCl.

The hydrolytic sol–gel approach in the presence of the selected ILs (Fig. 1) produces a quick and efficient TEOS hydrolysis in the first reaction step. This makes the system highly sensitive to the added diamine's basicity in the second step, not allowing the procedure to be accomplished with a strong base, like D230. The use of the non-hydrolytic sol–gel approach allowed slowing down of the first (protolysis) step without significantly affecting its efficiency. In this manner, systems that previously could only be obtained for rubbery epoxy networks,[8] could now also form glassy network-based nanocomposites. Thus, the already tough DGEBA-D230 network could be further reinforced by well-tuned filler morphology and interphase bonding. On the other hand, the non-hydrolytic sol–gel approach, with IL addition, worked only when a strong base was used in the second reaction step.

Thus, this system could not be used for obtaining a rubbery system using a weak base, like D2000 (Scheme 1). Interestingly, the non-hydrolytic sol–gel based DGEBA-D230 systems in the presence of ILs also worked with more reactive sol–gel precursors, like tetramethoxysilane (TMOS), producing an even higher silica condensation degree. As these systems are more sensitive to the reaction conditions,[31] demanding a more detailed study, their synergistic action with ILs will be presented in a forthcoming paper.

3.4 Nanocomposites interphase bonding

A strong interphase interaction seemed to be the reason for the dramatic properties enhancements when carboxylic-ILs were applied. Especially in the case of $C_3H_6CO_2$HMImCl, the reinforcement seemed to surpass the effect based on the fine silica morphology, since C_7O_3MImMeS was also able to *in situ* produce very small silica particles in epoxy systems.[8,9] The IL addition in both DGEBA-D230–TEOS and DGEBA-D2000–TEOS systems led to a gradual enhancement in modulus when compared to the neat matrices, which seemed to depend on both the IL's side-chain length and functional group.

For evaluating the carboxylic-ILs' reactivity with DGEBA, a model reaction using PGE was followed by a time dependent FTIR experiment at room temperature. As PGE presents identical epoxy group reactivity to DGEBA, it could give an insight into the filler–matrix interphase during the nanocomposite *in situ* formation. The main evaluation criterion was the ~915 cm^{-1} peak consumption, corresponding to the oxirane group C–O stretching.[32] As a manner of excluding dilution and background effects, the ~750 cm^{-1} peak integration, relative to the PGE aromatic C–H bending,[32] was used as a correction reference.

The $C_3H_6CO_2$HMImCl was reacted in a stoichiometric ratio with PGE. At room temperature, the IL presented high reactivity with PGE, since after 5 h of reaction approximately 50% of epoxy groups were already consumed. After 24 h of reaction, practically no epoxy groups were observed in the FTIR spectrum (Fig. 9).

When the same procedure was carried out replacing $C_3H_6CO_2$HMImCl with acetic acid, no peak consumption was observed even after 48 h. This indicates an imidazolium ring catalytic effect for opening the PGE epoxy groups. The carboxylic-ILs' reactivity with the epoxy matrix justifies the drastic differences in mechanical properties among the systems, *i.e.* when applying different or no ILs to identical systems. This could cause a different interphase composition in each system, based on a sequence of covalent and physical bonds (Scheme 2).

The IL-free nanocomposite presented defined brittleness, which was due to the confined interphase with plenty of H-bonds with the silica Si–OH groups. The C_7O_3MImMeS contributed in reinforcing the network by van der Waals interactions throughout the interphase, causing toughness improvement. On the other hand, the carboxylic-ILs caused drastic changes by covalently bonding to the network. This

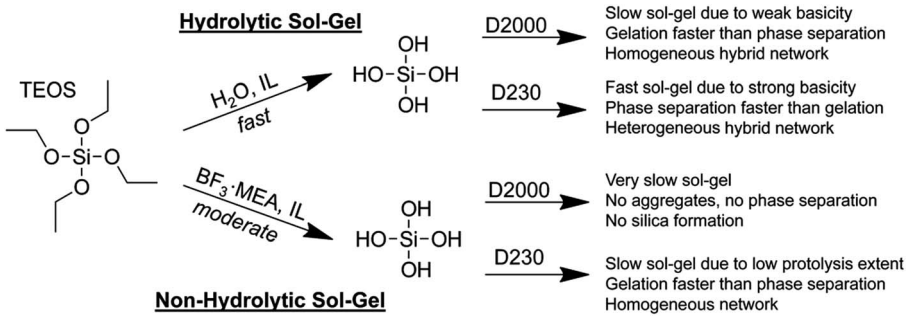

Scheme 1 Summary of characteristics of the epoxy–silica formed *via* hydrolytic and non-hydrolytic sol–gel processes in the presence of ILs.

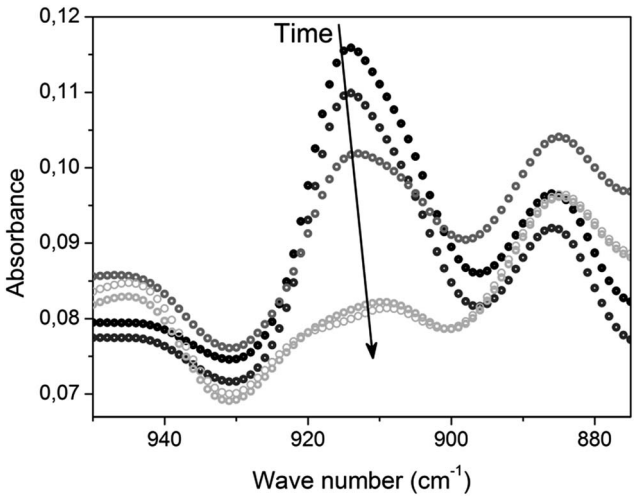

Fig. 9 Time dependent FTIR spectra of the reaction between PGE and $C_3H_6CO_2HMImCl$. Curves represent measurements at 30 min, 1 h, 5 h, 24 h and 48 h.

caused the modulus reinforcement together with flexibility for stress release, which strongly contributed to the toughness. The balance between adhesion strength and flexibility could be the key for balancing the interphase properties. Thus, the incorporation of $C_3H_6CO_2HMImCl$ strongly affected both flexibility and strength of the final nanocomposite, enabling the formation of the stiffest and toughest materials.

The strong mechanical properties contribution with such a small additive content makes these ILs very promising multi-task coupling agents for epoxy based nanocomposites.

4. Conclusions

Task-specific imidazolium ionic liquids (ILs) were used for morphology and interphase bonding control in the *in situ* epoxy–silica nanocomposites formation *via* the sol–gel process. Applying the ILs to the hydrolytic sol–gel process caused a fast TEOS hydrolysis process, allowing only rubbery epoxy–silica nanocomposites formation (using Jeffamine D2000 as the cross-linker). Nevertheless, the use of non-hydrolytic sol–gel (catalyzed by BF_3·MEA) allowed this drawback to be surpassed and also formed glassy epoxy–silica nanocomposites (using Jeffamine D230 as cross-linker), without application of water or co-solvents. The epoxy–silica interphase bonding was found to be crucial for both nanocomposite morphology and mechanical properties enhancement. The organic–inorganic system homogenization and improved silica nanodomains dispersion

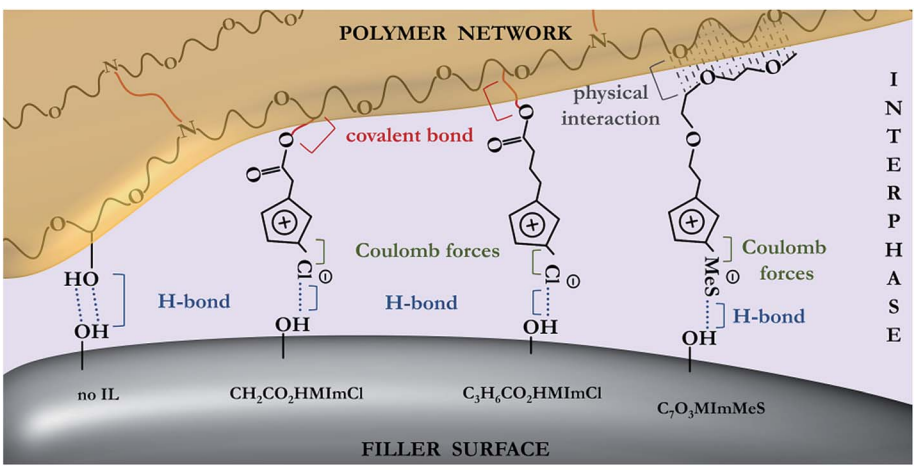

Scheme 2 Schematic representation of the interphase compositions depending on the IL applied, based on a sequence of covalent and physical bonds.

in the epoxy matrix were achieved for both the hydrolytic and non-hydrolytic sol–gel approaches. In the rubbery matrix, the IL application resulted in a significant system stiffening and toughening. In the glassy matrix, ILs led to the material's extensibility and toughness enhancement, without decreasing modulus by affecting the crosslinking density.

In both cases, the carboxylic-IL side chain length seemed to play a crucial role, as the systems with $C_3H_6CO_2$HMImCl presented the overall best results. The strong but ductile interphase, constituted by physical and chemical crosslinking, seemed to be the reason for the high nanocomposite reinforcement. When compared to the identical IL-free rubbery nanocomposite, the $C_3H_6CO_2$HMImCl system led to an increase of three times on Young's modulus, twice on tensile strength and ~150% on extensibility, producing a 7 times higher toughness. Most importantly, in the glassy nanocomposite, $C_3H_6CO_2$HMImCl led to 40% higher tensile strength and extensibility, producing an 80% higher toughness without modulus loss.

All the morphology control and mechanical properties enhancements were performed using a small silica content (~7.5 wt%) and a very small catalytic IL amount (0.2 wt%). These results outperform our own previous systems,[8,9] even when using 3 times smaller IL contents and without the addition of water or co-solvents, broadening the systems' possibilities for casting and molding applications without formation of residues.

Acknowledgements

The authors gratefully appreciate the financial support of the Brazilian funding agencies CAPES, CNPq and FAPERGS, and the Grant Agency of the Czech Republic (projects 14-05146S and P108/12/1459). R. K. Donato is thankful to FAPERGS-CAPES for the DOCFIX post-doctoral fellowship.

Notes and references

1 L. Matějka, in *Hybrid Nanocomposites for Nanotechnology*, Springer Verlag, New York, 2009, pp. 3–85.
2 J. Wen and J. E. Mark, *J. Appl. Polym. Sci.*, 1995, **58**, 1135.
3 L. Bokobza and J. P. Chauvin, *Polymer*, 2005, **46**, 4144.
4 G. Heinrich, M. Kluppel and T. A. Vilgis, *Curr. Opin. Solid State Mater. Sci.*, 2002, **6**, 195.
5 A. I. Medalia, *Rubber Chem. Technol.*, 1978, **51**, 437.
6 L. Matějka, O. Dukh and J. Kolarık, *Polymer*, 2000, **41**, 1449.
7 J.-P. Pascaut and R. J. J. Williams, in *Epoxy Polymers*, Wiley-VCH Verlag, Weinheim, 2010, p. 174.
8 R. K. Donato, L. Matějka, H. S. Schrekker, J. Plestil, A. Jigounov, J. Brus and M. Slouf, *J. Mater. Chem.*, 2011, **21**, 13801.
9 R. K. Donato, K. Z. Donato, H. S. Schrekker and L. Matějka, *J. Mater. Chem.*, 2012, **22**, 9939.
10 J. Dupont, R. F. de Souza and P. A. Z. Suarez, *Chem. Rev.*, 2002, **102**, 3667.
11 T. Welton, *Chem. Rev.*, 1999, **99**, 2071.
12 P. Wasserschied and T. Welton, *Ionic Liquids in Synthesis*, VCH Wiley, Weinheim, 2nd edn, 2008.
13 J. Lu, F. Yan and J. Texter, *Prog. Polym. Sci.*, 2009, **34**, 431.
14 D. Mecerreyes, *Applications of Ionic Liquids in Polymer Science and Technology*, Springer Verlag, Berlin, 2015, DOI: 10.1007/978-3-662-44903-5_1.
15 A. Martinelli, *Int. J. Mol. Sci.*, 2014, **15**, 6488.
16 R. K. Donato, M. Lavorgna, P. Musto, K. Z. Donato, A. Jager, P. Štepánek, H. S. Schrekker and L. Matějka, *J. Colloid Interface Sci.*, 2015, **77**, 447.
17 M. V. Migliorini, R. K. Donato, M. A. Benvegnu, R. S. Gonçalves and H. S. Schrekker, *J. Sol-Gel Sci. Technol.*, 2008, **48**, 272.
18 Y. Zhou, J. H. Schattka and M. Antonietti, *Nano Lett.*, 2004, **4**, 477.
19 K. Z. Donato, R. K. Donato, M. Lavorgna, L. Ambrosio, L. Matějka, R. S. Mauler and H. S. Schrekker, *J. Sol-Gel Sci. Technol.*, 2015, **76**, 414.
20 R. K. Donato, M. V. Migliorini, M. A. Benvegnú, M. P. Stracke, M. A. Gelesky, F. A. Pavan, C. M. L. Schrekker, E. V. Benvenutti, J. Dupont and H. S. Schrekker, *J. Sol-Gel Sci. Technol.*, 2009, **49**, 71.
21 J. Dupont, *J. Braz. Chem. Soc.*, 2004, **15**, 341.
22 S. Tang, G. A. Baker and H. Zhao, *Chem. Soc. Rev.*, 2012, **41**, 4030.
23 P. A. Hunt, C. R. Ashworth and R. P. Matthews, *Chem. Soc. Rev.*, 2015, **44**, 1257.
24 Z. Fei, D. Zhao, T. J. Geldbach, R. Scopelliti and P. J. Dyson, *Chem.–Eur. J.*, 2004, **10**, 4886.
25 H. S. Schrekker, D. O. Silva, M. A. Gelesky, M. P. Stracke, C. M. L. Schrekker, R. S. Goncalves and J. Dupont, *J. Braz. Chem. Soc.*, 2008, **19**, 426.
26 S. Ponyrko, L. Kobera, J. Brus and L. Matějka, *Polymer*, 2013, **54**, 6271.
27 M. V. Migliorini, R. K. Donato, M. A. Benvegnú, J. Dupont, R. S. Gonçalves and H. S. Schrekker, *Catal. Commun.*, 2008, **9**, 971.
28 C. J. Brinker and G. W. Scherer, *in Sol–Gel Science*, Academic Press, New York, 1989.
29 L. Matějka, K. Dusek, J. Plestil, J. Kriz and F. Lednicky, *Polymer*, 1998, **40**, 171.
30 Y. Li, J. Yu and Z.-X. Guo, *Polym. Int.*, 2003, **52**, 981.
31 S. Ponyrko, J. Kovarova, L. Kobera and L. Matějka, *J. Appl. Polym. Sci.*, 2014, **131**, 40899.
32 P. Larkin, in *Infrared and Raman Spectroscopy, Principles and Spectral Interpretation*, Elsevier, 2011.

Polymer Chemistry

PAPER

View Article Online
View Journal

Cite this: DOI: 10.1039/c5py01450f

Tailored high performance shape memory epoxy–silica nanocomposites. Structure design†

S. Ponyrko,[a] R. K. Donato[a,b] and L. Matějka*[a]

Received 8th September 2015,
Accepted 6th November 2015

DOI: 10.1039/c5py01450f

www.rsc.org/polymers

High performance shape memory (SM) epoxy–silica nanocomposites have been synthesized. The structure of the corresponding SM polymer was designed on the basis of the determined relationships between structure, mechanical properties and SM performance. The recovery stress, as a crucial SM property of high performance systems, is governed by the material toughness while the efficiency of the SM performance is controlled by morphological homogeneity and viscoelastic behaviour of the polymer as well as by experimental conditions of the SM procedure. The nanocomposites were prepared by *in situ* generation of nanosilica in the epoxy matrix. A non-aqueous sol–gel procedure was applied and the ionic liquid (IL) was used in the synthesis as a multifunctional agent controlling morphology and mechanical properties. The effect of nanosilica, IL, crosslinking density of the epoxy network, physical crosslinking as well as the application of the concept of bimodal networks on SM performance was evaluated and discussed. Based on the knowledge of the corresponding relationships and structural effects the SM nanocomposite was synthesized showing the high recovery stress σ_r = 3.9 MPa or high deformability ε_b = 103%. The study contributed to the better understanding of the SM behaviour of polymers.

1. Introduction

Shape-memory polymers (SMPs) are an important class of smart polymers capable of memorizing their shape. After a mechanical deformation and fixing a temporary shape they recover the original permanent shape upon external stimulation.[1,2] The recovery can be triggered by heat, light, electric or magnetic field, *etc*. The thermal-responsive SMPs are the most studied systems and will be the focus of this paper. In the past 10 years a remarkable advance in stimuli responsive SMPs has been achieved providing the potential applications in medical, aerospace, civil engineering, energy, and bionics areas.

The SMPs are composed of two phases – a permanent one and a switching phase which is sensitive to an external stimulus. The permanent phase, maintaining the dimensional stability, is the chemical or physical network. The switching phase enables a reversible transformation between hard and soft/liquid states. The most typical are the glassy and crystalline states serving to fix the temporary shape of a polymer. Thermally induced transformation of the switching phase, *i.e.* glass transition or melting, then leads to recovery of the original shape.

The shape memory (SM) properties of polymers are usually tested by the thermal SM cycle. It consists of (i) heating the sample above transformation temperature (T_{trans}), corresponding to T_g or T_m, up to deformation temperature T_d, (ii) deforming the sample into a temporary shape, (iii) cooling the sample below T_{trans} down to the setting temperature T_s while maintaining the deformation load; the temporary shape is quenched by vitrification or crystallization, (iv) the deformation load is released, (v) re-heating the sample above T_{trans} up to T_d. This step leads to a recovery to the original shape under nonconstrained conditions or to a stress recovery under constrained conditions, *i.e.* the sample is fixed at constant length. The SM behaviour of a SMP is characterized by the quantities, such as shape fixity R_f, shape recovery R_r, rate of recovery V_r and recovery stress σ_r. The first one indicates the ability of a polymer to fix the temporary shape after cooling and unloading, R_r and V_r describe the capacity of the material to recover the original shape and σ_r is a stress generated at the constrained recovery.[3] Generally, the high shape fixity requires a high modulus at the setting temperature, G_s, and scales with the expression $(1 - G_r/G_s)$, while the recovery is related mainly to the rubbery modulus G_r. The recovery stress increases with increasing G_r, and the nonconstrained recovery is faster at low G_r. Also broadness of the thermal transition plays a role. The sharp transition results in prompt fixing of the shape at cooling and triggering shape recovery at heating.

[a]Institute of Macromolecular Chemistry, Academy of Sciences of the Czech Republic, Heyrovsky Sq. 2, Prague, Czech Republic. E-mail: matejka@imc.cas.cz
[b]Laboratory of Technological Processes and Catalysis, Institute of Chemistry, Universidade Federal do Rio Grande do Sul, Av. Bento Goncalves 9500, Porto Alegre-RS, Brazil

†Electronic supplementary information (ESI) available. See DOI: 10.1039/c5py01450f

The typical SMPs are based on polyurethanes,[4] polyolefins,[5] acrylates,[6] polystyrene-based polymers[7] or epoxies.[8] With respect to another common shape memory material, shape memory alloys (SMA),[9,10] the SMPs are beneficial due to their variability, easier processability and larger attainable strain. The recoverable strain up to 700% has been reported in SMPs based on physically crosslinked thermoplastics.[4] However, the physical networks are prone to creep and irreversible plastic deformation resulting in a low shape fixity and recovery.[11] Therefore, covalently crosslinked networks, thermosets, are considered as more prospective shape memory candidates. They show a better shape fixity and recovery as well as a higher thermal and chemical stability. In general, however, the SMPs exhibit a low mechanical strength and stiffness resulting in poor SM properties such as a low recovery stress, being σ_r < 3 MPa and rate of recovery compared to SMA. This drawback has largely restricted the applications of SMPs.

The epoxy based materials are known to display superior mechanical properties. Moreover, a low curing shrinkage, versatile chemistry of curing and easy adjustable thermomechanical properties make the epoxy based glassy thermosets prospective SM materials, displaying excellent shape fixity and recovery, reaching 95–100%.[12] Despite their beneficial properties, however, not too many teams deal with the epoxy based SMPs due to a low deformability and high T_g of the corresponding systems.[13–19] Rousseau and Xie[20] studied the effect of the epoxy network structure on shape memory properties in order to give guidelines for the use of epoxy systems as high-performance SMPs. They investigated the networks of different crosslinking densities and flexibilities by using different amine crosslinkers or introducing the monoamine, and applying both aromatic and aliphatic epoxies. In this way, T_g and the rubbery modulus of networks were tuned in a wide range. However, the SM behaviour was found to be independent of a network structure, composition, crosslink density and viscoelasticity. All systems showed excellent SM performance with shape fixity and shape recovery approaching 100%. Only very slight differences were determined unveiling that SM properties decline at a low crosslinking density and a high chain flexibility. The recovery stress, however, was not reported.

The drawback of the epoxy-based SMPs is the low deformability: elongation at break ε_b < 30%, which limits their potential application. Several ways of increasing their deformability were reported. Gall *et al.* used the procedure of deformation at T close to T_g instead in the rubbery state.[21] This strategy makes it possible to increase ε_b from 30% to *ca.* 60%.[20] However, shape fixity was noticeably reduced. Williams *et al.*[22] described an SMP epoxy system with pendant alkyl chains undergoing self-assembly by tail-to-tail association thus forming physical crosslinks. This partially physically crosslinked SMP showed deformability ε_b as high as 75%. Highly deformable epoxy-based SMP has been recently investigated by Xie *et al.*[23] The composition of the networks based on the diepoxide E44 and Jeffamine D230 was tuned by varying epoxy/amine stoichiometric ratio, thus controlling the network crosslinking density. The networks of a low crosslinking density, at a high amine excess, were extended up to ε_b = 111 and 212%, in the rubbery state and at $T \sim T_g$, respectively. Despite the low crosslink density, the systems showed the perfect shape fixity, R_f > 99% and recovery ratio, R_r = 97–99.4%. The stress recovery was not reported. However, the deformability increased at the expense of stiffness and the modulus was reduced by 360% implying likely a severe decline of σ_r.

In order to overcome the main drawbacks of SMPs, a low stiffness, strength and a low recovery stress, attention has been paid to the polymer reinforcement. The polymer fillers are able to improve the mechanical performance and shape recovery stress of SMPs[24–27] and consequently the polymer composites/nanocomposites are prospective materials for SM systems.[28–31] Different types of reinforcing agents were used, such as exfoliated nanoclay,[32] microfibers,[33] carbon nanotubes,[34] and functionalized SiO_2 particles[35] enhancing mechanical and SM properties. Beloshenko *et al.*[36] revealed the importance of strength of a polymer–filler interphase. The composites with the strong polymer–silica and weak polymer-expanded graphite interactions displayed recovery stress σ_r = 1.1 and 0.6 MPa, respectively. Gall *et al.*[37] described the fabrication and characterization of the epoxy-based SMP composites filled with the nanoparticulate SiC. The modulus was enhanced and the recovery force in the nanocomposites was shown to increase by 50% with the addition of 20 wt% SiC. At a high content of nanofiller, however, a permanent deformation occurred deteriorating the SM properties. Just the permanent deformation and a decrease in attainable strain limit the application of composites/nanocomposites as a SM material.

In this work we aim to prepare and study the high performance epoxy-based SMP showing a high recovery stress and a high deformability, while keeping an excellent shape fixity and recovery. The study is focused on the design of the structure of the SMP and determination of relationships between the structure and SM properties of the investigated systems. The structural design makes it possible to control the thermomechanical, tensile mechanical and viscoelastic properties and thereby to optimize the SM behavior. We have investigated the reinforced systems, epoxy–silica nanocomposites, in order to enhance mechanical properties. The nanocomposites are more efficient than the classical composites due to a large interfacial area and a correspondingly stronger polymer–nanofiller interaction. The structural design takes into account (i) the structure of the epoxy matrix including the crosslinking density of the network, flexibility of polymer chains, physical crosslinking, as well as a concept of bimodal networks, (ii) the nanocomposite morphology involving the nanofiller content and quality of dispersion in the matrix as well as an interphase interaction. In addition to the material structure design the optimization of a SM procedure was also performed in order to fully exploit the potential of SMP materials.

The special approach has been applied for the synthesis of the epoxy–silica nanocomposites in order to tune their structure and morphology to be most suitable for the SMP system. The different types of epoxy–amine networks based on diglycidyl ether of bisphenol A (DGEBA) were used as polymer

matrices. The nanocomposites were prepared by *in situ* generation of nanosilica in the epoxy network, thus ensuring a good dispersion of nanofiller in the matrix. The non-aqueous sol–gel process was used to incorporate nanosilica. This procedure enables a better control of the nanocomposite morphology and a more efficient enhancement of mechanical properties compared to the classical aqueous sol–gel procedure.[38,39] In addition, the absence of water makes the synthesis easier. Moreover, the ionic liquids (ILs) were applied during synthesis making possible modification of the morphology and further homogenization by improvement of polymer–nanosilica interaction, as well as reinforcement of the nanocomposite.[40,41]

The novelty of this paper consists of the design and synthesis of high performance SMPs by application of epoxy–silica nanocomposites with a well controlled structure and thermomechanical properties using a non-aqueous sol–gel process under catalytic action of the ILs. The general relationships between the nanocomposite structure and SM properties were determined providing thus a better understanding of the SM behaviour.

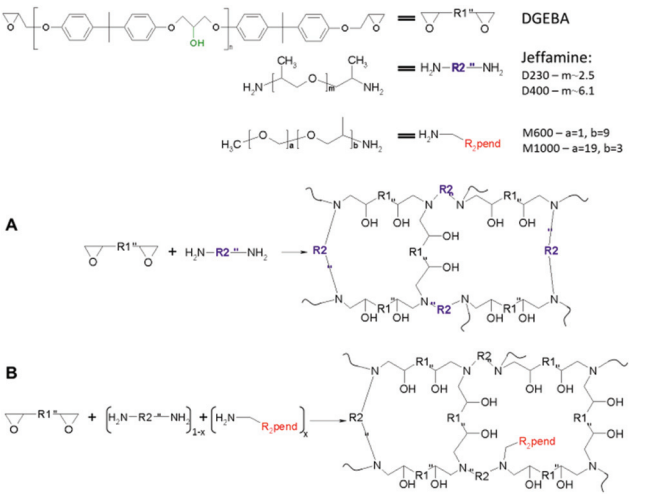

Scheme 1 Structure of the (A) networks DGEBA–D230 and DGEBA–D400, (B) networks with pendant chains DGEBA–D230–M.

2. Experimental

2.1. Materials

Diglycidyl ether of bisphenol A (DGEBA, n = 0.17) based resin with an equivalent weight of the epoxy groups E_E = 187 g mol^{-1} epoxy groups was obtained from Aldrich.

Crosslinking agents: poly(oxypropylene)diamines – Jeffamine® D230 and D400 were received from BASF, ethylenediamine (EDA) and 4,4′-methylenebis(3-methylcyclohexylamine) (Laromin) were obtained from Aldrich, the polyether monoamines Jeffamine® M600 and M1000 were purchased from Huntsman, and amine-terminated butadiene–acrylonitrile copolymer (Hycar ATBN 1300X16) was obtained from Nanoresis.

Inorganic components: tetramethoxysilane (TMOS) was purchased from Fluka. Borontrifluoride monoethylamine (BF_3MEA) was obtained from Aldrich.

The ionic liquids 1-decyl-3-methylimidazolium tetrafluoroborate ($C_{10}BF_4$), 1-butyl-3-methylimidazolium tetrafluoroborate (C_4BF_4) and 1-butyl-3-methylimidazolium chloride (C_4Cl) were obtained from Prof. Schrekker (Universidade Federal do Rio Grande do Sul, Porto Alegre-RS, Brazil).[42]

All chemicals were used without any further purification.

2.2. Synthetic procedures

2.2.1 Networks. The epoxy networks were prepared by the reaction of DGEBA with di- and monoamines at a total stoichiometric ratio of functional groups ($C_{epoxy} : C_{NH}$ = 1 : 1). The content of monoamines in the networks is characterized by molar fraction of amino groups x in the amine mixture belonging to monoamines; $x = [NH_2]_{mono}/([NH_2]_{mono} + [NH_2]_{di})$ (see Scheme 1B).

2.2.2 Nanocomposites. A two step synthesis was applied.[38] (i) 2 wt% of BF_3MEA with respect to TMOS was mixed with an epoxy resin for 30 min at 70 °C. After that, an optional content of TMOS was added to the DGEBA–BF_3MEA mixture and rapidly mixed for another 30 min. Then 0.2 wt% of ionic liquid was added (if mentioned in a sample code) to the mixture and mixed for further 30 min. (ii) Stoichiometric equivalent weight of diamine was added to the prereacted mixture of TMOS in the epoxy resin and mixed for 30 min. In the case of bimodal networks Laromin, ATBN together with EDA were added to the epoxy resin and stirred for 20 min. The following curing regime was applied: 90 °C for 2 h; 130 °C for 16 h and postcuring under vacuum for 5 h at 190 °C or 210 °C in the case of Laromin containing networks.

The content of silica in nanocomposites was indicated according to the weight fraction of TMOS with respect to DGEBA used for the nanocomposite synthesis. The amount of TMOS indicated as T7, 14, 25 and 40 corresponds to the 2.6, 5.4, 9.6 and 15.2 wt% of nanosilica, respectively.

The studied systems were designated according to the diamine of the network: D230, D400, ATBN (A), EDA (E), Laromin (L), the presence of monoamine MY (molar fraction x), the content of silica T(7–40) and the presence of IL (abbreviation). For example DGEBA–D230–M600(0.05)–T(14)–C_4Cl or the bimodal network DGEBA–A(0.3)–E(0.2)–L(0.5)–T(7)–$C_{10}BF_4$.

2.2.3 Dual SM nanocomposites. Two different amines D230 and D400 were used to prepare the dual SM nanocomposite according to the procedure discussed above. Both nanocomposite mixtures were placed on a Teflon wafer separated by a thin silicone bar. During the reaction at a high enough viscosity the silicone bar was removed and two halves of the specimen were mingled at the interphase.

2.3. Methods

The mechanical tests were performed by using an ARES G2 apparatus (TA Instruments).

2.3.1 Dynamic mechanical thermal analysis. The temperature dependence of the complex shear modulus of rectangular samples was measured by oscillatory shear deformation at a constant frequency of 1 Hz and at a heating rate of 3 °C min^{-1}. The glass transition temperature T_g was evaluated as a maximum of the loss factor tan δ. The rubbery modulus was determined at temperature $T = T_g + 30$ °C.

2.3.2 Tensile test. Tensile test experiments were performed at axial force with a constant linear speed of 0.06 mm min^{-1} (unless stated otherwise) at T_d = 100 °C or at T_d = 120 °C in the case of bimodal networks. Five rectangular specimens with dimensions 25 × 5 × 1 mm were tested for each sample. The toughness was evaluated as an area under the stress–strain curve.

2.3.3 Stress relaxation. Stress relaxation was measured by the transient stress relaxation mode at a strain λ = 1.07 at T_d = 100 °C.

2.4. Shape-memory properties

SM behaviour was followed in the temperature region T = 25–100 °C, with the setting temperature T_S = 25 °C, transition temperature $T_{trans} = T_g$ and deformation temperature T_d = 100 °C or T_d = 120 °C in the case of bimodal networks. The following parameters were determined to evaluate the shape-memory behaviour: shape fixity, recovery stress (at constrained mode) or recovery rate and extent of recovery (at unconstrained mode).

2.4.1 Shape fixity. Shape fixity was measured both in stretching (linear) and in bending modes. The sample was heated and deformed to the length l_d or to the angle Θ_d = 90° at the deformation temperature. Subsequently, the deformed sample was quickly cooled to the setting temperature and kept at T_S = 25 °C for 6 months. The change of the length and the angle in time was recorded.

Shape fixity was evaluated as $R_f = 1 - [(l_d - l_f)/l_d] \times 100\%$, where l_d and l_f are the lengths in the deformed state at deformation temperature and in the frozen state after 6 months, respectively. The bending mode was applied as well because of easy visualization of shape fixity.

2.4.2 Shape recovery. Shape recovery triggered by heating up to T_d was evaluated in the linear mode as $R_r = [1 - (l_r - l_0)/l_0] \times 100\%$, where l_0 is the initial non-deformed length and l_r is the recovered length.

2.4.3 Rate of shape recovery. The rate of shape recovery was evaluated in the bending mode by following the angle change of the deformed specimen in time.

2.4.4 Constrained recovery – recovery stress (σ_r). The recovery stress σ_r was measured on an ARES G2 equipped with a thermal chamber and a liquid nitrogen tank. The rectangular sample 25 × 5 × 1 mm was heated up to deformation temperature T_d and extended up to 60% of the previously determined strain at break, $\lambda_d = 0.6\lambda_b$, at a rate of 0.06 mm min^{-1}, unless stated otherwise. In all experiments $\lambda_d > 1.07$, which corresponds to the thermoelastic inversion point of epoxy systems.[13,43] The sample was subsequently cooled at a rate of 10 °C min^{-1} (unless stated otherwise) down to the setting temperature T_S while maintaining the load and kept for 10 minutes to completely freeze and store the stress within the sample. Only then the sample was unloaded. For the constrained recovery the sample was fixed, the length was kept constant and heated up to deformation temperature. The recovery stress triggered by heating was recorded.

3. Results and discussion

The epoxy–silica nanocomposites have been designed as promising high performance SMPs applicable in the temperature range between T_{room} and T = 100 °C.

3.1. Synthesis of SM networks and nanocomposites

The nanocomposites based on epoxy–amine networks were prepared and the following structural parameters or synthesis conditions were varied in order to modify the nanocomposite structure and morphology: (i) crosslinking density of the epoxy network, (ii) presence of long pendant chains in the network, (iii) content of nanosilica, (iv) presence of ILs at the synthesis.

3.1.1 Epoxy networks. Three types of the networks were synthesized. (i) The networks of different crosslinking densities were prepared by crosslinking DGEBA with diamines of different lengths, including poly(oxypropylene)diamines, Jeffamines D230 (M = 230) and D400 (M = 430) (see Scheme 1A), and amino-terminated butadiene–acrylonitrile copolymer, ATBN (M = 3600). (ii) The networks containing long pendant chains were prepared by partial substitution of diamines with monoamines, polyetheramines, Jeffamine M600 ($M \sim 600$) and M1000 ($M \sim 1000$) (Scheme 1B). (iii) The bimodal networks with the bimodal distribution of crosslinking density were prepared by crosslinking DGEBA with two diamines of different lengths, ATBN (M = 3600) and 4,4′-methylenebis(3-methylcyclohexylamine) (Laromin) (M = 238) (Scheme 2). The network involves long flexible sequences of ATBN (R3 sequence) and rigid sequences of Laromin (R4) as well as compatibilizing parts of EDA (R5).

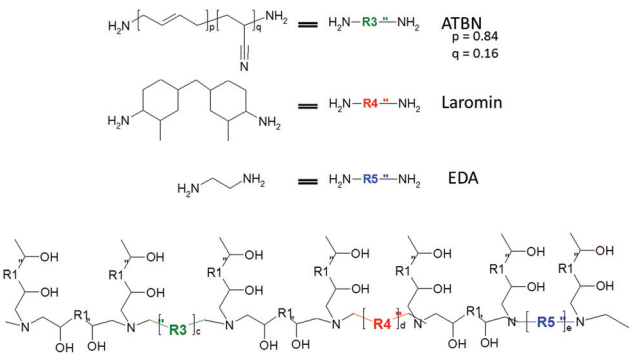

Scheme 2 Structure of the bimodal network.

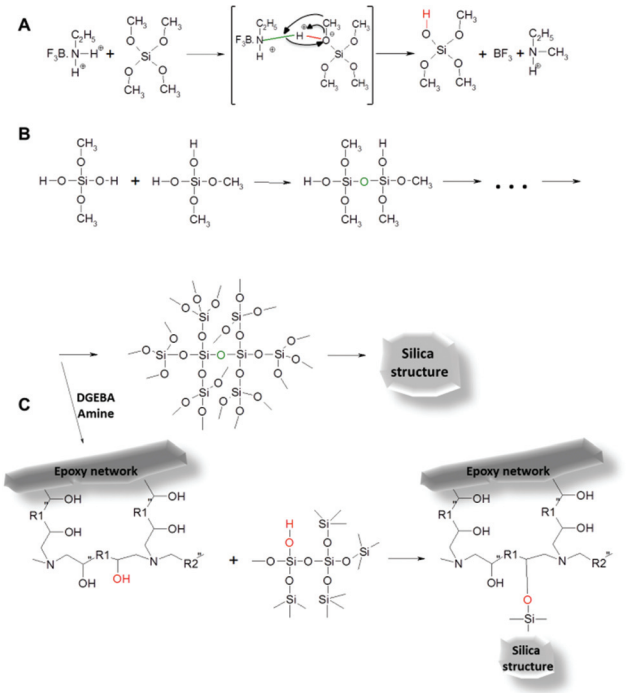

Scheme 3 Formation of epoxy–silica nanocomposites: (A) proteolysis of TMOS, (B) silica formation, (C) build-up of the nanocomposite, covalent bonding between the epoxy network and silica domain.

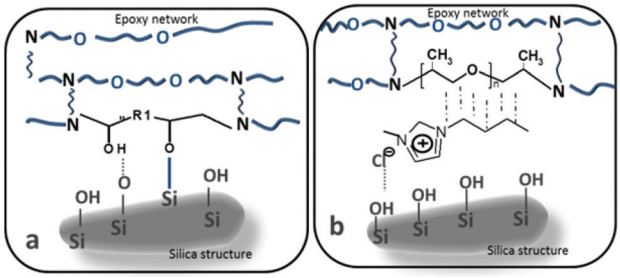

Scheme 4 Representation of the corresponding nanocomposite interphase interactions: (a) covalent grafting epoxy–silica; (b) physical interactions in the presence of IL.

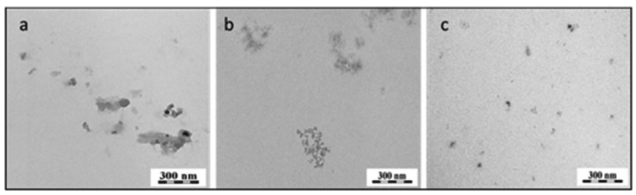

Fig. 1 TEM micrographs of the nanocomposite DGEBA–D400–T(14) prepared by (a) aqueous sol–gel process, (b) non-aqueous sol–gel process, (c) non-aqueous procedure in the presence of the IL C_4Cl.

3.1.2 Epoxy–silica nanocomposites. The nanocomposites were prepared by *in situ* generation of nanosilica within the epoxy–amine matrix by the non-aqueous sol–gel process (Scheme 3B). The non-hydrolytic polycondensation was initiated by proteolysis of TMOS using BF_3MEA (Scheme 3A).[38,39] During the nanocomposite formation the interphase epoxy–silica covalent grafting occurs[38] (Scheme 3C). The sequential synthesis was applied (see the Experimental section).

The imidazolium based ILs were used in the synthesis of the epoxy–silica nanocomposites serving as multifunctional agents for the sol–gel process. The IL acts as a catalyst, surfactant and an efficient agent controlling the silica structure as well as the nanocomposite morphology by forming strong physical interphase interactions, the silica–IL–epoxy matrix.[41]

The non-aqueous sol–gel procedure and application of ILs make it possible to control the interphase interaction, both covalent and physical (see Scheme 4) and fine tuning the structure and morphology of the nanocomposites as well as to enhance their mechanical properties.[38–41]

The applied synthesis leads to the formation of well homogeneous epoxy–silica nanocomposites. The TEM micrographs in Fig. 1 show a comparison of the morphology of the nanocomposites prepared by the classical aqueous sol–gel process, by the non-aqueous procedure and that prepared in the presence of the IL. While the reference "aqueous nanocomposite" exhibits non-uniform dense particles forming aggregates with a broad size distribution, the non-aqueous sol–gel process results in a finer morphology of loosely packed aggregates and the IL promotes the formation of morphology composed of uniformly dispersed particles without larger aggregates.

3.2. High performance SMP – design of structures

SMPs undergo a shape recovery triggered by heating above the transition temperature (unconstrained recovery). In the case of the fixed strain (constrained recovery) the material shows a recovery of the stress. This recoverable stress depends on the mechanical stress at the initial deformation in the rubbery state, which is internally stored into the polymer upon the cooling/fixing process. Under ideal conditions and no losses, at a perfect shape fixity and no stress relaxation it holds according to the theory of rubber elasticity.

$$\sigma_r \sim \sigma_d = G_r(\lambda_d - \lambda_d^{-2}) \quad (1)$$

where σ_r is the recovery stress, G_r and σ_d are the modulus and stress under deformation in the rubbery state, respectively, $\lambda(= l/l_0)$ is the deformation ratio, l and l_0 are the deformed and initial length of the sample, respectively. The stress at recovery thus depends on the rubbery modulus and deformation λ. Gall *et al.* observed that the recovery stress directly scales with the rubbery modulus and the network stress at the initial deformation.[44] Hence, the design of the polymer with a high rubbery modulus allowing a high deformation in the rubbery state is a way to the synthesis of high performance SMPs.

Moreover, the investigation is focused on the systems showing shape memory properties in the temperature region $T = T_{room} - 100$ °C (or 120 °C), where T_{room} is the setting tem-

perature T_s. Consequently, adjustment of T_g is necessary as well.

3.2.1 Control of the thermomechanical properties

Crosslinking density and chain flexibility. The thermomechanical properties of a prospective SMP are tuned in such a way to reach a high rubbery modulus while to keep T_g in the application window of a polymer.

The rubbery modulus of elasticity of polymer networks is determined mainly by the crosslinking density ν:

$$G_e = \nu RTA + \text{physical contribution} \quad (2)$$

G_e is the equilibrium shear modulus in the rubbery state, A is the front factor ($A = 1$ for affine networks, $A = (f - 2)/f$ for phantom networks, f is the functionality of a crosslinker).

Physical contribution to a modulus involves physical crosslinking by trapped chain entanglements or by formation of self-assembly domains acting as network junctions. The crucial contribution, however, is given by the presence of fillers in composites or nanocomposites. The hydrodynamic effect of fillers resulting in strain amplification, formation of a rigid interphase layer due to a polymer–filler interphase interaction giving rise to an increasing efficient fraction of a filler, physical crosslinking through filler domains or filler networks build-up at percolation of the filler structure are the reasons of a polymer reinforcement by a filler.

The increase in the crosslinking density of a network to enhance the modulus gives rise to an increase in T_g as well. Therefore, there are certain limits of crosslinking density in order to keep T_g in the application window of a SMP. In addition to the crosslinking density the chain stiffness or flexibility also affects the modulus by modifying the front factor A in eqn (2).[45] Stiff chains in a network lead to a higher modulus and higher T_g with respect to the network containing flexible chains.[20] Due to the simultaneous effect of a network structure on both the modulus and T_g a careful tuning of the polymer structure is necessary in order to optimize the thermomechanical properties for a SMP application.

We have studied the epoxy–amine networks of various crosslinking densities and flexibilities of network chains. They were prepared by using four amine crosslinkers: Jeffamines D230 and D400, Laromin and ATBN. Generally, it holds for the crosslinking density $\nu \sim 1/M_C$, where M_C is the molecular weight of the elastically active chain between crosslinks, that can be controlled, *e.g.*, by a structure of a crosslinker. The molecular weights of the applied amines are as follows: M(D230) = 230, M(D400) = 430, M(Laromin) = 238, M(ATBN) = 3600. Fig. 2 shows the effect of the length of the amines on the modulus in the rubbery state G' and T_g of the epoxy networks. The modulus increases in the series DGEBA–ATBN < DGEBA–D400 < DGEBA–D230 in accordance with increasing crosslinking density. The higher modulus of the DGEBA–Laromin network compared to DGEBA–D230, possessing approximately the same crosslinking density, is a result of a higher rigidity of the cycloaliphatic amine with respect to polyether network chains. The modulus of these networks enhances from

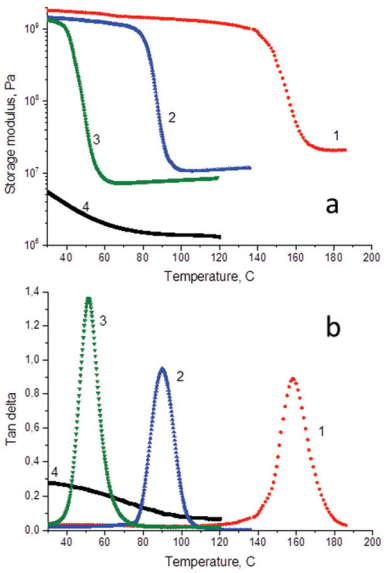

Fig. 2 Storage modulus (a) and loss factor tan δ (b) of epoxy networks as a function of temperature: 1 DGEBA–Laromin, 2 DGEBA–D230, 3 DGEBA–D400, 4 DGEBA–ATBN.

1.5 MPa up to 20 MPa. However, only the networks DGEBA–D400 and DGEBA–D230 display T_g in the suitable application window, at T_g = 50 °C and T_g = 91 °C, respectively.

Physical crosslinking. Introducing the physical crosslinks in a covalent network is another approach to increase the modulus. We have studied the epoxy networks DGEBA–D230 containing long pendant polyoxypropylene chains (see Scheme 1B). The incorporation of monoamines M600 and M1000 into the network results in lowering of the total amine functionality and in a decrease in the chemical crosslinking density. The rubbery modulus, however, on the contrary increases at a small amount of the monoamines as shown in Fig. 3. This is a result of physical crosslinking due to self-assembling or formation of entanglements between dangling chains. At a small fraction of the monoamines, x = 0.05, this effect dominates and the rubbery modulus enhances with respect to the unmodified DGEBA–D230 network. In contrast, the flexible pendant chains give rise to a decrease in T_g of the network. Consequently, the thermomechanical properties of these networks can be tuned by controlling chemical and physical crosslinking in such a way that the modulus increases and the T_g simultaneously diminishes. This approach is beneficial for our SMP by enhancing the rubbery modulus while keeping T_g in the application window. In the case of the network DGEBA–D230–M1000 (x = 0.05) the modulus grows from 10 MPa of the unmodified network to 14 MPa and the T_g decreases from 91 °C to 73 °C.

Nanofiller effect. The most pronounced reinforcement of the epoxy networks was achieved by incorporation of silica nanofillers. The thermomechanical behaviour of the nanocomposites DGEBA–D400–nanosilica is illustrated in Fig. 4. The rubbery modulus is significantly enhanced in the nanocompo-

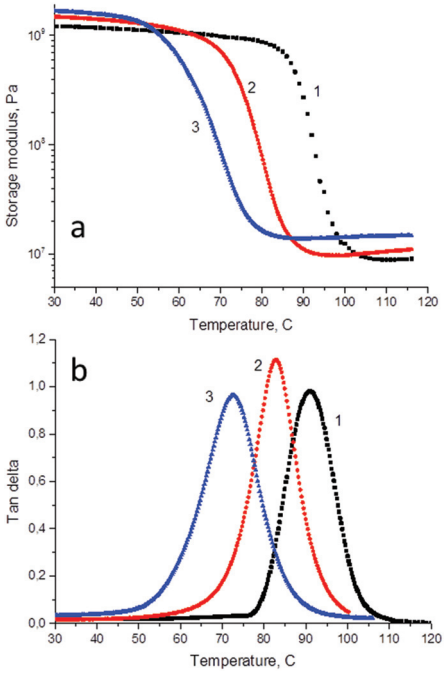

Fig. 3 Storage modulus (a) and loss factor tan δ (b) of the DGEBA–D230 with pendant chains as a function of temperature: 1 DGEBA–D230, 2 DGEBA–D230–M600 (x = 0.05), 3 DGEBA–D230–M1000 (x = 0.05).

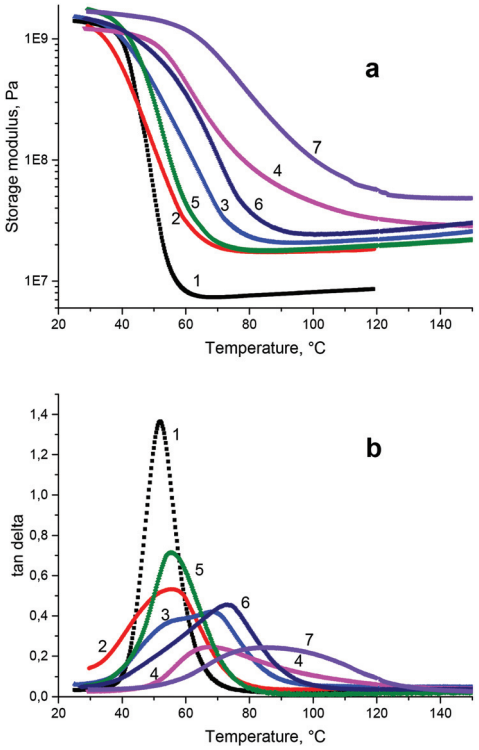

Fig. 4 Storage modulus (a) and loss factor tan δ (b) of the DGEBA–D400 based hybrids as a function of temperature: 1 DGEBA–D400, 2 DGEBA–D400–T(14), 3 DGEBA–D400–T(25), 4 DGEBA–D400–T(40), 5 DGEBA–D400–T(14)–C_4Cl, 6 DGEBA–D400–T(25)–C_4Cl, 7 DGEBA–D400–T(40)–C_4Cl.

sites by 100–250% with respect to the neat DGEBA–D400. The hybrid network containing 9.6 wt% silica (T25) and 15.2 wt% silica (T40) displays the modulus G_r = 20 MPa and 30 MPa, respectively. At the same time the T_g of the nanocomposites is raised due to immobilization of the network chains by interaction with silica domains and formation of a rigid interphase layer (see Scheme 4a). In the case of the nanocomposite DGEBA–D400–T(25) the glass transition temperature is increased by 15 °C. This T_g rise limits the application of silica reinforcement to the DGEBA–D400 matrix only because the DGEBA–D230 based nanocomposite does not fit in the application temperature window due to a very high T_g. The high content of silica is moreover manifested by broadening of glass transition. This is a result of a system inhomogeneity. The nanocomposite shows a wide distribution of chains' dynamics in the vicinity of the silica domain ranging from severely immobilized chain sequences to less restricted chains sterically far from the nanofiller. In addition, incompletely reacted siloxane/silica domains contribute to the broadness of the transition.[39] The wide transition limits the application of nanocomposites as a SMP. It gives rise to a slower recovery at heating and in the low temperature region the broad transition decreases the modulus at the setting temperature G_S which is responsible for the shape fixity. G_s is lowered by 20–30%, however, it is still high enough to provide the excellent shape fixity. Optimization of the silica content is thus necessary in order to avoid a very high T_g and an excessive widening of the glass transition.

Ionic liquids' effect. The IL increases both the rubbery modulus and T_g of the nanocomposite. Fig. 4 shows that this effect is more pronounced at a higher silica content (*cf.* curves 2 and 5 for T14, curves 3 and 6 for T25, curves 4 and 7 for T40). The modulus reaches 48 MPa in the case of DGEBA–D400–T40–IL. Crucial, however, is the effect of the IL on the morphology and homogenization of the nanocomposite as revealed in Fig. 1. The enhanced homogeneity due to an interphase interaction (see Scheme 4b) is reflected in thermomechanical properties. Fig. 4 displays a narrowing of glass transition of the nanocomposite promoted by the IL (*cf.* curves 5 and 2). The sharp transition results in a faster quenching and in a better shape fixity. This is, however, true only at a low and medium silica amount. The optimum nanocomposite thermomechanical properties were accomplished by using 5–10 wt% silica (the hybrids T(14)–(25)). At a higher TMOS content (T40), the T_g is too high and homogenization does not work; and glass transition is too broad (curve 7). Three types of ILs were used in the synthesis of nanocomposites; C_4Cl, C_4BF_4 and $C_{10}BF_4$. However, no difference in their effect on morphology and thermomechanical properties was observed.

The most suitable thermomechanical properties of the SMP were achieved by combination of the above discussed effects of the physical crosslinking by pendant chains and the reinforcement with nanosilica generated under IL assisted catalysis (see

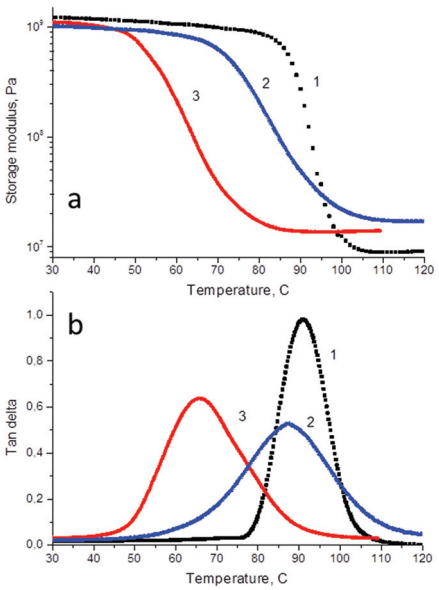

Fig. 5 Storage modulus (a) and loss factor tan δ (b) of the DGEBA–D230–T(7) with pendant chains: 1 DGEBA–D230, 2 DGEBA–D230–M600(0.05)–T(7), 3 DGEBA–D230–M1000(0.05)–T(7).

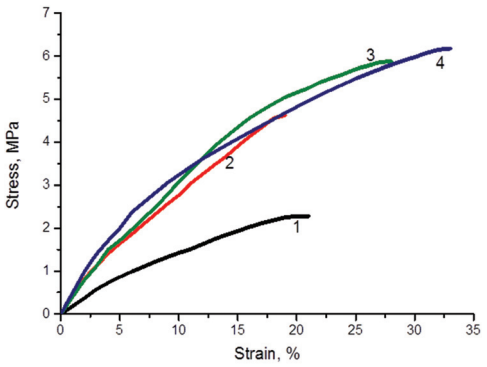

Fig. 6 Stress–strain behaviour of the SM network and nanocomposites at T_d: 1 DGEBA–D400, 2 DGEBA–D400–T(14), 3 DGEBA–D400–T(14)–C_4Cl, 4 DGEBA–D400–T(25)–C_4Cl.

Fig. 5). Because of the T_g lowering by plasticizing pendant chains also the higher-T_g network DGEBA–D230 could be used as a matrix for the epoxy–silica nanocomposite. The T_g of the corresponding DGEBA–D230–monoamine–nanosilica–IL system is kept in the application window. This complex nanocomposite profits as SMP from the following thermomechanical properties; (i) high modulus due to silica reinforcement and physical crosslinking, (ii) T_g in the application window due to a plasticizing effect of flexible pendant chains, (iii) narrow glass transition because of nanocomposite homogenization by the action of ILs.

The thermomechanical properties of the studied SM polymers are characterized in Table S1 (in the ESI†.)

3.2.2 Tensile stress–strain behaviour. The suitable thermomechanical properties of a material, including T_g, broadness of the transition, rubbery and setting moduli G_r, G_s, are prerequisite for an optimum shape memory behaviour. In addition, however, the structure design must take into account the material behaviour at deformation which is closely related to the shape memory process.

We have investigated the tensile stress–strain properties of the examined systems at T_d = 100 °C or 120 °C in the rubbery state. The results of the DGEBA–D400 based network and nanocomposites are displayed in Fig. 6. The polyether Jeffamine based epoxy networks DGEBA–D400 and DGEBA–D230 are considered to belong to the toughest epoxy thermosets. The DGEBA–D400 network (curve 1) shows an elongation at break ε_b = 20% in the rubbery state and tensile strength σ_b = 2.3 MPa. Fig. 6 reveals that the epoxy network modification leads to a dramatic improvement of tensile properties. Incorporation of nanosilica into the network (curve 2) brings about a significant enhancement of modulus and strength, while only a slight reduction of deformability (ε_b). Another improvement is achieved by application of the IL in the synthesis of nanocomposites (curves 3 and 4). The beneficial effect of the IL is manifested by a pronounced increase in toughness of the nanocomposites; both extensibility and tensile strength are enhanced. This is a result of modification of the epoxy–silica interphase by the IL (see Scheme 4b). The strong physical dynamic interphase interaction undergoes a breaking-formation process under stress which is responsible for the enhanced toughness. The material toughness corresponds to the mechanical energy absorbed by a material before break and generally it is characterized by the area under the stress–strain curve. The polymer toughness was found to be the decisive material property governing the shape memory behaviour as discussed below. A similar, but less pronounced trend in tensile behaviour was also observed at room temperature as shown in Table S2 (in the ESI†).

Highly deformable SM epoxy polymers – bimodal networks. The extensibility, *i.e.* strain at break λ_b, of a polymer network based material is related to the crosslinking density and generally it is expressed as $\lambda_b \sim M_c^{1/2}$. The polymer deformability thus could be increased at the expense of the modulus only, as $G \sim 1/M_c$.

The high-molecular weight amine crosslinker ATBN (M = 3600) allows to prepare the highly extensible epoxy network. Fig. 7 illustrates the corresponding stress–strain curve at T_d = 120 °C revealing the high elongation at break ε_b = 280% (curve 2). The DGEBA–ATBN elastomer is rubbery at room temperature and hence the combination with the high-T_g, but a less ductile, DGEBA–Laromin network (Fig. 7 curve 1 and Fig. 8 curve 1) was applied in order to increase T_g of the corresponding bimodal network. The bimodal network (see Scheme 2) of the molar composition, DGEBA–ATBN (n = 0.3) – Laromin (n = 0.7), exhibits still a high extensibility; ε_b = 100% (Fig. 7, curve 3) and T_g occurs in the application window, T_g = 85 °C (see Fig. 8, curve 2).

This system is phase separated, containing the mixed phase of partially miscible epoxy and rubbery components with a broad glass transition (T_g = 85 °C), and a dispersed rubbery

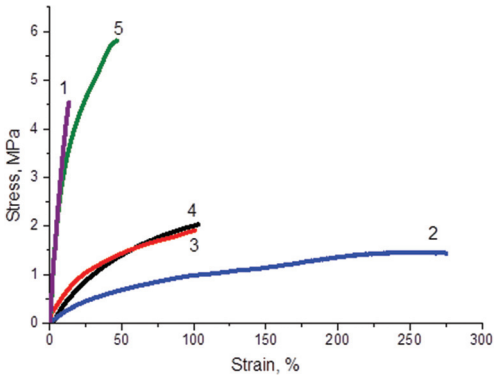

Fig. 7 Stress–strain behaviour of the SM nanocomposites at T_d: 1 DGEBA–Laromin, 2 DGEBA–ATBN, 3 DGEBA–A(0.3)–L(0.7), 4 DGEBA–A(0.3)–E(0.2)–L(0.5), 5 DGEBA–A(0.3)–E(0. 2)–L(0.5)–T(14).

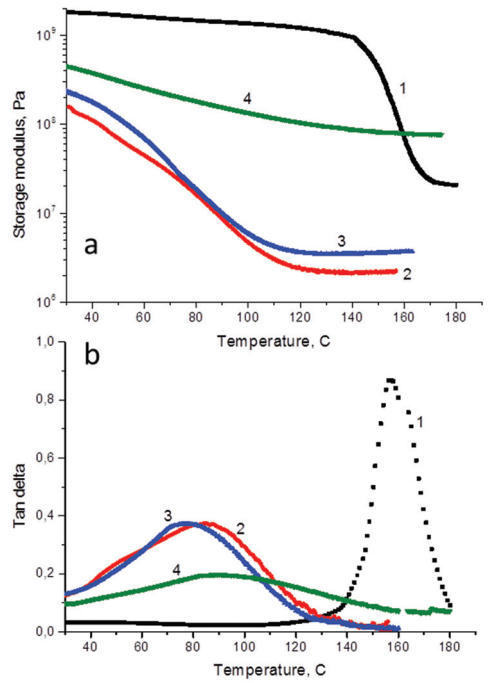

Fig. 8 Storage modulus (a) and loss factor tan δ (b) of the bimodal systems: 1 DGEBA–Laromin, 2 DGEBA–A(0.3)–L(0.7), 3 DGEBA–E(0.2)–A(0.3)–L(0.5), 4 DGEBA–A(0.3)–E(0.2)–L(0.5)–T(14).

phase (T_g = −45 °C, not shown in Fig. 8). The low temperature shoulder in addition to the maximum in the tan δ curve in Fig. 8b, however, reveals a partial phase separation and incompatibility of the two networks even within the "miscible phase". Because of a high fraction of the separated ATBN phase the modulus at room temperature is relatively low, G_s = 160 MPa, which results in a low shape fixity of the SMP. Improvement of compatibility was achieved by addition of a small amount of crosslinker ethylenediamine (EDA). The corresponding network DGEBA–A(0.3)–E(0.2)–L(0.5) shows a better compatibility as it is obvious from one loss factor peak in Fig. 8 (curve 3). The fraction of the dispersed rubbery phase was diminished, however, not eliminated. This modification leads to a slight reduction of T_g and narrowing of glass transition as well as to increase both G_r and G_s. However, G_s is still low (= 240 MPa) and the tensile properties are not significantly changed, ε_b = 103% (Fig. 7, curve 4). The substantial improvement of mechanical properties was achieved by using a nanofiller. The nanocomposite containing 5 wt% silica (T14) (Fig. 7, curve 5) displays enhancement of strength by 200% and G_r by more than an order of the magnitude up to 76 MPa. The extensibility is relatively high, ε_b = 47% and G_s increases. Even this nanocomposite involves a small fraction of the dispersed rubbery phase.

The bimodal network based nanocomposite is a very tough material. The following series displays the studied systems with increasing toughness as evaluated from the area under the stress–strain curve: DGEBA–D230 < DGEBA–D230–M–T < DGEBA–D400 < DGEBA–D400–T < DGEBA–D400–T–IL < DGEBA–A(0.3)–L(0.7) < DGEBA–A(0.3)–E(0.2)–L(0.5) < DGEBA–A(0.3)–E(0.2)–L(0.5)–T. The results thus unveil that toughness enhances by (i) increasing molecular weight of the amine crosslinker, (ii) incorporation of silica nanofiller, (iii) application of IL in the synthesis of nanocomposites, (iv) formation of bimodal networks. Based on this finding one can design the structure of a system in order to tune the toughness of a material.

3.2.3 Shape memory properties. The following SM characteristics were evaluated: shape fixity, shape recovery, rate of recovery and recovery stress.

Recovery stress. A comparison of thermomechanical, tensile and shape memory results demonstrates that the generally accepted prediction $\sigma_r \sim G_r$ is not well satisfied. For instance, the nanocomposites DGEBA–D400–T(14) and DGEBA–D400–T(14)–C_4Cl show the same rubbery modulus G_r, however the nanocomposite prepared in the presence of IL exhibits 4 times higher recovery stress. The results reveal that a recovery stress of a SMP is determined mainly by the material toughness. Fig. 9 illustrates the experimentally determined σ_r of the studied systems as a function of their toughness. The toughest nanocomposites based on bimodal networks and those pre-

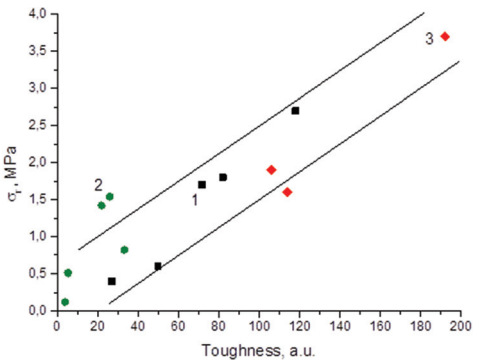

Fig. 9 The recovery stress in SMPs as a function of their toughness for: 1 – DGEBA–D400 and 2 – DGEBA–D230 based systems, 3 – DGEBA–ATBN–Laromin based bimodal systems.

pared by using IL exhibit the highest recovery stress. Particularly, the highest value was achieved in the bimodal nanocomposite network DGEBA–A(0.3)–E(0.2)–L(0.5)–T(14) showing σ_r = 3.7 MPa. Moreover, in contrast to an irregular scatter of experimental data in the case of the dependence σ_r *vs.* G_r, the plot σ_r *vs.* toughness in Fig. 9 displays an unambiguous universal trend involving all investigated systems. The structural effect on recovery stress exhibits a similar trend as for toughness. The recovery stress increases in the systems filled with silica and particularly in the nanocomposites prepared by using ILs. A slight enhancement was observed after incorporation of a small amount of pendant chains. Mainly, however, the recovery stress is enhanced in the nanocomposites based on bimodal networks. These structural effects in SM polymers on recovery stress are shown in Table S1 (in the ESI†). One has to take into account, however, that the comparison of the effect in different systems could be slightly distorted by the fact that the measurement was performed at the constant temperature T_d for all systems, excluding bimodal networks, disregarding T_g and the temperature difference ΔT (= $T_d - T_g$) in the particular system.

The limit of an achievable recovery stress is given by the stress at λ_d (= $0.6\lambda_b$, see the Experimental section) at deformation temperature (T_d). This is an ideal potential, however the real recovery stress is determined by the energy loss during the shape memory cycle. The efficiency to store the elastic energy and memorize the initial state during the cooling/heating processes is characterized approximately by the ratio σ_r/σ_d ($\sim\sigma_r/\sigma_b$). According to this criterion, the shape memory efficiency is reduced in the nanosilica filled system, however it is improved by application of the IL in the synthesis of nanocomposites.

The other SM properties correspond to typical epoxy systems exhibiting the excellent shape fixity and recovery as displayed in Table 1.

Shape fixity. All systems exhibit 100% shape fixity after 6 months with the exception of the bimodal networks containing ATBN. R_f depends on the modulus at the setting temperature G_s. A decrease in shape fixity occurs in polymers showing G_s < 500 MPa, which is the case of the bimodal networks (see Table S1†). The reduced fixity, R_f = 86%, was determined in the DGEBA–A(0.3)–E(0.2)–L(0.5) bimodal network displaying a low modulus, G_s = 240 MPa, as well as in the corresponding nanocomposite involving 5 wt% of nanosilica (T14), R_f = 95%, G_s = 450 MPa.

Shape recovery. The SMPs show almost complete shape (linear) recovery under nonconstrained conditions. A small reduction of shape recovery due to an irreversible deformation was observed in the systems with strong physical interactions and inhomogeneities. This is the case of the nanocomposites with a high nanosilica amount mainly in the bimodal networks and the networks with long pendant chains undergoing a disentanglement. The IL homogenizes the nanocomposite and prevents thereby this shape recovery reduction which results in perfect recovery, 99.7%.

Rate of recovery. The shape recovery is completed in 15–30 s. The slight slowing down within this range was observed in the silica containing nanocomposites in agreement with the general knowledge about a lower recovery speed in less homogeneous systems.

3.2.4 Viscoelasticity effect. The loss of the stored energy during the SM cycle consists of an irreversible plastic deformation as well as in viscoelastic properties and time dependent behaviour of polymers. It is reflected by a reduced shape fixity, incomplete shape recovery and a lower recovery stress, $\sigma_r < \sigma_d$. Therefore, the viscoelasticity effect and stress relaxation are to be taken into account in order to better understand the SM efficiency of polymers. The stress at deformation of a viscoelastic polymer includes the elastic, equilibrium part and the viscoelastic one,

$$\sigma(t) = \sigma_e + \sigma_0 \exp(-t/\tau)^m \quad (3)$$

where σ_0 and σ_e are the initial (at t = 0) and equilibrium stress at deformation, respectively, τ is the relaxation time.

The stress relaxation in the studied systems at the deformation temperature T_d is displayed in Fig. 10. The almost "ideal elastic" network DGEBA–D230 shows a very small viscoelastic effect. Due to a high chemical crosslinking density the stress relaxes quickly and levels off at the equilibrium value σ_e in 15 s (curve 1). The behaviour of a structurally heterogeneous bimodal network of a lower crosslinking density involves more

Table 1 Shape fixity R_f and recovery R_r of epoxy SMPs

SMP system	R_f, %	R_r, %
DGEBA–D400	100	99.95
DGEBA–D400–T(14)	100	99.5
DGEBA–D400–T(40)	100	98.2
DGEBA–D400–T(14)–C_4BF_4	100	99.7
DGEBA–D230–M600(0.1)	100	98.9
DGEBA–D230–M1000(0.1)	100	98.7
DGEBA–A(0.3)–E(0.2)–L(0.5)	86	99.9
DGEBA–A(0.3)–E(0.2)–L(0.5)–T(14)	95	97.9

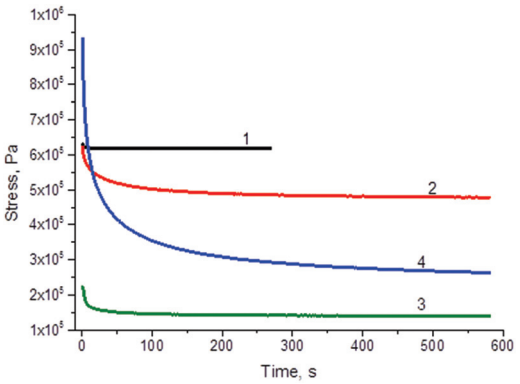

Fig. 10 Stress relaxation at T_d: 1 DGEBA–D230, 2 DGEBA–D230–T(14), 3 DGEBA–A(0.3)–E(0.2)–L(0.5), 4 DGEBA–A(0.3)–E(0.2)–L(0.5)–T(14).

viscoelasticity, however relaxation is fast (curve 3). Mainly the nanocomposites containing silica nanofillers exhibit a significant viscoelastic effect (curve 2 and 4) because of strong physical interactions and phase inhomogeneity. It is manifested by a pronounced and a relatively slow stress relaxation reaching the equilibrium value in $t > 10$ min. This is in agreement with literature data reporting an increased relaxation time with the incorporation of nanoparticles.[46]

The viscoelastic behaviour and relaxation of the studied systems are characterized in Table 2, where the viscoelasticity effect is expressed, for the sake of simplicity, as $\Delta\sigma_{VE} = (\sigma_0 - \sigma_e)/\sigma_0$. The following structural trends were determined to affect the polymer viscoelasticity: (i) increasing crosslinking density of a network leads to a higher elasticity and a faster relaxation, (ii) incorporation of dangling chains enhances viscoelasticity contribution and slows down the relaxation due to physical interactions: slow disentanglement, (iii) presence of a nanofiller results in a strong viscoelasticity effect and a slow relaxation, (iv) application of ILs reduces the viscoelasticity and accelerates relaxation because of the improvement of nanocomposite homogeneity (Table 2).

The strong viscoelastic behaviour could be a reason for the reduced SM efficiency of the nanocomposites. The results reveal that the IL reduces the viscoelastic effect and at the same time improves the SM efficiency corroborating thereby the above hypothesis. These findings unveil the correlation between morphological homogeneity, viscoelastic behaviour and shape memory efficiency. Minimizing the stress relaxation thus could be another way to improve SM efficiency and to reduce the loss of the stored energy.

Consequently, the effects of the nanocomposite structure and synthesis parameters are as follows: (i) silica nanofiller increases G_r, strength and toughness, however SM efficiency is reduced due to a broadening of glass transition and a strong viscoelasticity effect, (ii) the IL used for the synthesis improves homogeneity of a nanocomposite morphology, thereby reducing broadness of the glass transition and the viscoelasticity effect; in addition it enhances toughness due to the strong interphase interaction and improves SM performance, (iii) bimodal networks display a high toughness and deformability, being thus promising systems for high performance SMPs, (iv) physical crosslinking by long pendant chains increases G_r without an enhancement of T_g.

3.3. Optimization of the experimental SM procedure

In addition to material structural characteristics the experimental conditions of the SM procedure can also affect the SM performance. The technical conditions include the rate and extent of deformation, temperature at deformation, rate of cooling/heating processes, geometry (size) of a sample, *etc*. We have studied the effect of the rate of deformation and the rate of cooling. The relative rates of the time dependent processes, such as the experimental procedure and polymer relaxation, are crucial. Both slowing down the polymer relaxation and acceleration of experimental procedures prevent or minimize stress relaxation during these steps and enable the quenching of the relaxation process before reaching the equilibrium state.

The effect of the deformation and cooling rates on the recovery stress of the nanocomposite DGEBA–D400–T(14)–C_4BF_4 is shown in Table 3. The stress relaxation of this nanocomposite in the rubbery state is relatively slow. About 50% of the nonequilibrium stress is relaxed in 25 s at 100 °C, however the equilibrium is reached only in ~9 min. As a result, an effect of the experimental procedure could be expected when freezing the sample within 9 min, while the procedure will significantly affect the SM behaviour in the case of quenching in less than ~25 s. The table illustrates an enhancement of the recovery stress at increasing rates of both deformation and cooling. The effect of the rate of deformation was studied at the highest cooling rate in order to eliminate the influence of relaxation at a slow cooling. Similarly, the effect of the rate of cooling was followed at the highest deformation rate.

The deformation process takes either 1.5 s or up to 5 min according to the rate of deformation in the range 0.06–10 mm s^{-1}. At the highest rate the polymer has less time to relax. Thereby, the higher nonequilibrium stress is quenched by cooling, thus leading to the higher stress at recovery. The sample deformation at 100 °C is immediately followed by cooling with a delay of 1–2 s. According to the rate of cooling it takes about 1–8 min for the instrument to cool down

Table 2 Relaxation of SMPs at T_d = 100 °C

System	$\Delta\sigma_{VE}$	t_{relax}, min
DGEBA–D230	0.02	0.25
DGEBA–D230–M600(0.1)	0.12	2
DGEBA–D230–T(14)	0.30	>15
DGEBA–D400	0.18	7
DGEBA–D400–T(14)	0.23	>10
DGEBA–D400–T(14)–$C_{10}BF_4$	0.15	9
DGEBA–A(0.3)–E(0.2)–L(0.5)	0.59	5
DGEBA–A(0.3)–E(0.2)–L(0.5)–T(14)	0.75	>10

$\Delta\sigma_{VE}$ – viscoelasticity effect, t_{relax} – time of relaxation up to equilibrium of stress.

Table 3 Effect of the rate of deformation and the rate of cooling on recovery stress σ_r of the nanocomposite DGEBA–D400–T(14)–C_4BF_4

Rate of deformation, mm s^{-1}	Rate of cooling, °C min^{-1}	σ_r, MPa	
0.06	10	2.58	Reference conditions
0.06	50	2.64	
1	50	2.70	Effect of deformation rate
10	50	2.92	
10	10	2.77	Effect of cooling rate
10	30	2.78	
10	50	2.92	

the oven from 100 °C to the glassy state of the sample and freeze it (in this case T_g = 62 °C). The quick cooling leads to earlier quenching and increase in σ_r. By applying the highest rates, the recovery stress is enhanced by 15% with respect to the reference conditions used in all experiments. Under the optimized conditions the recovery stress σ_r = 3.9 MPa was determined in the case of the bimodal network based nanocomposite DGEBA–A(0.3)–E(0.2)–L(0.5)––T(14). The effect of the cooling rate is dependent on heat transfer, thermal conductivity of a material and geometry of a sample.

3.4. Dual SM material

The acquired knowledge was used to prepare the dual SM material, the two parts of which can be controlled at different temperatures. The sample in Fig. 11 is composed of two halves of different structures, *i.e.*, containing the networks of different T_gs as shown in Fig. 12. The left hand part is the material based on the DGEBA–D400 network while the right hand part involves the DGEBA–D230 network. The narrow middle interphase is the mixed type due to interdiffusion of the reaction mixtures in both parts. The shape recovery of the two parts is triggered by heating up to T_1 = 60 °C and to T_2 = 110 °C, respectively (*cf.* Fig. 12). Fig. 11 discloses that both temperatures T_{s_1} = 25 °C and T_{s_2} = 60 °C are applicable as the setting temperatures. However, the storage modulus at 60 °C is low, $G_{s(60\ °C)}$ = 300 MPa, resulting in poor shape fixity of the second right-hand part, being only 82% after 10 days.

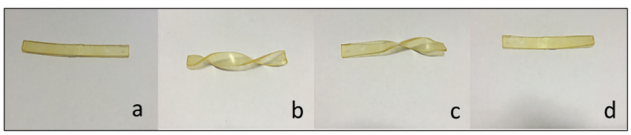

Fig. 11 Dual SM effect of the epoxy–silica nanocomposite DGEBA–D230/D400–T(14)–$C_{10}BF_4$: (a) initial shape, (b) heating up to 110 °C, deformed and cooled down to T_s, (c) heating up to 60 °C and (d) heating up to 110 °C.

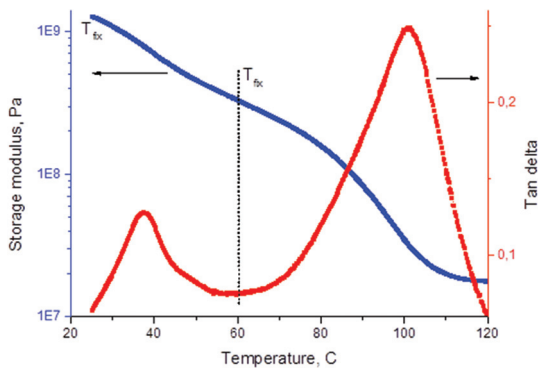

Fig. 12 Storage modulus and loss factor tan δ of the shape memory nanocomposite with the dual SM effect DGEBA–D230/D400–T(14)–$C_{10}BF_4$ as a function of temperature.

4. Conclusions

The paper deals with the structural design and synthesis of high performance epoxy based SM nanocomposites. They were prepared by *in situ* generation of nanosilica within the epoxy matrix and a special synthesis was employed in order to finely tune their structure. The non-aqueous sol–gel process and application of ILs in the synthesis made it possible to control the strength of the interphase, morphology and mechanical properties of the nanocomposites.

The investigation involved the determination of relationships between the structure, mechanical properties and the SM properties of the studied polymers. It was found that the recovery stress, as a crucial SM property of high performance systems, is governed by the material toughness, which can be considered as a potential of a material for the SM behaviour at the recovery under constrained conditions. However, a SM efficiency to exploit this potential depends on the material morphology and the viscoelastic behaviour of the polymer as well as on experimental conditions of the SM procedure. The shape fixity and recovery under nonconstrained conditions were proved to be controlled mainly by the material thermomechanical properties such as moduli at deformation and setting temperatures, G_r, G_s, the T_g and broadness of the glass transition.

Because of these correlations, the structure of the SM systems was designed in such a way to enable the control of (i) thermomechanical, (ii) tensile mechanical and (iii) viscoelastic properties in order to improve their SM performance. The thermomechanical properties were tuned and the T_g of SMPs was adjusted by optimization of the crosslinking density of the epoxy matrix and the flexibility of polymer chains, by introducing physical crosslinks and silica nanofillers to increase the rubbery modulus G_r and by application of the IL in the synthesis in order to narrow glass transition. Tensile properties and toughness were determined to be enhanced by the silica nanofiller and by application of the IL. Moreover, the bimodal epoxy networks showed a very high toughness and enabled a high extensibility of the SMP. The effect of polymer viscoelasticity and relaxation, as the properties deteriorating the efficiency of SM performance, is reduced by increasing system elasticity and homogeneity; by enhancing the crosslinking density and by application of the IL.

The characterization of nanocomposites as SMPs is as follows. The reinforcement by nanosilica increases G_r and toughness, as well as the recovery stress, however SM efficiency is reduced because of a strong viscoelasticity effect. Beneficial is the influence of the IL in strengthening the interphase interaction and improving the homogeneity of nanocomposite morphology. As a result, the toughness is increased and the viscoelasticity reduced, thereby enhancing the SM performance. Also the concept of bimodal networks is promising. Based on the knowledge of the corresponding relationships, the high performance epoxy based SM nanocomposite was synthesized showing the high recovery stress σ_r = 3.9 MPa or high deformability ε_b = 103%. Moreover, the study contributed to the better understanding of the SM behaviour of polymers.

Acknowledgements

The authors acknowledge the financial support from the Grant Agency of the Czech Republic (P108/12/1459). The authors thank to Prof. Schrekker (Universidade Federal do Rio Grande do Sul, Porto Alegre-RS, Brazil) for the ionic liquids. Sergii Ponyrko is thankful to the Charles University in Prague for the financial support.

References

1 N. Rapoport, *Prog. Polym. Sci.*, 2007, **32**, 962.
2 H. Y. Jiang, S. Kelch and A. Lendlein, *Adv. Mater.*, 2006, **18**, 1471.
3 C. Liu, H. Qin and P. T. Mather, *J. Mater. Chem.*, 2007, **17**, 1543.
4 H. Koerner, G. Price, N. A. Pearce, M. Alexander and R. A. Vaia, *Nat. Mater.*, 2004, **3**, 115.
5 C. Liu, S. B. Chun, P. T. Mather, L. Zheng, E. H. Haley and E. B. Coughlin, *Macromolecules*, 2002, **35**, 9868.
6 Y. Kagami, J. P. Gong and Y. Osada, *Macromol. Rapid Commun.*, 1996, **17**, 539.
7 K. Sakurai, H. Tanaka, N. Ogawa and T. Takahashi, *J. Macromol. Sci., Phys.*, 1997, **36**, 703.
8 J. Diani, Y. Liu and K. Gall, *Polym. Eng. Sci.*, 2006, **46**, 486.
9 J. M. Jani, M. Leary, A. Subic and M. A. Gibson, *Mater. Des.*, 2014, **56**, 1078.
10 K. Kumar and D. C. Lagoudas, *Shape memory alloys modelling and engineering applications chapter 1: introduction to shape memory alloys*, Springer, US, 2008.
11 A. Lendlein and R. Langer, *Science*, 2002, **296**, 1673.
12 I. A. Rousseau, *Polym. Eng. Sci.*, 2008, **48**, 2075.
13 I. A. Rousseau and T. Xie, *J. Mater. Chem.*, 2010, **20**, 3431.
14 D. M. Feldkamp and I. A. Rousseau, *Macromol. Mater. Eng.*, 2010, **295**, 726.
15 X. H. Jing, Y. Y. Liu, Y. X. Liu, Z. G. Liu and H. F. Tan, *J. Appl. Polym. Sci.*, 2014, **131**, 40853.
16 J. S. Leng, X. L. Wu and Y. J. Liu, *Smart Mater. Struct.*, 2009, **18**, 095031.
17 M. A. Di Prima, K. Galla, D. L. McDowella, R. Guldbergb, A. Linb, T. Sandersonc, D. Campbelle and S. C. Arzbergere, *Mech. Mater.*, 2010, **42**, 405.
18 R. Biju, C. Gouri and C. P. R. Nair, *Eur. Polym. J.*, 2012, **48**, 499.
19 X. L. Wu, S. F. Kang, X. J. Xu, F. Xiao and X. L. Ge, *J. Appl. Polym. Sci.*, 2014, **131**, 40559.
20 T. Xie and I. A. Rousseau, *Polymer*, 2009, **50**, 1852.
21 C. M. Yakacki, S. Willis, C. Luders and K. Gall, *Adv. Eng. Mater.*, 2008, **10**, 112.
22 A. B. Leonardi, L. A. Fasce, I. A. Zucchi, C. E. Hoppe, E. R. Soule, C. J. Perez and R. J. J. Williams, *Eur. Polym. J.*, 2011, **47**, 362.
23 N. Zheng, G. Fang, Z. Cao, Q. Zhao and T. Xie, *Polym. Chem.*, 2015, **6**, 3046.
24 J. Cui, K. Kratz, M. Heuchel, B. Hiebl and A. Lendlein, *Polym. Adv. Technol.*, 2011, **22**, 180.
25 Y. Bellouard, *Mater. Sci. Eng., A*, 2008, **481**, 582.
26 E. Hornbogen, *Adv. Eng. Mater.*, 2006, **8**, 101.
27 P. Miaudet, A. Derré, M. Maugey, C. Zakri, P. M. Piccione, R. Inoubli and P. Poulin, *Science*, 2007, **23**, 1294.
28 I. S. Gunes and S. C. Jana, *J. Nanosci. Nanotechnol.*, 2008, **8**, 1616.
29 J. S. Leng, X. Lan, Y. J. Liu and S. Y. Du, *Prog. Mater. Sci.*, 2011, **56**, 1077.
30 S. A. Madbouly and A. Lendlein, *Adv. Polym. Sci.*, 2010, **226**, 41.
31 Q. H. Meng and J. L. Hu, *Composites, Part A*, 2009, **40**, 1661.
32 M. S. Kim, J. K. Jun and H. M. Jeong, *Compos. Sci. Technol.*, 2008, **68**, 1919.
33 T. Ohki, Q. Q. Ni, N. Ohsako and M. Iwamoto, *Composites, Part A*, 2004, **35**, 1065.
34 Y. C. Jung, N. G. Sahoo and J. W. Cho, *Macromol. Rapid Commun.*, 2006, **27**, 126.
35 S. K. Lee, S. H. Yoon, I. Chung, A. Hartwig and B. K. Kim, *J. Polym. Sci., Part A: Polym. Chem.*, 2011, **49**, 634.
36 V. A. Beloshenko and Yu. V. Voznyak, *Polym. Sci., Ser. A*, 2009, **51**, 416.
37 K. Gall, M. L. Dunn, Y. Liu, D. Finch, M. Lake and N. A. Munshi, *Acta Mater.*, 2002, **50**, 5115.
38 S. Ponyrko, L. Kobera, J. Brus and L. Matějka, *Polymer*, 2013, **54**, 6271.
39 S. Ponyrko, J. Kovářová, L. Kobera and L. Matějka, *J. Appl. Polym. Sci.*, 2014, **131**(20), 40899.
40 R. K. Donato, K. Z. Donato, H. S. Schrekker and L. Matějka, *J. Mater. Chem.*, 2012, **22**, 9939.
41 R. K. Donato, L. Matějka, H. S. Schrekker, J. Pleštil, A. Jigounov, J. Brus and M. Šlouf, *J. Mater. Chem.*, 2011, **21**, 13801.
42 H. S. Schrekker, D. O. Silva, M. A. Gelesky, M. P. Stracke, C. M. L. Schrekker, R. S. Goncalves and J. Dupont, *J. Braz. Chem. Soc.*, 2008, **19**, 426.
43 L. Matějka, K. Dušek and M. Ilavský, *Polym. Bull.*, 1979, **1**, 659.
44 C. M. Yakacki, R. Shandas, D. Safranski, A. M. Ortega, K. Sassaman and K. Gall, *Adv. Funct. Mater.*, 2008, **18**, 2428.
45 E. Urbaczewski-Espuche, J. Galy, J.-F. Gerard, J.-P. Pascault and H. Sautereau, *Polym. Eng. Sci.*, 1991, **31**, 1572.
46 B. U. Ahn, S. K. Lee, S. K. Lee, J. H. Park and B. K. Kim, *Prog. Org. Coat.*, 2008, **62**, 258.